


7-2021

## Microfabrication and Electrochemical Characterization of a Novel SU-8 Probe with an Array of Individually Addressable Electrodes Suitable for Redox Cycling Experiments in Ultra-small Volumes

Mahsa Lotfi Marchoubeh  
*University of Arkansas, Fayetteville*

Follow this and additional works at: <https://scholarworks.uark.edu/etd>

 Part of the [Analytical Chemistry Commons](#), [Animal Experimentation and Research Commons](#), [Animal Studies Commons](#), [Materials Chemistry Commons](#), [Molecular and Cellular Neuroscience Commons](#), and the [Organic Chemistry Commons](#)

---

### Citation

Lotfi Marchoubeh, M. (2021). Microfabrication and Electrochemical Characterization of a Novel SU-8 Probe with an Array of Individually Addressable Electrodes Suitable for Redox Cycling Experiments in Ultra-small Volumes. *Graduate Theses and Dissertations* Retrieved from <https://scholarworks.uark.edu/etd/4170>

This Dissertation is brought to you for free and open access by ScholarWorks@UARK. It has been accepted for inclusion in Graduate Theses and Dissertations by an authorized administrator of ScholarWorks@UARK. For more information, please contact [scholar@uark.edu](mailto:scholar@uark.edu).

Microfabrication and Electrochemical Characterization of a Novel SU-8 Probe with an Array of Individually Addressable Electrodes Suitable for Redox Cycling Experiments in Ultra-small Volumes

A dissertation submitted in partial fulfillment  
of the requirements for the degree of  
Doctor of Philosophy in Chemistry

by

Mahsa Lotfi Marchoubeh  
Isfahan University of Technology  
Bachelor of Science in Chemistry, 2008  
Isfahan University of Technology  
Master of Science in Chemistry, 2011

July 2021  
University of Arkansas

This dissertation is approved for recommendation to the Graduate Council.

---

Ingrid Fritsch, Ph.D.  
Dissertation Director

---

Julie Stenken, Ph.D.  
Committee Member

---

Charles Wilkins, Ph.D.  
Committee Member

---

David Paul, Ph.D.  
Committee Member

---

Suresh Thallapuranam Kumar, Ph.D.  
Committee Member

## Abstract

Redox cycling is an electrochemical technique that utilizes closely spaced generator and collector electrodes to cycle reversible redox species between their oxidative states. With advantages in signal amplification, selectivity of species based on their electrochemical reaction mechanism, and limited or no background subtraction, this technique is well suited for selective detection of important electrochemically active molecules such as dopamine at basal or slowly changing levels.

Miniaturized medical devices have become an area of great interest for measurement of chemicals in limited volumes with low concentrations or in sensitive tissues. A probe on a polymeric SU-8 substrate with suitable dimensions and robustness for *in vivo* neural measurements was developed and tested *in vitro*. The probe's unique construction using microfabrication processes and a laser-machining procedure is described in detail. The probe features an array of individually addressable electrodes, each 100  $\mu\text{m}$  long, 4  $\mu\text{m}$  wide and with a 100  $\mu\text{m}$  gap in between, on a shank that is 6 mm long and 100  $\mu\text{m}$  wide. The probe is insulated by a thin layer of SU-8 with only the electrodes near the tip and the contact pads exposed. Evaluation of tissue after probe insertion into a rat brain indicates minimal damage comparable to FSCV electrodes and less extensive than the microdialysis probe.

The electrodes on the probe were characterized electrochemically and redox cycling on the array was evaluated *in vitro* in the presence of model compounds (potassium ferricyanide and ruthenium (III) hexamine chloride) and dopamine, and the responses were compared to theory. The amplification factors, percent collection efficiencies and detection limits are determined from calibration curves. The best detection limits obtained for dopamine at the generator

electrodes and collector electrodes during redox cycling are 800 nM and 1.10  $\mu$ M, respectively.

These values lie in the physiological concentration range of dopamine. The features and the results suggest that the probe is ready for further analysis *in vivo*.

Finally, potential future designs for the probe are proposed and their expected current is calculated using theoretical approximations. All of the proposed designs fit on the same footprint as the current probe (70- $\mu$ m wide and 100- $\mu$ m long window) and have dimensions achievable with available micro and nanofabrication tools.

## **Acknowledgements**

I would like to thank my advisor Dr. Ingrid Fritsch who has guided and supported me throughout my education at the University of Arkansas. Her scientific insights and mentorship have been invaluable to me. She invested in me as a scientist, let me learn and grow along the way and always lifted me up. I would also like to thank my committee, Dr. Charles Wilkins, Dr. Julie Stenken, Dr. Suresh Thallapuranam Kumar and Dr. David Paul for their advice, support, and comments. The environment and opportunities they provided for me, along with their moral and professional support was an essential part of my accomplishments. My lab mates and friends also played a role, and I am forever thankful to them.

I would also like to thank my collaborators, Dr. Adrian Michael at the University of Pittsburgh and Dr. Julie McPherson at the University of Warwick and their research groups for their contributions to my research. Their help and support opened numerous doors for me and widened my horizons. The staff at the QNF micro/nanofabrication facility at the University of Pittsburgh and The High-Density Electronics Center at the University of Arkansas are also appreciated, as they provided valuable insights for this project. Special thanks go to my funding sources specially the University of Arkansas's College of Arts of Sciences Travel grant and the Women's giving Circle. These financial supports gave me the opportunity to travel and get hands on experience with state-of-the-art research.

Finally, I would like to thank my husband, parents, and family for their unconditional support of my goals and ambitions. I am forever indebted to them for their love, encouragement and understanding.

## Contents

|   |    |
|---|----|
| 1. Introduction   | 1  |
| 1.1 Neurotransmitters   | 2  |
| 1.1.1 Catecholamines  | 3  |
| 1.1.2 Other Interfering Electrochemically Active Species in the Brain   | 4  |
| 1.1.3 Nonelectroactive Species in the Brain   | 6  |
| 1.1.4 <i>In vivo</i> Neural Probes and Chemical Analysis of Catecholamines  | 6  |
| 1.2 Considerations for a neural probe   | 13 |
| 1.3 Overview of the Studies Described in this Dissertation  | 14 |
| 1.4 Figures   | 16 |
| 1.5 References  | 20 |
| 2. Miniaturized Probe on Polymer SU-8 with Array of Individually Addressable<br>Microelectrodes for Electrochemical Analysis in Neural and other Biological Tissues | 30 |
| 2.1 Abstract  | 32 |
| 2.2 Introduction  | 33 |
| 2.3 Materials and Methods   | 37 |
| 2.3.1 Chemicals and Materials   | 37 |
| 2.3.2 Fabrication of the Electrodes   | 39 |
| 2.3.3 Shaping of the Probes   | 42 |
| 2.3.4 Electrochemical Studies   | 43 |

|       |  |    |
|-------|--|----|
| 2.3.5 | Assessment of Tissue Damage.....   | 44 |
| 2.4   | Results and Discussion.....  | 46 |
| 2.4.1 | Probe design and rationale .....   | 46 |
| 2.4.2 | Characterization by Cyclic Voltammetry of Individual Electrodes with a Model<br>Compound   | 47 |
| 2.4.3 | Redox Cycling and Calibration Curves for a Model Compound.....   | 48 |
| 2.4.4 | Redox Cycling and Calibration Curves for Dopamine .....  | 52 |
| 2.5   | Insertion of probe and assessment of resulting tissue damage in rat brain .....  | 54 |
| 2.6   | Conclusions .....  | 54 |
| 2.7   | Supporting Information .....   | 56 |
| 2.8   | Conflicts of Interest .....  | 56 |
| 2.9   | Ethics Approval.....   | 56 |
| 2.10  | Source of Biological Material .....  | 56 |
| 2.11  | Statement on Animal Welfare .....  | 57 |
| 2.12  | Acknowledgements .....   | 57 |
| 2.13  | Figures.....   | 58 |
| 2.14  | References .....   | 68 |
| 2.S   | Supplementary Information: Miniaturized Probe on Polymer SU-8 with Array of Individually<br>Addressable Microelectrodes for Electrochemical Analysis in Neural and other Biological<br>Tissues | 74 |

|       |   |     |
|-------|---|-----|
| 3.    | In situ Quantitative Analysis of Dopamine and Theoretical Considerations for Design Optimization for Redox Cycling at a Coplanar Array of Individually Addressable Electrodes with Dimensions Suitable for <i>in vivo</i> Detection on SU-8 Polymeric Substrate | 77  |
| 3.1   | Abstract .....  | 78  |
| 3.2   | Introduction .....  | 79  |
| 3.3   | Materials and Methods .....   | 83  |
| 3.3.1 | Chemicals and Materials .....   | 83  |
| 3.3.2 | Design and Microfabrication of the Device .....   | 84  |
| 3.3.3 | Characterization of Individual Electrodes .....   | 84  |
| 3.4   | Results and Discussion.....   | 86  |
| 3.4.1 | Electrochemical Performance of the Device using Model Compounds .....   | 86  |
| 3.4.2 | Capacitive Behavior of the Microelectrodes on SU-8 .....  | 90  |
| 3.4.3 | A Model Electrochemical Circuit for a Band Electrode on SU-8 Substrate in KCl91   |     |
| 3.4.4 | Redox Cycling of Dopamine using the Device.....   | 93  |
| 3.4.5 | Design optimization of the electrode array .....  | 95  |
| 3.5   | Conclusions .....   | 98  |
| 3.6   | Figures .....   | 100 |
| 3.7   | References .....  | 107 |
| 3.S   | Supplemental information: In situ Quantitative Analysis of Dopamine and Theoretical Considerations for Design Optimization for Redox Cycling at a Coplanar Array of Individually  |     |



## Addressable Electrodes with Dimensions Suitable for *in vivo* Detection on SU-8 Polymeric

|  |     |
|--|-----|
| Substrate  | 115 |
| 4. Conclusion and Future Work  | 120 |
| 4.1 Conclusion.....  | 121 |
| 4.2 Future Work .....  | 123 |
| 4.2.1 Differentiation of catecholamines and their quantification <i>in vitro</i> ..... | 123 |
| 4.2.2 Optimization of the probe .....  | 125 |
| 4.3 References .....   | 127 |
| 5. Appendix  | 129 |

## List of Publications

**Chapter 2.** Miniaturized probe on polymer SU-8 with array of individually addressable microelectrodes for electrochemical analysis in neural and other biological tissues.

Mahsa Lotfi Marchoubeh, Samuel J. Cobb, Miguel Abrego Tello, Mengjia Hu, Andrea Jaquins-Gerstl, Elaine M. Robins, Julie V. McPherson, Adrian C. Michael, Ingrid Fritsch

Anal Bioanal Chem (2021). <https://doi.org/10.1007/s00216-021-03327-2>

## **1. Introduction**

## 1.1 Neurotransmitters

Neurotransmitters are signaling molecules in the brain that convey an impulse from the pre-synaptic neuron to the post-synaptic one.<sup>1</sup> These molecules are stored in vesicles at the end of pre-synapse neurons and are released into the synaptic cleft by stimuli. The released neurotransmitter then binds to its receptor at the post-synaptic neuron and consequently transduces the chemical signal into electrochemical transmission via changes in neuronal cell membrane potentials (i.e., depolarization or hyperpolarization).<sup>1</sup> Excess neurotransmitter is then removed by reuptake into the pre-synaptic neuron, diffusion, or metabolized by enzymes, ending the signal. Most neurotransmitters are either small amine molecules, amino acids, or neuropeptides.

Neurotransmitters are associated with a myriad of neurological disorders and therefore their detection and quantification have been points of great interest to scientists. Because these chemicals are present in very low concentrations (for example, dopamine's extracellular concentration range is 20-1200 nM)<sup>2</sup> and are very short-lived (for example, dopamine is cleared from the synapse between 10-200 ms after release),<sup>3</sup> there is a great need for sensitive, selective and fast detection methods for these chemicals at physiological concentrations.<sup>4</sup>

Some small amine neurotransmitters (e.g. catecholamines) are electrochemically active (able to transfer electrons on the surface of an electrode at the right potential) with reasonable potential ranges achieved by laboratory potentiostats. Compounds such as hydrogen peroxide are produced from enzymatic reactions with some of the non-electrochemically active neurotransmitters (e.g. acetylcholine, present in sub-nanomolar concentrations).<sup>5</sup> Hydrogen peroxide is then electrochemically measured and associated with the concentration of the species.<sup>6,7</sup> Here, we will focus on the detection of catecholamines.

### 1.1.1 Catecholamines

Catecholamines contain one amine and a dihydroxyphenyl group as the catechol nucleus. They include three species: dopamine (DA, 3,4-dihydroxyphenethylamine,) epinephrine also known as adrenaline (EP, (R)-4-(1-Hydroxy-2-(methylamino)ethyl)benzene-1,2-diol) and norepinephrine also known as noradrenaline (NE, 4-[(1R)-2-amino-1-hydroxyethyl]benzene-1,2-diol) ((Fig 1).

Catecholamines are derived in the biosynthetic pathway from tyrosine.<sup>8</sup> The rate-limiting step in the synthesis is the hydroxylation of tyrosine to 3,4-dihydroxyphenylalanine (DOPA) with tyrosine hydroxylase. Dopamine is formed by the decarboxylation of L-DOPA. Norepinephrine is formed after transfer of a hydroxyl group onto the  $\beta$ -position of the side chain via dopamine- $\beta$ -hydroxylase. The amine of norepinephrine can be methylated by phenylethanolamine-N-methyltransferase to form epinephrine.

Dopamine (DA), also known as the central neurotransmitter has many different functions, including roles that it plays in the “reward” system, adaptive behavior, and voluntary movements. It has been closely entwined with substance abuse<sup>9, 10</sup> and its treatment, as well as depression, Parkinson’s disease<sup>11-13</sup> and Huntington’s disease.<sup>14</sup> Norepinephrine (NE) is closely related to stress levels. It is involved in regulation of functions such as attention and arousal, because it increases the level of excitatory activity.<sup>15,16</sup> Epinephrine (EP) is a hormone released from the adrenal medulla which is a part of the adrenal glands on top of the kidney, it is known to be involved with fight or flight decisions. Exercise is the biggest contributor to secretion of EP in the bloodstream.<sup>17</sup>

Catecholamine neurotransmitters are well suited for electrochemical detection because the potential required for their oxidation is well within normal voltage windows where carbon

and metal electrodes are electrochemically inert in physiological buffer.<sup>18</sup> In the oxidation process of catecholamines, the catechol group loses two hydrogens and two electrons to form orthoquinone groups. The following chemistry involves internal cyclization of the orthoquinone group to form a leucoaminochrome. This leucoaminochrome can react with orthoquinones to remake the catecholamine and an aminochrome species. The leucoaminochrome and the aminochrome molecules are electrochemically inactive in the potential windows of catecholamine oxidation on the most common electrodes (Fig. 2).<sup>19</sup>

Catecholamines go through a  $2e^-/2H^+$  oxidation at +0.2 V vs Ag/AgCl (saturated KCl) reference electrode in pH=7.4 at physiological conditions.<sup>20</sup> Because they coexist in certain parts of the brain,<sup>21-23</sup> it is important to be able to distinguish between them. Simple electrochemical techniques, such as cyclic voltammetry (CV) are not well suited to achieve this for dopamine and norepinephrine due to their similar oxidation potentials and shape of voltammograms. More advanced and complicated electrochemical techniques are required for differentiation of these chemicals in real time.

### **1.1.2 Other Interfering Electrochemically Active Species in the Brain**

The brain's extracellular fluid consists of many electroactive chemicals that are considered interference to detection of catecholamines. Interferences fall into two main categories, the chemicals whose oxidation signal overlaps with the one of the catecholamines, and the chemicals that in some way change the concentration of catecholamines in the brain.

The most studied electrochemical interference for catecholamines is ascorbic acid (AA). It is one of the most prevalent molecules in the brain (30 -800  $\mu\text{M}$ )<sup>24</sup> and serves as an antioxidant to clear oxygen or nitrogen-based radicals. It is also a co-factor in several enzyme reactions including catecholamine synthesis.<sup>25, 26</sup> Ascorbic acid is also oxidized at a similar potential as the

catecholamines and because of its high concentration, its peak dominates the oxidation peak of catecholamines.<sup>27, 28</sup> Various strategies have been utilized to be able to detect dopamine in the presence of AA. These methods mainly involve modification of the electrode to selectively detect dopamine (e.g. Nafion)<sup>29, 30</sup> or taking advantage of the irreversibility and slow kinetics of the redox reaction of AA.<sup>31 32, 33</sup>

Other electrochemically-active species include uric acid (UA), L-3, 4-dihydroxyphenylalanine (L-dopa), a precursor to DA, and metabolites of catecholamines: 3, 4-dihydroxyphenylacetic acid (DOPAC), homovanillic acid (HVA), and 3-methoxytyramine (3-MT). Another important neurotransmitter (serotonin, 5-HT) and its metabolites (5-hydroxyindoleacetic acid, 5-HIAA) can coexist with DA in certain regions of the brain. Most of these interfering species have similar electrode potentials to that of DA, close to +0.2 V vs Ag/AgCl (Saturated KCl) reference electrode.<sup>34, 35</sup> Any *in vivo* electrochemical experiment should take into consideration the existence of these chemicals and devise methods to eliminate or account for these interferences to be able to accurately detect catecholamines. Most common electrochemical techniques are not capable of differentiating between these chemicals and the catecholamines and therefore there is a need for an electrochemical detection method that can selectively detect catecholamines.

Another species present in the brain is oxygen. The partial pressure of oxygen in the brain is usually between 30-35 mm Hg (about 0.08 ppm in a healthy brain).<sup>36</sup> Due to its high concentration in brain, it will have a significant impact in oxidizing chemicals such as catecholamines, ascorbic acid and others.<sup>1</sup> It needs to be taken into consideration in electrochemical research involving the brain. For *in vitro* experiments with the final goal of *in*

*in vivo* qualification or quantification of catecholamines, it is important to have controlled oxygen levels close to the ones in the brain.

Hydrogen concentration affects the chemical balances of catecholamines and their reduced species (orthoquinones) (Fig. 2). In addition, the oxidation of catecholamines on electrodes leads to changes in the pH. Based on the Nernst equation, changes in the pH of the system can lead to changes in the oxidation potential of catecholamines. For most *in vitro* studies, the pH of aCSF (artificial cerebral spinal fluid) is adjusted to be 7.2-7.4 either by adding acids and bases or by bubbling of carbon dioxide gas.<sup>37-40</sup> It is important to consider the pH in experimental and theoretical evaluations of these systems.

### **1.1.3 Nonelectroactive Species in the Brain**

Non-electroactive species present in the complex biological environment of the brain can affect catecholamine detection. These species include proteins such as albumin and lipids (which will be more abundant when cell membranes are damaged due to insertion of the probe in tissue). These compounds can adhere to the surface of the electrodes and foul them. The fouling of electrodes can cause shifts in the potentials of oxidation and reduction, diminishing sensitivity and worsen detection limits. Other chemicals such as GABA (gamma amino butyric acid), glucose, glutamate, lactate, and choline are also present in the brain, but their detection requires electrode modification. They are not likely to directly affect catecholamine concentrations.

### **1.1.4 *In vivo* Neural Probes and Chemical Analysis of Catecholamines**

Studies to achieve sensitive and selective detection of neurotransmitters with high temporal and spatial resolution have been underway for decades. The most prominent approaches to detection of neurotransmitters *in vivo* are microdialysis sampling coupled with a detection method and electrochemical methods.<sup>21</sup> These are further discussed below. Imaging



methods such as positron emission tomography (PET) and functional magnetic resonance imaging (fMRI) have been used to track neurotransmitter activity in the brain, but these techniques do not exhibit suitable spatial and temporal resolution to gain insights into release and uptake mechanisms at the neuronal levels.<sup>34, 41, 42</sup>

#### **1.1.4.1 Microdialysis Sampling Coupled with a Detection Method**

Microdialysis, a sampling method, has become an indispensable tool for investigations of neurochemicals in the brain.<sup>43-46</sup> A probe with a tip diameter of 200-400  $\mu\text{m}$  made of a semi permeable membrane collects extracellular fluid. Small molecules such as the amine neurotransmitters will cross the membrane because of concentration gradient. The inlet tubing perfuses fluids such as extracellular fluid or pharmaceutical agents and the outlet tubing collects the sample called the dialysate. The dialysate is analyzed for presence and concentration of molecules. The perfusion inside the probe controlled with a slow rate ( $< 3 \mu\text{l}/\text{min}$ ) will carry the analyte to a detector. The detector (mass spectrometry, absorbance spectrophotometry, fluorescence, or electrochemical detectors) will play a role in defining the temporal resolution and sensitivity.<sup>44,47</sup>

A notable advantage of microdialysis when coupled with detection methods is its high selectivity and sensitivity. Another advantage of microdialysis is that the versatility of choosing the detector can lead to identification and quantification of a wide variety of *in vivo* analytes. Also, the fabrication of the probe is relatively easy and reproducible. Microdialysis can also be utilized to deliver drugs into the tissue.<sup>47,48-50</sup> Reports have indicated that the size of the microdialysis probe may lead to tissue damage, resulting in an immune response, and therefore impact the analysis results.<sup>51</sup> The damage can cause various electrochemically active and fouling chemicals to be released in the sampling region due to immune response which will affect

accuracy and alter the chemical composition of the tissue. The probes can go up to 1 mm in outer diameter which will cause low spatial resolution of sampling. The rate of perfusion inside the membrane is typically  $<3 \mu\text{l}/\text{min}$ , and depends on membrane properties, and detection method. Each sampling-detection procedure can take a few seconds<sup>52, 53</sup> to 20-30 min<sup>44, 45</sup> leading to temporal resolutions not suitable for real time analysis of chemicals in the brain.

#### **1.1.4.2 Electrochemical Methods**

Electrochemical detection of neurotransmitters has been a subject of interest since the 1960s with Ralph Adams as the pioneer.<sup>28</sup> Catecholamines undergo a  $2e^-/2H^+$  oxidation reaction and are therefore detectable using electrochemical techniques. Electrochemical sensors are inexpensive and easy to operate devices for selective and sensitive detection of molecules in real time. Advances in microfabrication, have allowed electrochemical devices to become miniaturized and portable for applications in medical fields.

A variety of electrochemical techniques, electrode material and modification methods have been utilized to electrochemically detect catecholamines.<sup>32, 54</sup> The following section focuses on Fast Scan Cyclic Voltammetry (FSCV), as the most widely used electrochemical technique for detection of catecholamines, followed by redox cycling, which is the method the work presented in this dissertation utilizes to detect catecholamines *in vitro*.

##### **1.1.4.2.1 Fast Scan Cyclic Voltammetry**

FSCV is currently the most widely used electrochemical method for making relatively continuous DA measurements at carbon fiber electrodes (CFEs).<sup>9, 55, 56, 57</sup> The method exhibits low detection limits (low nM) due to high surface area of the electrodes and the pre-absorption of dopamine on the surface of the electrode held at a reducing potential.<sup>2, 58</sup> The small diameter carbon fiber electrodes (5-15  $\mu\text{m}$  diameter) used in FSCV will cause little tissue damage.<sup>3</sup>

Detecting dopamine using FSCV at CFEs *in vivo* has been largely explored. The high speed of the technique (300 V/s to 600 V/s coupled with potential waveform to enhance adsorption between scans) allows rapid monitoring of dopamine every 100 ms.<sup>2</sup> It uses a time scale so short as to exclude kinetically slow oxidation processes, such as that exhibited by ascorbic acid.<sup>2, 33, 34</sup>

It has long been recognized that DA adsorbs to the surface of the carbon microfiber electrode used for FSCV. This adsorption is both as an advantage and a disadvantage. The adsorption preconcentrates DA on the electrode therefore, improving the limit of detection. However, the electrode's response becomes slower due to this adsorption. Many groups utilize deconvolution techniques to remove this lag of the signal.<sup>2, 34, 59</sup>

Since the diameter of the CFE is very small, the electrode can be placed and make measurements very close to the point where DA gets released from the vesicle.<sup>58</sup> Uptake mechanisms and dilution due to diffusion lead to diminishing concentrations of DA far away from the point of release; the proximity of the CFE to release site leads to detection of DA molecules before they are affected by the two mentioned processes and therefore it is generally believed that the values obtained using FSCV for DA are more accurate in terms of local concentration than the ones from microdialysis.<sup>40</sup>

In addition, CFEs have such narrow diameters that tissue damage can be assumed to be negligible. In fact, the track of the carbon fiber exposed tip cannot be observed by electron microscopy of the nano-bead perfused brain slides and therefore the track of the glass capillary is followed to the smallest visible extent and that is assumed to be where the CFE tip has affected the tissue. This is considered a major advantage over microdialysis probes that cause substantial tissue damage as can be seen by the disappearance of blood vessels around the probe's track.<sup>40, 51,</sup>

Due to very high scan rates used in FSCV, high enough background currents are generated that create analytical challenges in measuring basal levels concentrations due to the need to subtract the background current. The need to scan background current in FSCV leads to its inability to measure basal or slow changing concentrations of catecholamines. However, by stimulation of nerves, catecholamine transients can be measured after using the background-subtraction methods.<sup>34</sup>

In addition to large backgrounds, FSCV has difficulty discriminating among multiple neurotransmitters. Quantitative measurement of individual components within a mixture of neurochemicals including DA, 5-HT, DOPAC, HVA, 3-MT, L-dopa, UA and AA has been made in Wightman's laboratory.<sup>61</sup> However, FSCV signals of the neurotransmitters dopamine and norepinephrine are similar and these two compounds cannot be differentiated using this technique.<sup>23</sup> Due to this, FSCV probe is usually inserted into a part of the brain that is known to have higher concentrations of the target neurotransmitter.<sup>62</sup> These regions might even exhibit the absence of specific interferences or the interferent might be eliminated by administration of specific receptor antagonists or transporter inhibitor.<sup>2</sup> Another solution is to stimulate the release of a specific catecholamine (for example DA).<sup>63</sup> Considering the drawback of FSCV, the need for methods that do not require background subtraction, and can differentiate catecholamines arises.

#### **1.1.4.2.2 Redox Cycling**

Redox cycling is a powerful technique that involves closely spaced electrodes having opposing potentials<sup>20, 64-70</sup> and diffusional shuttling of molecules between them. Redox cycling utilizes at least two closely spaced electrodes whose potentials are controlled independently of each other. One is held at a "generating" potential and the other at an opposite "collecting"

potential, where electrical currents are measured independently at each. The current magnitude is associated with the slope of the concentration gradient (arrival rate) of the electroactive species reaching that electrode. The potential at which the electrode is poised can also help identify what electroactive species are present. Because regeneration of the starting species can occur at the nearby collector electrode upon arrival of the generated species, redox cycling provides the advantage of signal amplification at the generator. The amplification improves with diminishing gaps because steeper concentration gradients are achieved.

Extensive dimensional and diffusional studies in a multitude of chemical environments have been performed by redox cycling, such as those by Niwa and co-workers<sup>71-73</sup>, Amatore and co-workers<sup>65, 74-78</sup>, Fritsch and co-workers<sup>67, 79</sup>, and Aoki and co-workers<sup>71, 80</sup>. In redox cycling, there is control over where, when and at what potential electroactive species can be generated and collected. A major advantage of redox cycling is its ability to provide insight into the mechanisms and kinetics of following reactions that occur while generated and regenerated species diffuse between collector and generator electrodes, respectively. Likewise, the selective detection of one electrochemically active species over another based on their relative electron transfer rates is also possible.

Strategic application of different potentials and different potential waveforms at the generators and collectors can contribute to the extent of specificity that is not possible at a single electrode. For example, the potential at the generator can be swept slowly across a range while the collector is held at a fixed value at which only certain generated products that arrive at the collector are active. In a different scenario, the potential at both the generator and collector can be held constant (as is done through chronoamperometry, CA) to follow temporal events more precisely in the surrounding environment. The temporal resolution of this method is limited by

the transit times between the two sets of electrodes, which in turn makes it a factor of the gap. A large advantage of a slow sweep and a constant potential over the fast sweep in FSCV is that charging current at the generator is either much lower (depending on the sampling time) or eliminated at the collector, respectively.<sup>81, 82</sup> This minimizes the need for subtraction of background current, therefore making it a more suitable method to measure both transient release of chemical species and basal variations.<sup>67</sup> In the case of varying basal levels of catecholamines, gradual changes in solution composition that also change charging current makes precise background subtraction difficult without subtracting out the faradaic signal, too.<sup>58</sup> CA has been used *in vivo* at single carbon fiber electrodes, as well, but it suffers from low sensitivity due to the shallow concentration gradients from diffusional depletion at long times, unlike redox cycling that refreshes the species at the nearby electrodes.<sup>81</sup>

In an ECC' mechanism (Fig. 2), catecholamines undergo a two-electron oxidation (E) to yield o-quinone.<sup>19</sup> The o-quinone form can then go through an internal cyclization reaction (C) to yield the leucoaminochrome. The leucoaminochrome and o-quinone forms can react with each other (C') to yield the original catecholamine and the aminochrome form. The internal cyclization reaction that is involved in the C part of the mechanism occurs at different rates for the different catecholamines. The apparent rate constants at pH=7.4 in phosphate buffer have been reported to be  $0.13 \pm 0.05 \text{ s}^{-1}$ ,  $0.98 \pm 0.52 \text{ s}^{-1}$  and  $87 \pm 10 \text{ s}^{-1}$  for DA, NE and EP, respectively.<sup>28</sup> Due to the difference in these rate constants, the species can be distinguished by spatial distribution based on the survival of the o-quinone from the following chemistry. Step C in the mechanism can also affect the number of times the species can go back and forth between two oppositely polarized electrodes and therefore the amplification of the signal, depending on the species.

## 1.2 Considerations for a neural probe

A neural probe is a device that can be inserted into a nervous system tissue (the spine, nerves, and the brain) and make measurements or deliver chemicals.<sup>83</sup> Due to sensitivity of these tissues with regards to tissue damage, their size has always been a major consideration.<sup>83</sup> Microdialysis probes used for sampling the extracellular fluid and carbon fiber microelectrodes used for FSCV experiments have been studied extensively with regards to their tissue damage and the immune response caused by these devices.<sup>51, 84, 85</sup> Microfabricated devices however are more recent and only a few probes have been reported with suitable dimensions for *in vivo* redox cycling neural measurements.<sup>86, 87</sup> These probes are fabricated on silicon nitride and their microfabrication processes (specially the patterning of the substrate and insulation layer) is reported to be difficult and irreproducible. In addition, silicon nitride is a brittle substance and the concern with breakage during insertion and the tissue damage caused by the mechanical mismatch between the tissue and the device prevent these devices to be implanted in the live brain for more than a few hours.<sup>88</sup> Due to these concerns probes on polymeric substrates have gained popularity over the years.<sup>89-93</sup> The four most common polymers used for these probes include polyimide, parylene, BCB and SU-8.<sup>89-93</sup> Of these polymers, the first three require mechanical reinforcement to be able to penetrate the tissue. This mechanical reinforcement can come in the form of a dissolvable coating (e.g. maltose)<sup>94</sup> whose impact on the chemical composition of the surroundings is unknown. SU-8 is a photo-patternable negative resist (Fig. 3) that polymerizes under UV light (350 nm). SU-8 shows minimal biotoxicity and is considered biocompatible for neural recordings.<sup>90, 95, 96</sup> It also shows suitable chemical and mechanical properties for *in vivo* measurements and its high resistivity ( $1.8 \times 10^{17} \Omega$ ) makes it a great candidate for a non-conductive substrate on which the electrodes can be patterned. In chapter

two of this dissertation, a detailed discussion on probe dimensions and choice of material is presented.

### **1.3 Overview of the Studies Described in this Dissertation**

The main objective of this project is to construct an electrode-array with individually addressable electrodes on a probe intended for *in vivo* measurements and to characterize the probe's performance *in vitro* for measuring dopamine at low concentrations using redox cycling. To achieve this goal, conventional microfabrication techniques in combination with laser micromachining were utilized to fabricate the novel, miniaturized device with suitable dimensions and robustness for *in vivo* measurements inside a rat's brain. Fabrication of a device with such small dimensions and shaping it into the needle was a major hurdle for this project and it hindered the progress towards detection of dopamine *in vivo*. Electrochemical studies were performed on the device (whether laser micromachined into the needle-like shape or cut in the shape of a rectangular chip) to characterize the probe using model compounds, followed by *in vitro* detection of dopamine. Each chapter in this dissertation is written in a manuscript format.

Chapter 2 discusses the design and fabrication of the SU-8 probe and its characterization along with proof-of-concept dopamine detection. Details of microfabrication process and laser micromachining are discussed in this chapter. The electrodes are individually characterized and compared to expected performance based on theory and other relevant reports in the literature. The redox cycling method is evaluated by values such as amplification factor and collection efficiency; these values along with detection limits are reported for the model compound and dopamine. Chapter 2S, provides supplemental information for chapter 2.

Chapter 3 focuses on electrochemical detection of dopamine and its behavior during redox cycling. The device used for this chapter has the same electrode design as in Chapter 2,



however the lifted SU-8 substrate is in the form of a chip and not laser micromachined into the needle-shaped probe. Electrochemical responses to model compounds and dopamine are compared with theory. A detailed discussion about the quality of the insulation layer and how that may influence the electrochemical response is provided. A section of this chapter also discusses future designs and optimization for the electrode geometry. Chapter 3S, provides supplemental information for chapter 3.

Chapter 4 provides a conclusion for the work and proposes future work to achieve the goals for this project. This chapter discusses possible future design considerations, microfabrication approaches and prospects and challenges of *in vivo* analysis using the probe developed for this dissertation.

## 1.4 Figures

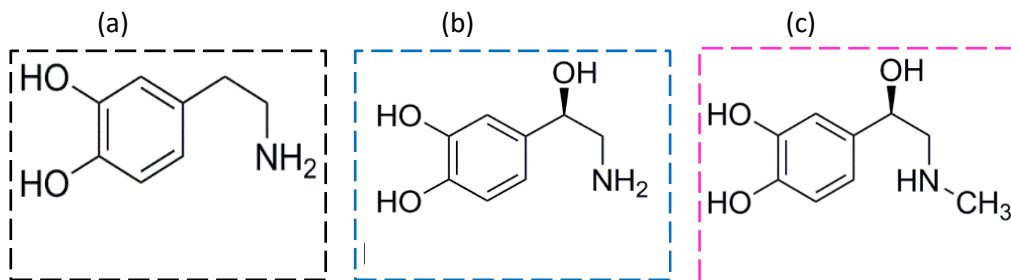


**Fig. 1** Chemical structures of (a) dopamine, (b) norepinephrine and (c) epinephrine

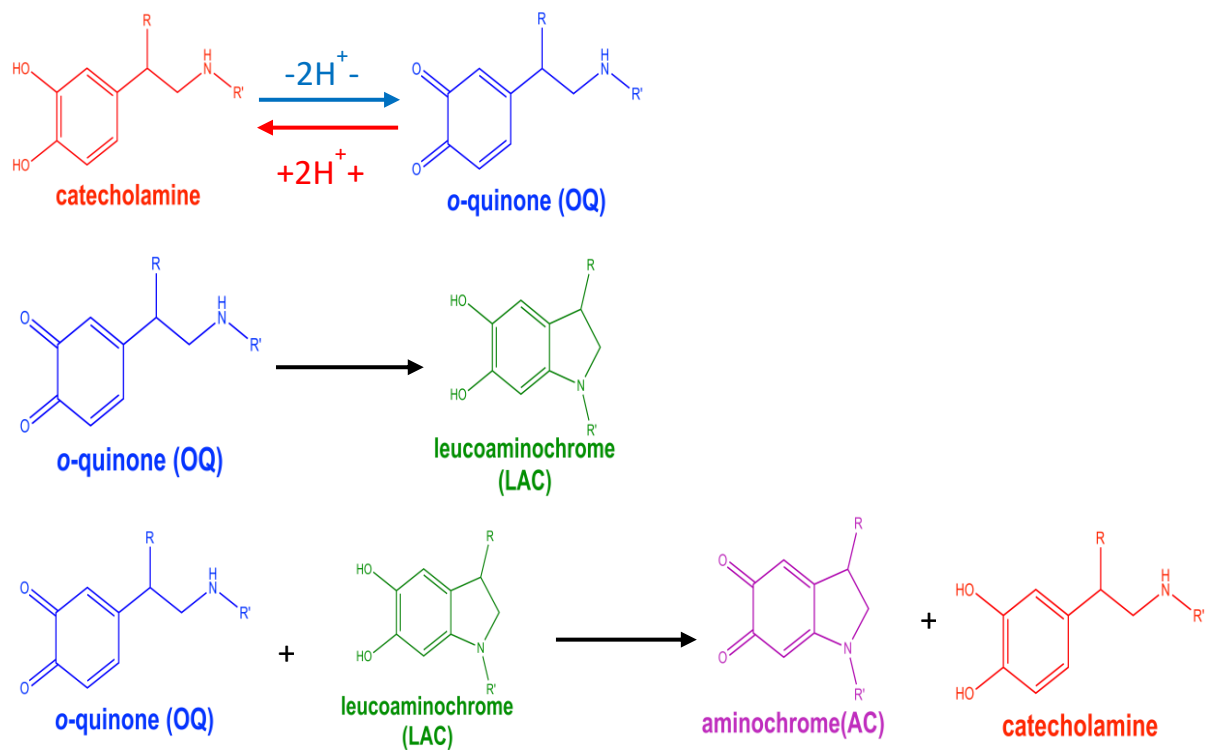


**Fig 2.** Electrochemical oxidation reaction of catecholamines and their following chemistry

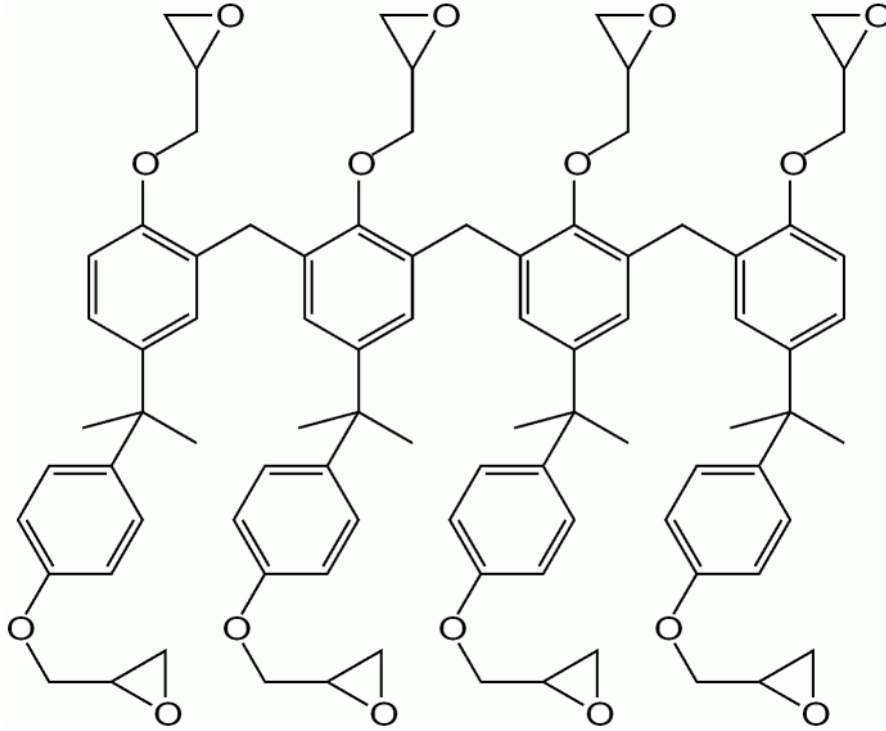


**Fig. 3** Chemical structure of polymerized SU-8

## 1.5 References

1. Kandel, E. R.; Schwartz, J. H.; Jessell, T. M.; Siegelbaum, S.; Hudspeth, A. J.; Mack, S., *Principles of neural science*. McGraw-hill New York: 2000; Vol. 4.
2. Robinson, D. L.; Venton, B. J.; Heien, M.; Wightman, R. M., Detecting subsecond dopamine release with fast-scan cyclic voltammetry in vivo. *Clinical Chemistry* **2003**, *49* (10), 10.
3. Jaquins-Gerstl, A.; Michael, A. C., A review of the effects of FSCV and microdialysis measurements on dopamine release in the surrounding tissue. *Analyst* **2015**, *140*, 3696-3708.
4. Wightman, R. M.; May, L. J.; Michael, A. C., Detection of dopamine dynamics in the brain. *Analytical chemistry* **1988**, *60* (13), 769A-793A.
5. De Bundel, D.; Sarre, S.; Van Eeckhaut, A.; Smolders, I.; Michotte, Y., Critical Evaluation of Acetylcholine Determination in Rat Brain Microdialysates using Ion-Pair Liquid Chromatography with Amperometric Detection. *Sensors (Basel, Switzerland)* **2008**, *8* (8), 5171-5185.
6. Tsai, H.-c.; Doong, R.-a., Simultaneous determination of pH, urea, acetylcholine and heavy metals using array-based enzymatic optical biosensor. *Biosensors and Bioelectronics* **2005**, *20* (9), 1796-1804.
7. Shimomura, T.; Itoh, T.; Sumiya, T.; Mizukami, F.; Ono, M., Amperometric biosensor based on enzymes immobilized in hybrid mesoporous membranes for the determination of acetylcholine. *Enzyme and Microbial Technology* **2009**, *45* (6-7), 443-448.
8. M., T., Recent advances in methods for the analysis of catecholamines and their metabolites. *Analytical and Bioanalytical Chemistry* **2006**, *386*, 506-514.
9. Wightman R. M., M. L. J., Michael A. C., Detection of dopamine dynamics in the brain. *Analytical Chemistry* **1988**, *60* (13), 769A-779A.
10. Koob, G. F., Addiction is a Reward Deficit and Stress Surfeit Disorder. *Frontiers in Psychiatry* **2013**, *4*, 72.
11. Fix, J. D., *Neuroanatomy*. Wolters Kluwer/Lippincott Williams & Wilkins: Philadelphia, 2008.

12. Vazey, E.; Aston-Jones, G., The emerging role of norepinephrine in cognitive dysfunctions of Parkinson's disease. *Frontiers in Behavioral Neuroscience* **2012**, *6*, 48.
13. Turk, A. Z.; Lotfi Marchoubeh, M.; Fritsch, I.; Maguire, G. A.; SheikhBahaei, S., Dopamine, vocalization, and astrocytes. *Brain and Language* **2021**, *219*, 104970.
14. Cepeda, C.; Murphy, K. P. S.; Parent, M.; Levine, M. S., The role of dopamine in Huntington's disease. *Prog Brain Res* **2014**, *211*, 235-254.
15. D., F. J., *Neurotransmitters and pathways*. In *Neuroanatomy*. 4th ed.; Lippincott Williams & Wilkins: Philadelphia: 2008.
16. Bear, M. F.; Connors, B. W.; Paradiso, M. A., *Neuroscience : exploring the brain*. 3rd ed.; Lippincott Williams & Wilkins: PA, 2007.
17. Kjaer, M.; Christensen, N. J.; Sonne, B.; Richter, E. A.; Galbo, H., Effect of exercise on epinephrine turnover in trained and untrained male subjects. *Journal of Applied Physiology* **1985**, *59* (4), 1061-1067.
18. Adams, R. N.; Marsden, C. A., Electrochemical detection methods for monoamine measurements in vitro and in vivo. In *Handbook of psychopharmacology*, Springer: 1982; pp 1-74.
19. Ciolkowski, E. L.; Maness, K. M.; Cahill, P. S.; Wightman, R. M.; Evans, D. H.; Fosset, B.; Amatore, C., Disproportionation during electrooxidation of catecholamines at carbon-fiber microelectrodes *Analytical Chemistry* **1994**, *66* (21), 3611-3617.
20. Aggarwal, A.; Hu, M.; Fritsch, I., Detection of dopamine in the presence of excess ascorbic acid at physiological concentrations through redox cycling at an unmodified microelectrode array. *Analytical and bioanalytical chemistry* **2013**, *405*.
21. Greco, S.; Danysz, W.; Zivkovic, A.; Gross, R.; Stark, H., Microdialysate analysis of monoamine neurotransmitters—A versatile and sensitive LC–MS/MS method. *Analytica Chimica Acta* **2013**, *771*, 65-72.
22. Cooper, B. R.; Mark Wightman, R.; Jorgenson, J. W., Quantitation of epinephrine and norepinephrine secretion from individual adrenal medullary cells by microcolumn high-performance liquid chromatography. *Journal of Chromatography B: Biomedical Sciences and Applications* **1994**, *653* (1), 25-34.

23. Nakatsuka, N.; Andrews, A. M., Differentiating Siblings: The Case of Dopamine and Norepinephrine. *ACS Chemical Neuroscience* **2017**, *8* (2), 218-220.
24. Stamford, J. A.; Kruk, Z. L.; Millar, J., Regional differences in extracellular ascorbic acid levels in the rat brain determined by high speed cyclic voltammetry. *Brain research* **1984**, *299* (2), 289-295.
25. Moretti, M.; Fraga, D. B.; Rodrigues, A. L. S., Ascorbic Acid to Manage Psychiatric Disorders. *CNS Drugs* **2017**, *31* (7), 571-583.
26. Harrison, F. E.; May, J. M., Vitamin C function in the brain: vital role of the ascorbate transporter SVCT2. *Free Radical Biology and Medicine* **2009**, *46* (6), 719-30.
27. Lane, R. F.; Hubbard, A. T., Differential double pulse voltammetry at chemically modified platinum electrodes for in vivo determination of catechol amines. *Analytical Chemistry* **1976**, *48* (9), 1287-1293.
28. Hawley, M. D.; Tatawawadi, S. V.; Piekarski, S.; Adams, R. N., Electrochemical Studies of the Oxidation Pathways of Catecholamines. *Journal of the American Chemical Society* **1967**, *89* (2), 447-450.
29. Salimi, A.; Abdi, K.; Khayatian, G.-R., Amperometric detection of dopamine in the presence of ascorbic acid using a nafion coated glassy carbon electrode modified with catechin hydrate as a natural antioxidant. *Microchimica Acta* **2004**, *144* (1-3), 161-169.
30. Shahrokhian, S.; Zare-Mehrjardi, H. R., Application of thionine-nafion supported on multi-walled carbon nanotube for preparation of a modified electrode in simultaneous voltammetric detection of dopamine and ascorbic acid. *Electrochimica acta* **2007**, *52* (22), 6310-6317.
31. Ensafi, A. A.; Taei, M.; Khayamian, T.; Arabzadeh, A., Highly selective determination of ascorbic acid, dopamine, and uric acid by differential pulse voltammetry using poly (sulfonazo III) modified glassy carbon electrode. *Sensors and Actuators B: Chemical* **2010**, *147* (1), 213-221.
32. Ribeiro, J. A.; Fernandes, P. M. V.; Pereira, C. M.; Silva, F., Electrochemical sensors and biosensors for determination of catecholamine neurotransmitters: A review. *Talanta* **2016**, *160*, 653-679.



33. Nagles, E.; Ibarra, L.; Llanos, J. P.; Hurtado, J.; García-Beltrán, O., Development of a novel electrochemical sensor based on cobalt (II) complex useful in the detection of dopamine in presence of ascorbic acid and uric acid. *Journal of Electroanalytical Chemistry* **2017**, *788*, 38-43.
34. Robinson, D. L.; Hermans, A.; Seipel, A. T.; Wightman, R. M., Monitoring rapid chemical communication in the brain. *Chemical Reviews* **2008**, *108* (7), 2554-2584.
35. Roy, P. R.; Saha, M. S.; Okajima, T.; Park, S. G.; Fujishima, A.; Ohsaka, T., Selective detection of dopamine and its metabolite, DOPAC, in the presence of ascorbic acid using diamond electrode modified by the polymer film. *Electroanalysis: An International Journal Devoted to Fundamental and Practical Aspects of Electroanalysis* **2004**, *16* (21), 1777-1784.
36. Carreau A., E. H.-R. B., Matejuk A., Grillon ., Kieda C., Why is the partial oxygen pressure of human tissues a crucial parameter? Small molecules and hypoxia *Journal of Cellular and Molecular Medicine* **2011**, *15* (6).
37. Aggarwal, A.; Hu, M.; Fritsch, I., Detection of dopamine in the presence of excess ascorbic acid at physiological concentrations through redox cycling at an unmodified microelectrode array. *Analytical and Bioanalytical Chemistry* **2013**, *405* (11), 3859-3869.
38. Borland, L. M.; Shi, G.; Yang, H.; Michael, A. C., Voltammetric study of extracellular dopamine near microdialysis probes acutely implanted in the striatum of the anesthetized rat. *Journal of neuroscience methods* **2005**, *146* (2), 149-158.
39. Gu, H.; Varner, E. L.; Groskreutz, S. R.; Michael, A. C.; Weber, S. G., In vivo monitoring of dopamine by microdialysis with 1 min temporal resolution using online capillary liquid chromatography with electrochemical detection. *Analytical chemistry* **2015**, *87* (12), 6088-6094.
40. Jaquins-Gerstl, A.; Michael, A. C., Comparison of the brain penetration injury associated with microdialysis and voltammetry. *Journal of neuroscience methods* **2009**, *183* (2), 127-135.
41. Luijten, M.; Veltman, D. J.; Hester, R.; Smits, M.; Nijs, I. M. T.; Peppinkhuizen, L.; Franken, I. H. A., The role of dopamine in inhibitory control in smokers and non-smokers: A pharmacological fMRI study. *European Neuropsychopharmacology* **2013**, *23* (10), 1247-1256.
42. Pavese, N.; Evans, A. H.; Tai, Y. F.; Hotton, G.; Brooks, D. J.; Lees, A. J.; Piccini, P., Clinical correlates of levodopa-induced dopamine release in Parkinson disease. *Neurology* **2006**, *67* (9), 1612.

43. Zestos, A. G.; Kennedy, R. T., Microdialysis Coupled with LC-MS/MS for In Vivo Neurochemical Monitoring. *The AAPS Journal* **2017**, *19* (5), 1284-1293.
44. Watson, C. J.; Venton, B. J.; Kennedy, R. T., In vivo measurements of neurotransmitters by microdialysis sampling. *Analytical Chemistry* **2006**, *78* (5).
45. Schlitz, K. N.; Kennedy, R. T., Time-Resolved Microdialysis for In Vivo Neurochemical Measurements and Other Applications. *Annual Review of Analytical Chemistry* **2008**, *1*, 627-661.
46. Paul, D.; Stenken, J., A review of flux considerations for in vivo neurochemical measurements. *Analyst* **2015**, *140*.
47. Darvesh, A. S.; Carroll, R. T.; Geldenhuys, W. J.; Gudelsky, G. A.; Klein, J.; Meshul, C. K.; Van der Schyf, C. J., In vivo brain microdialysis: advances in neuropsychopharmacology and drug discovery. *Expert Opinion on Drug Discovery* **2011**, *6* (2), 109-127.
48. Zhang, M. Y.; Beyer, C. E., Measurement of neurotransmitters from extracellular fluid in brain by in vivo microdialysis and chromatography-mass spectrometry. *Journal of Pharmaceutical and Biomedical Analysis* **2006**, *40* (3), 492-499.
49. Michael, A. C.; Borland, L., *Electrochemical methods for neuroscience*. CRC press: 2006.
50. Sun, L.; Stenken, J. A.; Brunner, J. E.; Michel, K. B.; Adelsberger, J. K.; Yang, A. Y.; Zhao, J. J.; Musson, D. G., An in vivo microdialysis coupled with liquid chromatography/tandem mass spectrometry study of cortisol metabolism in monkey adipose tissue. *Analytical Biochemistry* **2008**, *381* (2), 214-223.
51. Nesbitt, K. M.; Jaquins-Gerstl, A.; Skoda, E. M.; Wipf, P.; Michael, A. C., Pharmacological mitigation of tissue damage during brain microdialysis. *Analytical chemistry* **2013**, *85* (17), 8173-8179.
52. Lada, M. W.; Vickroy, T. W.; Kennedy, R. T., High Temporal Resolution Monitoring of Glutamate and Aspartate in Vivo Using Microdialysis On-Line with Capillary Electrophoresis with Laser-Induced Fluorescence Detection. *Analytical Chemistry* **1997**, *69* (22), 4560-4565.
53. Ngernsutivorakul, T.; Steyer, D. J.; Valenta, A. C.; Kennedy, R. T., In Vivo Chemical Monitoring at High Spatiotemporal Resolution Using Microfabricated Sampling Probes and

Droplet-Based Microfluidics Coupled to Mass Spectrometry. *Analytical Chemistry* **2018**, *90* (18), 10943-10950.

54. Jackowska, K.; Krysinski, P., New trends in the electrochemical sensing of dopamine. *Analytical and Bioanalytical Chemistry* **2013**, *405* (11), 3753-3771.

55. Garris P.A., K. M., Bunin M.A., Michael D., Walker Q.D., Wightman R.M., Dissociation of dopamine release in the nucleus accumbens from intracranial self-stimulation. *Nature* **1999**, *398* (6722), 67-69.

56. Cahill P.S., W. Q. D., Finnegan J.M., Mickelson G.E., Travis E.R., Wightman R.M., Microelectrodes for the measurement of catecholamines in biological systems. *Analytical Chemistry* **1996**, *68* (18), 3180-3186.

57. Yavich L. , T. J., In vivo voltammetry with removable carbon fibre electrodes in freely-moving mice: dopamine release during intracranial self-stimulation. *Journal of Neuroscience Methods* **2000**, *104* (1), 55-63.

58. Venton, B. J.; Cao, Q., Fundamentals of fast-scan cyclic voltammetry for dopamine detection. *Analyst* **2020**, *145* (4), 1158-1168.

59. Hu, M.; Fritsch, I., Application of Electrochemical Redox Cycling: Toward Differentiation of Dopamine and Norepinephrine. *Analytical Chemistry* **2016**.

60. Clapp-Lilly, K. L.; Roberts, R. C.; Duffy, L. K.; Irons, K. P.; Hu, Y.; Drew, K. L., An ultrastructural analysis of tissue surrounding a microdialysis probe. *Journal of Neuroscience Methods* **1999**, *90* (2), 129-142.

61. Heien, M. L. A. V.; Johnson, M. A.; Wightman, R. M., Resolving neurotransmitters detected by fast-scan cyclic voltammetry. *Analytical chemistry* **2004**, *76* (19), 5697-5704.

62. Park, J.; Wheeler, R. A.; Fontillas, K.; Keithley, R. B.; Carelli, R. M.; Wightman, R. M., Catecholamines in the bed nucleus of the stria terminalis reciprocally respond to reward and aversion. *Biological psychiatry* **2012**, *71* (4), 327-334.

63. Adams, R. N., Probing brain chemistry with electroanalytical techniques. *Analytical Chemistry* **1976**, *48* (14), 1126A-1138A.

64. He, D.; Yan, J.; Zhu, F.; Zhou, Y.; Mao, B.; Oleinick, A.; Svir, I.; Amatore, C., Enhancing the Bipolar Redox Cycling Efficiency of Plane-Recessed Microelectrode Arrays by Adding a Chemically Irreversible Interferent. *Anal. Chem. (Washington, DC, U. S.)* **2016**, *88* (17), 8535-8541.
65. Oleinick, A.; Yan, J.; Mao, B.; Svir, I.; Amatore, C., Theory of Microwell Arrays Performing as Generators-Collectors Based on a Single Bipolar Plane Electrode. *ChemElectroChem* **2016**, *3* (3), 487-494.
66. Alayo, N.; Fernández-Sánchez, C.; Baldi, A.; Esquivel, J. P.; Borrisé, X.; Pérez-Murano, F., Gold interdigitated nanoelectrodes as a sensitive analytical tool for selective detection of electroactive species via redox cycling. *Microchimica Acta* **2016**, *183* (5), 1633-1639.
67. Hu, M.; Fritsch, I., Redox cycling behavior of individual and binary mixtures of catecholamines at gold microband electrode arrays. *Analytical Chemistry* **2015**, *87* (4), 2029-2032.
68. Oleinick, A.; Zhu, F.; Yan, J.; Mao, B.; Svir, I.; Amatore, C., Theoretical Investigation of Generator-Collector Microwell Arrays for Improving Electroanalytical Selectivity: Application to Selective Dopamine Detection in the Presence of Ascorbic Acid. *ChemPhysChem* **2013**, *14* (9), 1887-1898.
69. Straver, M. G.; Odijk, M.; Olthuis, W.; van den Berg, A., A simple method to fabricate electrochemical sensor systems with predictable high-redox cycling amplification. *Lab on a Chip* **2012**, *12* (8), 1548-1553.
70. Aggarwal, A. Studies Toward the Development of a Microelectrode Array for Detection of Dopamine through Redox Cycling. Dissertation, University of Arkansas, 2011.
71. Aoki, K.; Morita, M.; Niwa, O.; Tabei, H., Quantitative analysis of reversible diffusion-controlled currents of redox soluble species at interdigitated array electrodes under steady-state conditions. *Journal of electroanalytical chemistry and interfacial electrochemistry* **1988**, *256* (2), 269-282.
72. Hayashi K., I. Y., Kuriata R., Sunagawa K, Niwa O., Tate A., The highly sensitive detection of catecholamines using a microfluidic device integrated with an enzyme-modified pre-reactor for intererent elimination and interdigitated array electrode. *Journal of Electroanalytical Chemistry* **2005**, *579*, 215-222.

73. Niwa, O.; Morita, M.; Tabei, H., Highly sensitive and selective voltammetric detection of dopamine with vertically separated interdigitated array electrodes. *Electroanalysis* **1991**, 3 (3), 163-168.
74. Zhu, F.; Yan, J.; Pang, S.; Zhou, Y.; Mao, B.; Oleinick, A.; Svir, I.; Amatore, C., Strategy for increasing the electrode density of microelectrode arrays by utilizing bipolar behavior of a metallic film. *Anal. Chem. (Washington, DC, U. S.)* **2014**, 86 (6), 3138-3145.
75. Amatore, C.; Da Mota, N.; Lemmer, C.; Pebay, C.; Sella, C.; Thouin, L., Theory and Experiments of Transport at Channel Microband Electrodes under Laminar Flows. 2. Electrochemical Regimes at Double Microband Assemblies under Steady State. *Anal. Chem. (Washington, DC, U. S.)* **2008**, 80 (24), 9483-9490.
76. Amatore, C.; Sella, C.; Thouin, L., Electrochemical time-of-flight responses at double-band generator-collector devices under pulsed conditions. *J. Electroanal. Chem.* **2006**, 593 (1-2), 194-202.
77. Amatore, C.; Pebay, C.; Servant, L.; Sojic, N.; Szunerits, S.; Thouin, L., Mapping electrochemiluminescence as generated at double-band microelectrodes by confocal microscopy under steady state. *ChemPhysChem* **2006**, 7 (6), 1322-1327.
78. Amatore, C.; Belotti, M.; Chen, Y.; Roy, E.; Sella, C.; Thouin, L., Using electrochemical coupling between parallel microbands for in situ monitoring of flow rates in microfluidic channels. *J. Electroanal. Chem.* **2004**, 573 (2), 333-343.
79. Vandaveer, W. R.; Woodward, D. J.; Fritsch, I., Redox cycling measurements of a model compound and dopamine in ultrasmall volumes with a self-contained microcavity device. *Electrochimica Acta* **2003**, 48 (20), 3341-3348.
80. Aoki, K., analysis of reversible diffusion-controlled currents of redox soluble species at interdigitated arrays electrodes under steady state conditions. *J. Electroanal. Chem.* **1988**, 256, 269-282.
81. Roberts, J. G.; Sombers, L. A., Fast-Scan Cyclic Voltammetry: Chemical Sensing in the Brain and Beyond. *Analytical Chemistry* **2018**, 90 (1), 490-504.
82. Rodeberg, N. T.; Sandberg, S. G.; Johnson, J. A.; Phillips, P. E. M.; Wightman, R. M., Hitchhiker's Guide to Voltammetry: Acute and Chronic Electrodes for in Vivo Fast-Scan Cyclic Voltammetry. *ACS Chemical Neuroscience* **2017**, 8 (2), 221-234.

83. HajjHassan, M.; Chodavarapu, V.; Musallam, S., NeuroMEMS: Neural Probe Microtechnologies. *Sensors (Basel, Switzerland)* **2008**, *8* (10), 6704-6726.
84. Stenken, J. A.; Church, M. K.; Gill, C. A.; Clough, G. F., How minimally invasive is microdialysis sampling? A cautionary note for cytokine collection in human skin and other clinical studies. *The AAPS journal* **2010**, *12* (1), 73-78.
85. Jaquins-Gerstl, A.; Michael, A. C., A review of the effects of FSCV and microdialysis measurements on dopamine release in the surrounding tissue. *Analyst (Cambridge, U. K.)* **2015**, *140* (11), 3696-3708.
86. Xi, Y. Interdigitated array electrode microprobe: Design, fabrication and characterization. University of Arkansas, 2005.
87. Dengler, A. K.; McCarty, G. S., Microfabricated Microelectrode Sensor for Measuring Background and Slowly Changing Dopamine Concentrations. *Journal of electroanalytical chemistry (Lausanne, Switzerland)* **2013**, *693*, 28-33.
88. Chen, C.-H.; Chuang, S.-C.; Su, H.-C.; Hsu, W.-L.; Yew, T.-R.; Chang, Y.-C.; Yeh, S.-R.; Yao, D.-J., A three-dimensional flexible microprobe array for neural recording assembled through electrostatic actuation. *Lab on a Chip* **2011**, *11* (9), 1647-1655.
89. Pang, C.; Cham, J.; Nenadic, Z.; Musallam, S.; Tai, Y.-C.; Burdick, J.; Andersen, R., A new multi-site probe array with monolithically integrated parylene flexible cable for neural prostheses. *Conf Proc IEEE Eng Med Biol Soc* **2005**, *7*, 7114-7.
90. Nemani, K. V.; Moodie, K. L.; Brennick, J. B.; Su, A.; Gimi, B., In vitro and in vivo evaluation of SU-8 biocompatibility. *Materials Science and Engineering: C* **2013**, *33* (7), 4453-4459.
91. Kim, E. G. R.; John, J. K.; Tu, H.; Zheng, Q.; Loeb, J.; Zhang, J.; Xu, Y., A hybrid silicon-parylene neural probe with locally flexible regions. *Sensors and Actuators B: Chemical* **2014**, *195*, 416-422.
92. Lotfi Marchoubeh, M.; Cobb, S. J.; Tello, M. A.; Hu, M.; Jaquins-Gerstl, A.; Robbins, E. M.; Macpherson, J. V.; Michael, A. C.; Fritsch, I., Miniaturized probe on polymer SU-8 with array of individually addressable microelectrodes for electrochemical analysis in neural and other biological tissues. *Analytical and Bioanalytical Chemistry* **2021**, 1-15.

93. Keekeun Lee, J. H., Ryan Clement, Biocompatible benzocyclobutene (BCB)-based neural implants with micro-fluidic channel. *Biosensors and bioelectronics* **2004**, *20*, 404-407.
94. Zhuolin Xiang, S.-C. Y., Ning Xue, Tao Sun, Ultra-thin flexible polyimide neural probe embedded in dissolvable maltose-coated microneedle. *J. Micromech Microeng.* **2014**, *24*, 11-20.
95. Huang, S.-H.; Lin, S.-P.; Chen, J.-J. J., In vitro and in vivo characterization of SU-8 flexible neuroprobe: From mechanical properties to electrophysiological recording. *Sensors and Actuators A: Physical* **2014**, *216*, 257-265.
96. Krishnamurthy, N.; Moodie, K.; B Brennick, J.; Su, A.; Gimi, B., *In vitro and in vivo evaluation of SU-8 biocompatibility*. 2013; Vol. 33, p 4453-9.

## **2. Miniaturized Probe on Polymer SU-8 with Array of Individually Addressable**

### **Microelectrodes for Electrochemical Analysis in Neural and other Biological Tissues**

Mahsa Lotfi Marchoubeh, Samuel J. Cobb, Miguel Abrego Tello, Mengjia Hu, Andrea Jaquins-Gerstl, Elaine M. Robins, Julie V. McPherson, Adrian C. Michael, Ingrid Fritsch



This chapter is reformatted from a letter submitted to *Analytical Bioanalytical Chemistry*

## 2.1 Abstract

An SU-8 probe with an array of nine, individually addressable gold microband electrodes (100  $\mu\text{m}$  long, 4  $\mu\text{m}$  wide, separated by 4  $\mu\text{m}$  gaps) was photolithographically fabricated and characterized for detection of low concentrations of chemicals in confined spaces and *in vivo* studies of biological tissues. The probe's shank (6 mm long, 100  $\mu\text{m}$  wide, 100  $\mu\text{m}$  thick) is flexible, but exhibits sufficient sharpness and rigidity to be inserted into soft tissue. Laser micromachining was used to define probe geometry into its shape through the SU-8 layers to access an underlying sacrificial aluminum layer that was etched to free the probes from a silicon wafer. Perfusion with fluorescent nanobeads showed that, like a carbon fiber electrode, the probe produced no noticeable damage when inserted into rat brain, in contrast to damage from an inserted microdialysis probe. The individual addressability of the electrodes allows single and multiple electrode activation. Redox cycling is possible, where adjacent electrodes serve as generators (that oxidize or reduce molecules) and collectors (that do the opposite) to amplify signals of small concentrations without background subtraction. Information about electrochemical mechanisms and kinetics may also be obtained. Detection limits for potassium ferricyanide in potassium chloride electrolyte of 2.19, 1.25 and 2.08  $\mu\text{M}$ , and for dopamine in artificial cerebral spinal fluid of 1.94, 1.08 and 5.66  $\mu\text{M}$  for generators alone and for generators and collectors during redox cycling, respectively, were obtained.

## 2.2 Introduction

Major technological advances have been made in the field of electrochemical sensors that are capable of detecting chemicals in confined spaces<sup>1,2</sup>. However, improving the design of probes so that they may be inserted into tissue and detect small amounts of biological molecules with minimal damage remains an area of need<sup>3</sup>. To address this, we have developed a semi-flexible probe with suitable dimensions that are designed specifically for detection of molecules *in vivo* and other small volume systems. The probe consists of an array of parallel, individually-addressable microband electrodes that are suitable for redox cycling (generation-collection) experiments where selective activation/deactivation is possible. Redox cycling is a powerful technique that involves diffusional shuttling of molecules between closely spaced electrodes having opposing potentials that oxidize and then re-reduce them<sup>4-7</sup>. Electrochemical signals amplify when the gaps between the electrodes narrow. When performed at steady state, where the potentials of the generators and collectors are held constant, the arrival of an analyte can be detected by redox cycling in real time without needing to subtract a charging current (unlike transient methods) while sustaining the amplified signal. In addition, the monitoring of the currents at the different electrodes, which can be affected by the fate of the molecules while in transit, can lead to quantifying the composition of a sample and a deeper understanding of the kinetics and mechanisms of the chemical system<sup>4,7,8</sup>.

A significant body of work involving needle-like probes for *in vivo* analysis focuses on interfacing to, stimulating and understanding brain function<sup>9</sup>. These probes involve different measurement modalities that contribute complementary information and have various specifications. This prior knowledge was drawn upon to design and construct the redox cycling probe described herein. That body of work also offers a context in which to compare the

performance of our probe. The sampling of extracellular fluid with microdialysis probes, for example, allows for extensive chemical analysis, although not in real time, and they can damage tissue while eliciting an immune response that eventually obscures sampling effectiveness<sup>10</sup>. Thus, narrower probes are desirable. Another modality involves wire-like electrodes, one to two orders of magnitude thinner than microdialysis probes, that record voltage pulses associated with real-time firing of neurons but do not acquire chemical information<sup>11</sup>. Direct measurement of chemical changes in real time is also possible at similarly-shaped, carbon fiber electrodes (4-50  $\mu\text{m}$  in diameter) and at microelectrodes patterned on substrates suitable for *in vivo* insertion<sup>12, 13</sup>, but with electrochemical methods like fast scan cyclic voltammetry (FSCV)<sup>14</sup>.

This latter approach targets small electroactive molecules, which are detected directly in response to timed stimuli<sup>15</sup>. Electrochemical sensing of other small molecules, often facilitated by enzymes and mediators, have also been reported, but have been deployed to a lesser extent on probes for tissue insertion<sup>16, 17</sup>. Although more challenging to fabricate, probes with multiple, individually-addressable electrodes offer several benefits. These include redundant sensing (in case of failure), spatial mapping, replicate analysis of a single analyte and simultaneous analysis of multiple analytes<sup>18-20</sup>.

To our knowledge, there are only two examples of a multi-electrode probe where the electrodes are close enough together for diffusion layers of adjacent sites to overlap on the time scale of the experiment so that redox cycling is possible<sup>12, 21</sup>. Redox cycling on a probe would be especially attractive in a dynamically changing biological system as an alternative to FSCV, where detection of basal levels of chemicals has been a major challenge<sup>14, 15</sup>. While there have been advances in basal dopamine detection at carbon fiber electrodes using fast scan controlled

adsorption voltammetry<sup>22</sup> and square wave voltammetry<sup>23</sup>, these techniques have much slower timescales than FSCV.

The multielectrode probes suitable for redox cycling have consisted of IDAs and fabricated by photolithography on silicon nitride, but elaborate substrate thinning and etching procedures were used to release them from the substrate<sup>12, 21</sup>. A dual electrode probe that avoids photolithography altogether, involves two, closely spaced carbon fibers<sup>24</sup> and is capable of combining FSCV with amplification because of the short transit time across a 180 nm nanogap. A limitation of IDAs and the electrode configurations is the fixed electrode number and width/gap geometry for a given device. To better understand the effect of diffusion and following chemistry in addition to the feasibility of differentiating between chemicals, individually addressable electrodes are desirable. This is because they offer unique spatio-temporal analysis capabilities. Activation of generator and collector electrodes at various separations from each other has allowed for differential detection of the three catecholamines from each other without fabricating a new device<sup>4, 25</sup>.

The choice of the substrate material is particularly important, not only for the application but also in determining the fabrication approach. Silicon-based and ceramic substrates have employed photolithographic techniques to fabricate relatively complex and advanced, multisite neural probes<sup>12, 13, 17, 26, 27</sup>. Despite their advantages, complications with tissue damage during and after insertion of brittle silicon shanks remain a concern. This is mainly due to the mechanical mismatch between the soft neural tissue and the stiff probe. The desire for less rigidity and hardness has led to introduction of polymeric substrates into microfabricated neural probe technology. Parylene<sup>28</sup>, polyimide<sup>29</sup> and SU-8<sup>30</sup> are the most common polymers used to fabricate implantable neural probes.

Of the different polymers investigated, SU-8 is believed to have optimal properties compared to parylene and polyimide. The major setback with these other two polymers is their lack of stiffness, and therefore they easily buckle during insertion into the brain<sup>29,31</sup>. In addition, polyimide has a relatively high moisture uptake (~4 wt%) which will ultimately lead to changes in the performance of the electrodes<sup>32</sup>. SU-8 has been shown to exhibit suitable flexibility to minimize tissue damage, and sufficient rigidity for insertion into the brain<sup>33</sup> without mechanical reinforcement. In addition, SU-8's biocompatibility, in terms of cell viability, hemolytic activity, effect of leachates, and histocompatibility has been studied and results suggest suitability for neural implants<sup>34</sup>. Therefore, SU-8 was chosen as a substrate for our probes. Also, photolithography was used in our work to pattern an array of individually-addressable, gold/chromium electrodes spaced apart by only a few micrometers (described further below) on the SU-8 substrate. However, to construct a suitable probe shape that is thin enough for minimal tissue damage can be extremely challenging using photolithography alone. Thus, an alternative approach to shape the substrate was employed here to resolve this complication.

Laser micromachining offers such an alternative route to fabricate complex geometries on the microscale in materials from diamond<sup>35</sup> to polymers that cannot be processed by photolithography<sup>36</sup>, or the workflow doesn't allow for it<sup>37</sup>, for instance, due to the chemicals or process used interacting adversely with another element of the device. This can streamline device fabrication as the material is cut in a single step as opposed to the several steps required for most photolithography processes, which are usually conducted in a cleanroom environment. Laser micromachining has been used to produce devices as diverse as microelectrodes<sup>37</sup>, electrochemical sensors<sup>35</sup>, fuel cells<sup>36</sup> and micro-electromechanical systems (MEMS). SU-8 has been processed using excimer laser micromachining to give features on the order of 100  $\mu\text{m}$ <sup>37</sup>,

and it has been shown that the process does not affect the material's cytotoxicity<sup>38</sup>, making it a viable technique for producing electrode arrays for biological applications. Furthermore, the technique is ideal for device prototyping in research environments as the design can be iterated without the time or expense of producing a new photomask. Consequently, laser micromachining was investigated as a means of defining our distinctive probe shape in SU8.

The work here presents the design and fabrication of a probe on SU-8 that can be easily lifted off a wafer after laser micromachining with a shape that provides ease of connectivity to an edge connector on one end and insertion into tissue on the other. The probe has nine individually addressable, co-planar, microband gold electrodes that were photolithographically fabricated near the tip and can be used to perform generation-collection experiments by strategic activation. Electrochemical characterization of each electrode was performed, and the redox cycling behavior of the electrodes was assessed with the model compound potassium ferricyanide in potassium chloride electrolyte and with dopamine in artificial cerebral spinal fluid and compared to theoretically expected responses. The suitability of the dimensions of the probe shank for insertion into rat brain and extent of tissue damage were also established in anticipation of future studies *in vivo*.

## **2.3 Materials and Methods**

### **2.3.1 Chemicals and Materials**

Unless otherwise stated, chemicals were reagent grade and used without further purification. Hexylmethyldisilazane (HMDS), acetone (ACS reagent,  $\geq 99.5\%$ ) and isopropyl alcohol (IPA,  $\geq 99.7\%$ ) were obtained from Sigma Aldrich. Water (ACS reagent grade, 18 M $\Omega$  cm or greater) was obtained from Ricca Chemical (Arlington, TX, USA). Dopamine hydrochloride, calcium chloride, sodium dihydrogen phosphate monohydrate, and 4-(2-

hydroxyethyl)-1-piperazineethanesulfonic acid (HEPES) (all ACS grade) were obtained from Alfa Aesar (Ward Hill, MA, USA). Magnesium sulfate, potassium ferricyanide (99.8% pure) and sodium chloride were obtained from EMD Chemicals (Gibbstown, NJ, USA). Sodium hydrogen carbonate was obtained from J.T. Baker (Phillipsburg, NJ, USA). Sodium sulfate was obtained from Aldrich Chemical (St. Louis, MO, USA). D(+)-glucose (anhydrous) and potassium chloride were obtained from BDH/VWR (Radnor, PA, USA). Carbon fiber microelectrodes were constructed from T650 fibers from Cytac LLC (Piedmont, SC, USA) in a borosilicate glass housing from A-M Systems (Sequim, WA, USA) sealed with Spurr Epoxy from Polysciences Inc. (Warrington, PA, USA) with a nichrome lead wire from Goodfellow (Oakdale, PA, USA). Components for artificial cerebrospinal fluid (aCSF, 142 mM NaCl, 1.2 mM CaCl<sub>2</sub>, 2.7 mM KCl, 1.0 mM MgCl<sub>2</sub>, 2.0 mM NaH<sub>2</sub>PO<sub>4</sub>, pH 7.4) and phosphate buffered saline (PBS, 137 mM NaCl, 2.7 mM KCl, 10 mM Na<sub>2</sub>HPO<sub>4</sub>, 1.8 mM KH<sub>2</sub>PO<sub>4</sub>) were purchased from Sigma-Aldrich. Concentric microdialysis probes (280 μm o.d., 4 mm long) were constructed with hollow fiber dialysis membrane (Spectra-Por RC Hollow Fiber, MWCO: 13,000, 160 μm i.d., Spectrum Laboratories, Inc., Rancho Dominguez, CA) and fused silica outlet lines (150 μm o.d., 75 μm i.d., Polymicro Technologies, Phoenix, AZ) as described elsewhere<sup>39</sup>. Perfusion solutions include 4% paraformaldehyde (electron Microscopy Sciences), in 0.1 M phosphate buffer pH 7.3 and a 0.1% solution of yellow-green fluorescent nanobeads as received (0.1 μm diameter, FluoSpheres® carboxylate-modified polystyrene microsphere suspensions (2% solids) in water plus 2 mM sodium azide, Molecular Probes, Inc., Eugene, OR) in PBS. Sucrose was obtained from Fisher (Fisher Scientific, Pittsburgh, PA).

Silicon (100) wafers (125 mm diameter, 650 μm thickness, 2 μm thermally grown silicon dioxide) used as the substrate material during probe fabrication, were purchased from Silicon



Quest International, Santa Clara, CA. Chromium adhesion and gold electrode layers were deposited on the silicon wafers using chromium coated tungsten rods (Kurt J. Lesker Company, Clairton, PA) and the small pieces of gold (99.99%) placed in a molybdenum boat (Kurt J. Lesker Company, Pittsburg, PA). Aluminum pellets (99.99%, from Alfa Aesar, Ward Hill, MA) in a molybdenum boat were used to deposit the sacrificial layer. The chromium mask was designed in house using AutoCAD<sup>®</sup> 2017 and manufactured by Advance Reproduction Corporation, North Andover, MA. The S1805 positive photoresist (Rohm and Haas Electronic Materials LLC, Marlborough, MA), AZ 300 MIF developer (AZ Electronic Materials, Somerville, gold etchant (Transene, GE8148) and chromium etchant (HTA Enterprise, CEP200) were used to pattern electrodes. SU-8 3050, SU-8 2000, adhesion promoter (Omniccoat), and SU-8 developer were obtained from MicroChem (Newton, MA).

### **2.3.2 Fabrication of the Electrodes**

The design of the electrodes, insulation layer and substrate shape are shown in Fig. 1. To pattern the electrodes and insulate them on the SU-8 probe, conventional photolithography was employed. The bare wafer was first rinsed thoroughly with a sequence of acetone, IPA, and water, and then dehydrated in a convection oven (Blue M Convection oven, Baker Furnace Inc., Brea, CA) at 200 °C for 20 min. Then, the silicon wafers were coated with an Al layer (~50 nm) by thermal evaporation (Edwards 306 Auto thermal evaporator, Edwards Electronics, Clinton, MA). This acted as a sacrificial layer that was dissolved to release the probes from the wafer in the last step. Omniccoat (MicroChem, Newton, MA) was used in an attempt to improve adhesion to the Al layer, but it caused SU-8 to lift off in an unexpected manner especially at baking and development steps. Hexamethyldisilazane (HMDS) did not improve adhesion, either. Therefore,

SU-8 was spin-coated (Eaton spin coater, Excel TeQ, Boston, MA) onto the aluminum-coated wafer directly and without an adhesion promoter.

The SU-8 layer (SU-8 3050) was spin coated onto the rinsed and dried Al-coated carrier wafer at 2500 rpm. It was observed that pouring SU-8 directly out of the bottle (versus dispensing it through a syringe) minimizes trapping of air bubbles. These bubbles make the surface of the SU-8 non-uniform and lead to imperfect contact of the chromium photomask with the wafer. Solvent was removed by pre-exposure baking on a hotplate at 95 °C. Use of a hotplate instead of an oven was critical at this stage. In an oven, a crust forms on the surface of the SU-8 layer due to heating from the outside, inward, which traps solvent inside and prevents it from evaporating. The manufacturer suggests ramping the temperature of the hotplate up and down. Without these ramps, the internal stress within the SU-8 film causes the SU-8 to exhibit a curl after the probe release step. However, there is a tradeoff between the ramps and the bake time. Long ramps mean increased time on the hotplate, which leads to SU-8 sheets that are not photo-definable. In the cases described below, the wafer was pre-baked with a 70 °C/h ramp from 65 to 95 °C. The wafer was held at 95 °C for 20 min and then the cool-down ramp was achieved by turning the hotplate off and letting the wafer cool to 55 °C, which took about 1 h.

For the thick SU-8, a ring of polymer with an increased height that forms around the rim of the wafer, called an edge bead, can prevent the mask from making sufficient contact with the wafer, and substantially deteriorate the spatial resolution of the transferred pattern. In the literature, there are multiple ways of addressing edge bead issues of photoresists. For this study, we removed them by creating an edge bead mask, where the blank mask was modified to be dark field around the edges of the wafer (Fig. 2(a)). Thus, when the rest of the SU-8 substrate layer was cross linked by exposure through this mask, the edge bead was unaffected and could be

dissolved away in the subsequent developer solution. The exposure under the edge bead mask was performed right after the pre-bake step with a dosage of  $300 \text{ mJ/cm}^2$  using a Karl Suss MA150 mask aligner (Suss Microtec, Garching, Germany). A short post developer bake was performed by moving the wafer from a  $45 \text{ }^\circ\text{C}$  hotplate to a  $65 \text{ }^\circ\text{C}$  hotplate (keeping the wafer on each hotplate for 1 min) to the  $95 \text{ }^\circ\text{C}$  hotplate for 5 min and then repeating the process in reverse order.

The postbaked wafer was strongly agitated in the SU-8 developer solution for 20 min to dissolve the edge beads. The wafer was subsequently rinsed with IPA and inspected. If the presence of white residue over the un-crosslinked areas was observed, further development was performed to remove this uncrosslinked SU-8. To dry the wafer, it was put in the spin coater and spun at 1000 rpm. Then, 50 mL of IPA were dispensed through the hole in the lid of the spin coater onto the spinning wafer, once the dispensing of IPA finished, the spinner was allowed to ramp down to zero rpm over 10 s. The wafers were placed in an oxygen plasma cleaner (Model: APE 110, LFE plasma systems, Clinton, MA) at 60 sccm oxygen flow, 60 W for 2 min. This step is recommended because it also roughens the surface of the SU-8 so that the adhesion of the subsequent metal layers is improved<sup>40</sup>. A Cr layer ( $\sim 8 \text{ nm}$ ) and Au layer ( $\sim 100 \text{ nm}$ ) were thermally evaporated onto the SU-8-coated substrate. Then, positive photoresist was spin coated at 3000 rpm for 30 s and baked on a hotplate at  $65 \text{ }^\circ\text{C}$  for 30 s. See Fig. 2(b).

The electrodes, leads and contact pads were then patterned into the resulting metal film using conventional photolithography methods. See Fig. 3(a)-3(c). In short, the positive resist was exposed through the electrode chrome mask at a  $70 \text{ mJ/cm}^2$  exposure rate (Fig. 3(a)). The wafer was developed for 45 s in the AZ-300 MIF solution and the metals were etched using their respective wet etchant solutions (15 s for gold and 5 s for Cr) (Fig 3(b)). The protective

photoresist layer was then flood exposed for 1 min and developed for 2 min, and the wafer was cleaned from residual photoresist by using a plasma cleaner at 60 sccm oxygen flow, 40 W for 1 min.

A thin SU-8 layer (SU-8 2002) was then spin coated at 100 rpm for 30 s, baked on a 65 °C hotplate for 30 s and moved to the 95 °C hotplate for 2 min. The wafer was allowed to cool for 20 min after being taken off the hotplate. The wafer was then patterned using the insulation layer mask at 275 mJ/cm<sup>2</sup>. The wafer was post baked for 2 min on a 65 °C hotplate and developed in the SU-8 developer solution for 1 min (Fig 3(c)). This step created openings through the insulator layer over the array electrodes and over the contact pads.

### **2.3.3 Shaping of the Probes**

The shapes of the individual probes were produced by cutting a trench through the SU-8 layers of the patterned and insulated wafers, which allowed access of etchant to the underlying Al sacrificial layer (Fig. 3(c)). A 355 nm Nd:YAG 34 laser micromachiner (E-355H-ATHI-O system, Oxford lasers, UK) was used with 2 passes at a pulse fluence of 29 J cm<sup>-2</sup> and pulse spacing of 3 μm to minimize burning the material. The Al layer was subsequently etched overnight in a static solution of concentrated KOH in a chemical release step. The probes could then be lifted individually from the substrate (Fig. 3(d)).

Scanning electron microscopy (SEM) was performed by a Philips XL30 ESEM with 1000x magnification, using a secondary electron detector, 10 kV acceleration voltage and at a pressure of 0.4 to 1.1 Torr.

### 2.3.4 Electrochemical Studies

Electrochemical experiments were performed with a bipotentiostat (CHI 750A, 760E and 760B, CH Instruments, Austin, TX), equipped with a Faraday cage and a picoamp booster (CH Instruments, Austin, TX). The reference electrode was Ag|AgCl in saturated KCl and the working electrode was a Pt flag. A Molex zero insertion force (ZIF) edge connector with 1.00 mm pitch and 9 circuits (part number 52610-0972) was used to connect the device to the bipotentiostat. Because the edge connector is small and fragile, it was soldered onto a circuit board (OSHPark company) and the board was connected to the pin header leading to wires that could be clamped to the potentiostat's leads.

Electrochemical characterization of individual electrodes (Fig. S1) on the probe was performed by cyclic voltammetry (CV) in a 1.02 mM solution of  $[\text{Fe}(\text{CN})_6]^{3-}$  and 0.1 M KCl. The potential was swept at 0.020 V/s from 0.550 V to -0.150 V and back to 0.550 V vs Ag|AgCl (saturated KCl).

Redox cycling involved activating five adjacent band electrodes in the array at a time, where the second and fourth were shorted together to serve as generators and the first, third, and fifth were shorted together to serve as collectors. CV was performed at the generators at 0.020 V/s, and the collectors were held at a constant potential equal to the starting potential of the CV at the generators. Before each redox cycling run, the CV response was recorded at the shorted generators, with the collectors at open circuit. For the solutions containing  $[\text{Fe}(\text{CN})_6]^{3-}$  in 0.1 M KCl, CV at 0.020 V/s was performed at the generators from 0.550 V to -0.150 V and back to 0.550 V vs Ag|AgCl (saturated KCl), while the collectors were held at a constant anodic potential of 0.550 V. Concentration studies were performed by spiking a solution of 0.10 M KCl in the electrochemical cell with different volumes of a stock solutions of 0.21 mM, 5.18 mM, or

9.94 mM  $[\text{Fe}(\text{CN})_6]^{3-}$  in 0.10 M KCl, to achieve consecutively higher concentrations of  $[\text{Fe}(\text{CN})_6]^{3-}$ : 1.0  $\mu\text{M}$ , 2.0  $\mu\text{M}$ , 4.5  $\mu\text{M}$ , 13.0  $\mu\text{M}$ , 20.4  $\mu\text{M}$ , 99.7  $\mu\text{M}$ , 226.5  $\mu\text{M}$ , 410.9  $\mu\text{M}$ , and 1.2 mM.

For solutions containing dopamine in artificial cerebral spinal fluid (aCSF) (consisting of 100 mM NaCl, 5.0 mM KCl, 1.2 mM  $\text{NaH}_2\text{PO}_4$ , 5.0 mM  $\text{NaHCO}_3$ , 10 mM glucose, 2.5 mM HEPES, 1.2 mM  $\text{MgSO}_4$ , 1.0 mM  $\text{CaCl}_2$  at 7.4 pH), CV at 0.020 V/s was performed at the generators from -0.100 to 0.500 V and back to -0.100 V vs Ag|AgCl (saturated KCl), while the collectors were held at a constant cathodic potential of -0.100 V. Concentration studies were performed by spiking a solution of aCSF in the electrochemical cell with different volumes from a freshly prepared stock solution of 0.52 mM dopamine in fresh aCSF to achieve consecutively higher concentrations of dopamine: 2.2  $\mu\text{M}$ , 3.6  $\mu\text{M}$ , 10.7  $\mu\text{M}$  and 49.1  $\mu\text{M}$ . To minimize oxidation of catecholamines by oxygen, the Faraday cage and all the solutions containing aCSF and dopamine were purged with argon prior to and during the experiments. The probe was kept dry in an enclosed container before the initial electrochemical studies involving  $[\text{Fe}(\text{CN})_6]^{3-}$ . The probe was then stored in water between the initial studies with the model compound and subsequent dopamine studies.

To measure plateau current from CV responses, a tangent to the background current early in the forward sweep was first extrapolated through plateau current region. Then, the difference was taken between the plateau current (the current at -0.100 V for  $[\text{Fe}(\text{CN})_6]^{3-}$  and 0.400 V for dopamine) and the value of the extrapolated background current at that same potential.

### **2.3.5 Assessment of Tissue Damage**

A microdialysis probe (made in house, 280  $\mu\text{m}$  o.d.<sup>41</sup>), a carbon fiber electrode (made in house, 7  $\mu\text{m}$  in diameter and 350  $\mu\text{m}$  in length of electroactive region) and a “blank SU-8 probe”

(SU-8 substrate with non-patterned Cr and Au layers on top) were implanted into rat brain. Each probe was inserted into a different rat and on a different day. The SU-8 probe was removed after 1 h and both the microdialysis probe and carbon fiber were removed after 4 h. An aCSF solution was perfused at 1.67  $\mu\text{L}/\text{min}$  through the microdialysis probe while in the tissue using a syringe pump. The probe was perfused prior to insertion to confirm that there were no leaks and was perfused continuously throughout the experiment. The University of Pittsburgh's Institutional Animal Care and Use Committee reviewed and approved all procedures involving animals. Male Sprague–Dawleys (Charles River, Raleigh, NC) were anesthetized with isoflurane (5% initially, 2.5% for maintenance) and maintained at a body temperature of 37 °C using a heat blanket (Harvard Apparatus; Holliston, MA). The anesthetized rat was placed in a stereotaxic frame (David Kopf, Tujunga, CA) and the dura mater was exposed by craniotomy and removed to allow insertion of one type of probe in the dorsal striatum at AP, +1.0 mm; ML, +3.8 mm; and DV, 4.8 mm, and held there for a given time while the animal was still anesthetized.

Once the probe was taken out, the tissue was fixed by transcardial perfusion with 200 mL phosphate buffer saline (1x PBS: 155 mM NaCl, 100 mM phosphate, pH 7.40) followed by 250 mL of 4 % paraformaldehyde (PFA) and 50 mL of 0.1 % fluorescent nanobeads (Invitrogen, Eugene, OR). The brain was removed and then post fixed for 2 h in 4 % PFA, soaked overnight in 30 % sucrose at 4 °C for cryoprotection. The brain was removed from sucrose solution and frozen by dipping in liquid nitrogen-cooled 2-methylbutane and stored at -80 °C until sliced. Horizontal tissue sections (perpendicular to the insertion track) were cut at 30  $\mu\text{m}$  using a cryostat. Sections were covered with gelvatol (Electron Microscopy Sciences) mounting medium (polyvinyl alcohol, glycerol, Tris buffer pH 8.5, and sodium azide in water) and covered with a cover slip. Fluorescence microscopy was performed with a 20 $\times$  objective (Olympus BX61,

Olympus; Melville, NY) and filter sets (Laser: Diode laser : 488nm) as appropriate for the nanobeads and IgG-CY3 (Chroma Technology, Rockingham, VT). The center of the probe track in each slice was positioned so that it was in the middle of the microscope viewing area. Image processing was performed with Metamorph/Fluor 7.1 software (Universal Imaging Corporation; Molecular Devices).

## **2.4 Results and Discussion**

### **2.4.1 Probe design and rationale**

The completed probe and SEM image of the probe tip are shown in Fig. 4. It was carefully designed based on several criteria and a schematic with all of the dimensions is in Fig. 1(a). Critical for *in vivo* studies are the dimensions of the shank, which needs to be narrow enough to minimize tissue damage upon insertion and long enough to reach regions of interest. The shank of our probe is 6 mm for feasibility of *in vivo* dopamine measurement in the dorsal striatum and the nucleus accumbens of the rat, where structures of common interest are located about 4 mm and 3.2 mm deep in the rat brain, respectively (depth of the region is reported after clearing the skull). The 100- $\mu\text{m}$  width of the shank is a compromise between being broad enough to accommodate an array of microband electrodes easily constructed with conventional photolithography and allow sufficient space flanking the outermost electrodes to avoid damage during the shaping step, while being narrow enough to minimize tissue damage. It is known that widespread tissue damage and glial response can occur after insertion of a 280- $\mu\text{m}$  diameter microdialysis probe has a radius that extends to 300  $\mu\text{m}$ <sup>10</sup>. However, penetration injury surrounding a narrow 7- $\mu\text{m}$  carbon microfiber electrode is merely 3  $\mu\text{m}$ , which is smaller than the diffusion sphere of dopamine (100  $\mu\text{m}$  wide and  $100 \pm 10$   $\mu\text{m}$  deep), and can be placed closer to dopamine-releasing terminals<sup>10</sup>. The electrode design on the probe consists of nine parallel,



individually addressable bands, each of 4  $\mu\text{m}$  width, with 4  $\mu\text{m}$  gaps between them (Fig. 1(b)). (Actual measured width of the fabricated electrodes was 3.8  $\mu\text{m}$  with 4.2  $\mu\text{m}$  gaps.) These dimensions were chosen because they are easily resolved with conventional photolithography and results can be compared with our prior redox cycling studies on arrays having the same width and gap measurements<sup>4,42</sup>. A thin insulating layer of SU-8 covers the leads on the probe and leaves an opening of  $76 \times 100 \mu\text{m}^2$  near the tip that exposes the band electrodes for electrochemical analysis. This opening also defines the electroactive length of the electrodes to 100- $\mu\text{m}$ , which is similar to the length of conventional carbon fiber electrodes used for *in vivo* measurements in the striatum<sup>15,43</sup>. The exposed contact pads allow for connection to the bipotentiostat through the edge connector. The shape of the tip was designed to come to a point, because it is conventionally accepted that increased sharpness helps improve insertion in biological tissue<sup>44</sup>.

#### **2.4.2 Characterization by Cyclic Voltammetry of Individual Electrodes with a Model Compound**

CV in a 1.02 mM solution of the model compound  $[\text{Fe}(\text{CN})_6]^{3-}$  and 0.1 M KCl was used to characterize the probe electrodes. Sigmoidally shaped responses for each of the nine electrodes are shown in Fig. S-1 of Supporting Information. The scan rate is slow enough to achieve an average quasi-steady state plateau current,  $i_{\text{qss}}$ , at 0 mV vs. Ag/AgCl (sat'd KCl) of  $-4.72 \pm 0.13 \text{ nA}$  for electrodes 1 through 8 ( $\pm$  one standard deviation). The magnitude of electrode 9's plateau current is only  $-2.95 \text{ nA}$ . This is due to partial coverage of that electrode by the nearby top insulation layer.

The  $i_{\text{qss}}$  from a potential step experiment with a microband electrode is expressed by Eq.

1<sup>45</sup>,

$$i_{qss} = \frac{2\pi nFlC^*D}{\ln\left(\frac{64Dt}{w^2}\right)} \quad (1)$$

where  $w$  is the electrode width (3.8  $\mu\text{m}$ ),  $l$  is the electrode length (100  $\mu\text{m}$ ),  $C^*$  is the bulk and initial concentration of the oxidized form of the redox species ( $1.02 \times 10^{-6} \text{ mol/cm}^3$ ),  $n$  is the number of moles of electrons needed to reduce a mole of  $[\text{Fe}(\text{CN})_6]^{3-}$  ( $n = 1$ ),  $F$  is the Faraday constant (96485.3 C/mol  $e^-$ ),  $D$  is the diffusion coefficient for  $[\text{Fe}(\text{CN})_6]^{3-}$  ( $7.20 \times 10^{-6} \text{ cm}^2/\text{s}$  at 25  $^\circ\text{C}$ )<sup>46</sup> and  $t$  is the time after stepping to a diffusion-limited potential. For a slow scan rate, the plateau current of the CV response at a microband electrode can be estimated by this equation. Here,  $t$  is taken as the time for the CV to sweep from  $E_{1/2}$  to 0 V, where the plateau current was measured,  $t = 0.25 \text{ V} / 0.02 \text{ V/s} = 12.5 \text{ s}$ . With these parameters, Eq. 1 yields  $i_{qss} = -4.53 \text{ nA}$ , which is outside the 95% confidence interval of the experimental data. A plausible explanation comes from the uncertainty in estimating  $t$  for Eq. 1 from a CV response and the derivation of Eq. 1, where the current approximates a two-dimensional diffusion and therefore ignores end effect contributions. It has been suggested that the length-to-width ratio should be 50 for end effects to be negligible<sup>47</sup>. Our length-to-width ratio is only 25. The five adjacent electrodes that had the most similar CV responses (3 through 7) were then selected to perform the redox cycling experiments. Throughout this paper, the electrodes in the array that are activated for the redox cycling studies are referred to as the “first” through “fifth” electrodes, to facilitate discussion.

### 2.4.3 Redox Cycling and Calibration Curves for a Model Compound

To determine the performance of redox cycling at the array on the probe, five adjacent electrodes were activated in solutions of different concentrations of  $[\text{Fe}(\text{CN})_6]^{3-}$  in 0.1 M KCl. The second and fourth electrodes were shorted together and served as generator electrodes. The first, third, and fifth electrodes were shorted together and served as collector electrodes. CV was

used at the generator electrodes, instead of a potential step, given its diagnostic power to view electrochemistry throughout a potential range rather than at a single value. The potential was initially swept cathodically (between 0.550 and -0.150 V), at 0.020 V/s to ensure a steady state redox cycling response across the 4- $\mu\text{m}$  gap, with the collectors held at a constant anodic potential of 0.550 V which is sufficient to oxidize cathodically-generated  $\text{Fe}(\text{CN})_6^{4-}$  and increasing the flux of  $\text{Fe}(\text{CN})_6^{3-}$ . The electrochemical responses are shown in Fig. 5.

At first, CV was performed at the shorted generators,  $i_{\text{GEN}}$ , while the collector electrodes were left at open potential and are sigmoidally-shaped (Fig. 5 (c1) and (c2)), similar to the single electrode responses (Fig. S1 in the Supporting Information). The solution containing 1.02 mM  $[\text{Fe}(\text{CN})_6]^{3-}$  has a cathodic plateau current of -7.63 nA, only 1.6 times (not 2 times) the average of the individual electrode plateau currents, because of shielding effects, when diffusion layers of the closely spaced, similarly biased electrodes overlap. To approximate the diffusion length in one dimension, we use  $x = \sqrt{2Dt}$  where  $x$  is the root mean squared distance that molecules diffuse in time  $t$ <sup>45</sup>. For  $D = 7.20 \times 10^{-6} \text{ cm}^2/\text{s}$  and  $t = 12.5 \text{ s}$ ,  $x = 137 \mu\text{m}$ , which extends well beyond the gap of 12  $\mu\text{m}$  between the generators and confirms that shielding takes place.

The experiment was then repeated with the collector electrodes turned held at constant oxidizing potential to achieve redox cycling. The current responses at the generators,  $i_{\text{GEN/RC}}$  are shown in Figs. 5 (b1) and (b2), and those at the collectors,  $i_{\text{COLL/RC}}$ , are shown in Figs. 5 (a1) and (a2). During CV, as the potential at the generator nears the half-wave potential of the redox species,  $E_{1/2}$ , and shows current due to reduction of  $[\text{Fe}(\text{CN})_6]^{3-}$ , the anodic current at the collector electrode increases as  $[\text{Fe}(\text{CN})_6]^{4-}$ , arriving from the generator electrode, oxidizes back to its starting form,  $[\text{Fe}(\text{CN})_6]^{3-}$ . In the return sweep, at potentials more positive of  $E_{1/2}$ , the collector current drops toward zero, as  $[\text{Fe}(\text{CN})_6]^{4-}$  is no longer produced at the generators.

Linear calibration curves for the absolute values of background-subtracted plateau currents of  $i_{\text{GEN}}$ ,  $i_{\text{GEN/RC}}$ , and  $i_{\text{COLL/RC}}$  at 0.400 V were produced for a series of concentrations of  $[\text{Fe}(\text{CN})_6]^{3-}$  and yielded the following slopes (calibration sensitivities):  $0.0064 \pm 0.0002$ ,  $0.0112 \pm 0.001$ , and  $0.00777 \pm 0.0007$  nA/ $\mu\text{M}$ , respectively. See Fig. 6. That for  $i_{\text{GEN/RC}}$  is greater than for  $i_{\text{GEN}}$  by a factor of  $1.76 \pm 0.06$ , because of the enhanced concentration gradient established by re-oxidization of the reduced form at the neighboring collector electrodes. This ratio is called the amplification factor:

$$A_f = \frac{i_{\text{GEN/RC}}}{i_{\text{GEN}}} \quad (2)$$

The calibration sensitivity of the anodic  $i_{\text{COLL/RC}}$  is greater than that for the cathodic  $i_{\text{GEN}}$  because of the concentration gradient established by reduction of the oxidized form at the generator electrodes. The ratio of the slopes of  $i_{\text{COLL/RC}}$  and  $i_{\text{GEN/RC}}$  is  $69.15 \pm 0.73\%$ . This quantity represents the percent collection efficiency,  $\%C_e$ , which is a measure of the relative number of molecules recycled between generator and collector electrodes:

$$\%C_e = 100\% \left( \frac{i_{\text{COLL/RC}}}{i_{\text{GEN/RC}}} \right) \quad (3)$$

The amplification factor and collection efficiency depend on the relative widths and numbers of generators to collectors and the size of the gaps between them. Comparisons of our results can be made to those obtained with similar array designs reported previously. The electrode lengths and model compounds are different but should not affect  $A_f$  and  $\%C_e$  substantially. One is by Aggarwal et. al. (2 mm-long electrodes, but with the same electrode widths, gaps and configuration as the work described here), who report an  $A_f$  of 1.4 and  $\%C_e$  of 60.6% for 5.0 mM  $\text{Ru}(\text{NH}_3)_6^{3+}$ <sup>5</sup>. Another is the  $\text{Si}_3\text{N}_4$  probe, which exhibited an  $A_f$  of 1.5 and

2.0 and %C<sub>e</sub> of 54.0 and 65.0% for 1 mM Ru(NH<sub>3</sub>)<sub>6</sub><sup>3+</sup> on the 2-pair and 3-pair IDA (250-μm long and 3-μm wide electrodes with 2-μm gaps), respectively <sup>21</sup>.

The experimental calibration sensitivity for *i*<sub>GEN/RC</sub> is a factor of 0.67 at the Aggarwal microband electrode array <sup>5</sup> compared to the theoretical slope (0.016 nA/μM) of the diffusion limited current, *i*<sub>lim</sub>, vs. C\* using Eq. 4 <sup>48</sup> for redox cycling,

$$i_{lim} = m \ln FC^* D \left[ 0.637 \ln \left( 2.55 \left( 1 + \frac{w}{w_g} \right) - \left( \frac{0.19}{\left( 1 + \frac{w}{w_g} \right)^2} \right) \right) \right]. \quad (4)$$

Here, *i*<sub>lim</sub> is the same at the generators and collectors, *m* is number of generators and collectors (*m* = 2.5, accounting for a total of five electrodes used in redox cycling experiments in this paper), *w* is the width of an individual electrode, where generator and collector widths are equal (*w* = 3.8 μm) and *w<sub>g</sub>* is the width of the gap between anodes and cathodes (*w<sub>g</sub>* = 4.2 μm). The value we use for *D* (6.93 × 10<sup>-6</sup> cm<sup>2</sup>/s) in Eq. 4 is the average of *D<sub>O</sub>* and *D<sub>R</sub>* for potassium ferri- and ferrocyanide in 0.1 M KCl at 25 °C reported by Konopka et al. <sup>46</sup>. This is because the expression of Eq. 4 assumes that the diffusion coefficients of reduced and oxidized forms are the same <sup>48</sup>. Eq. 4 makes several assumptions: (1) the array comprises of so many electrodes that the edge effects of the outermost electrodes are negligible; (2) the length-to-width ratio for each electrode is so large that end effects can be ignored; (3) the diffusion coefficients of reduced and oxidized forms of redox species are the same; (4) the system is at steady state; and (5) *w* > 0.18 *w<sub>g</sub>*. The experimental slope is a factor of 0.46 of that predicted by Eq. 4. This can be explained at least partially by the fact that the first two assumptions do not apply to our probe design. (It has been shown previously that with increasing numbers of pairs of generators and collectors that |*i*<sub>COLL/RC</sub>| approaches that of |*i*<sub>GEN/RC</sub>| <sup>49, 50</sup>.)

Detection limits for  $[\text{Fe}(\text{CN})_6]^{3-}$  were 2.19  $\mu\text{M}$ , 1.25  $\mu\text{M}$  and 2.08  $\mu\text{M}$ , for  $i_{\text{GEN}}$ ,  $i_{\text{GEN/RC}}$ , and  $i_{\text{COLL/RC}}$ , respectively. These were determined by the quotient of three times the standard deviation of the background current and the slope of the calibration curve. The background was obtained by performing CV in the blank KCl solution ( $N = 4$ ). For the most part, these detection limits are higher than detection limits using redox cycling reported elsewhere but for different model compounds (e.g. 10.0 nM  $[\text{Ru}(\text{NH}_3)_6]^{3+}$ <sup>51</sup> and 20 nM of  $[\text{Ru}(\text{NH}_3)_6]^{3+}$ <sup>21</sup>). This is likely due to the fact that our probe has at least one or more of the following: shorter electrodes, fewer pairs of them and wider gaps.

#### 2.4.4 Redox Cycling and Calibration Curves for Dopamine

Redox cycling of dopamine in aCSF *in vitro* and at the same probe electrodes as for the model compound was performed to demonstrate an application to an analyte of biological significance and a target for future *in vivo* studies. The potential was swept between -0.100 V to 0.500 V at 0.020 V/s to oxidize the dopamine to the o-quinone, with the collectors held at a constant potential of -0.100 V to reduce the o-quinone form back to dopamine. The redox cycling responses are shown in Fig. 7. As in the ferricyanide solutions, the generator and collector electrode responses in the dopamine solutions are sigmoidal and similar in behavior, except in opposite directions of potential and current, because dopamine is in its reduced form. However, not all background currents align when overlaid for reasons that are unknown and are being investigated at this time.

Linear calibration curves for  $i_{\text{GEN}}$ ,  $i_{\text{GEN/RC}}$ , and  $i_{\text{COLL/RC}}$  were produced from the background-subtracted plateau currents at 0.4 V for a series of concentrations of dopamine and yielded the following calibration sensitivities:  $0.021 \pm 0.002$ ,  $0.0420 \pm 0.0004$ , and  $0.0328 \pm 0.0003$  nA/ $\mu\text{M}$ , respectively. See Fig. 8. As for  $[\text{Fe}(\text{CN})_6]^{3-}$ , the calibration sensitivities for

dopamine also increase in the order of  $i_{\text{GEN}}$ ,  $i_{\text{COLL/RC}}$  and  $i_{\text{GEN/RC}}$ . These values are higher by a factor of  $\sim 3.8$  compared to those obtained for  $[\text{Fe}(\text{CN})_6]^{3-}$ . The calibration sensitivity based on Eq. 4 (using  $D = 7.5 \times 10^{-6} \text{ cm}^2/\text{s}$ <sup>52</sup>) is  $0.035 \text{ nA}/\mu\text{M}$ . The expected increase is only 2.2 times that for  $[\text{Fe}(\text{CN})_6]^{3-}$ , which should result from an increase in  $n$  from 1 to 2 and a slightly larger diffusion coefficient for dopamine. The unexpectedly higher experimental response could be due to increasingly clean electrode surfaces and hydration of SU-8<sup>53</sup> over extended use and storage in aqueous solution between the  $[\text{Fe}(\text{CN})_6]^{3-}$  and dopamine studies. (More studies would be needed to understand this effect).

The amplification factor for dopamine for redox cycling at the probe's array using five electrodes is  $2.01 \pm 0.16$ , obtained from the ratio of the slopes of calibration curves for  $i_{\text{GEN/RC}}$  and  $i_{\text{GEN}}$ . The percent collection efficiency for dopamine during redox cycling is  $78 \pm 1\%$ , obtained from the ratio of the slopes for  $i_{\text{COLL/RC}}$  and  $i_{\text{GEN/RC}}$ . These numbers are only slightly higher, by 1.1 times, than those obtained for the model compound, because it is the electrode array geometries that contribute to these numbers, and that little to no effect is expected on Af and Ce% of enhancement to the electroactivity of the electrodes (assuming all electrodes are similarly enhanced).

The calculated detection limits for dopamine with this probe are  $1.94 \mu\text{M}$ ,  $1.08 \mu\text{M}$  and  $5.66 \mu\text{M}$  for  $i_{\text{GEN}}$ ,  $i_{\text{GEN/RC}}$ , and  $i_{\text{COLL/RC}}$ , respectively. To our knowledge, a detection limit of  $10 \text{ nM}$  dopamine is the lowest value demonstrated by redox cycling, using the vertical-stacked, interdigitated microelectrode arrays<sup>51</sup>. However, that particular device is not suitable for *in vivo* measurements because of the large footprint with more and longer electrodes and narrower gaps compared to this work. The insertable  $\text{Si}_3\text{N}_4$  probe with IDA electrodes has reported detection

limits of 1.0  $\mu\text{M}$  of dopamine at the collector electrode at a 5-pair IDA <sup>21</sup>, consistent with our results.

## **2.5 Insertion of probe and assessment of resulting tissue damage in rat brain**

Fig. 9 shows fluorescence microscopy images of tissue sections from the dorsal striatum of rat brain where three different probes had been inserted and vascularization labeled by subsequent perfusion with fluorescent nanobeads. The white outlines indicate that of the probe traces in the tissue. The control image was obtained from the opposite hemisphere of the brain in which the SU-8 probe was inserted. In the case of the 7- $\mu\text{m}$  carbon microfiber, the track of the glass pipet encapsulating the carbon fiber was followed to the smallest visible extent. The trace of the electrode itself is very hard to find under the microscope and its size and shape can only be estimated, because the diameter of the electrode is so small <sup>10</sup>. As for the microdialysis probe, the tissue damage is substantial as can be seen by the absence of blood vessels around the probe's track. The SU-8 probe shows relatively low tissue damage as seen by the presence of many blood vessels around the track. Note, the time differences of these devices in Fig. 9 is 4 h and 1 h. The dwelling time of each device is indicative of the timeframe typically used in brain tissue. For example, 4 h is a very common timescale for microdialysis probe implantation, although current literature cite up to 10 days of dwelling time <sup>41, 54</sup>. Damage to the tissue from the SU-8 probe is most similar to that of the carbon fiber microelectrode (Fig. 9 b and c). Regardless of these timeframes it is clear that the SU-8 probe offers the benefits of the smaller single carbon fiber electrodes but with the additional capabilities of multiple electrodes and redox cycling.

## **2.6 Conclusions**

The studies here emphasize the fabrication of a flexible SU-8 probe with an array of individually-addressable microband electrodes and the preliminary results of their redox cycling



behavior. The dimensions and shape are suitable for *in vivo* measurements. Because the electroactive tip occupies a volume of only about 1  $\mu\text{L}$ , analysis in other kinds of ultrasmall samples of this size is possible. The electrode fabrication process was performed with modifications to established lithographical procedures, and the shape of the probe was accomplished by laser cutting through the SU-8 substrate and lift off by dissolving the metallic sacrificial layer. Tissue damage in rat dorsal striatum was minimal. Redox cycling produced predictable behavior and detection limits for a model compound and dopamine, comparable to other microelectrode arrays reported in the literature, accounting for the different designs and geometries, but most of which are not on tissue-insertable probes. A unique contribution is that the probe electrodes can be independently activated to allow for other electrochemical detection methodologies such as those that investigate following chemistry and kinetics or differentiate between analytes in mixtures based on these phenomena.

There remains a need to lower detection limits further to be able to measure physiologically relevant concentrations of dopamine<sup>55</sup>. To do so, narrowing the separation between generators and collectors while maintaining the same footprint can be considered. Achieving more electrode pairs with smaller gaps with stacked electrode arrays that also use the space perpendicular to the probe surface would further enhance signals. For an increasing number of electrodes to remain individually addressable, the need for more space for the leads should also be accounted for. Other possible modifications to improve detection limits include lengthening the electrodes, if larger detection regions are acceptable, and widening the probe shank to accommodate more electrodes, if tissue damage is tolerable. A more quantitative investigation of electrochemical performance of the array design, analysis of contributions of the SU-8 substrate and electrode imperfections toward electrochemical signal, and an assessment of

alternative electrode dimensions that fit on the probe and improve detection limits will be reported elsewhere.

## **2.7 Supporting Information**

Supporting information includes CV responses for individual electrodes in the ferricyanide solution.

## **2.8 Conflicts of Interest**

The authors declare that they have no conflicts of interest.

## **2.9 Ethics Approval**

The University of Pittsburgh's Institutional Animal Care and Use Committee reviewed and approved all procedures involving animals.

## **2.10 Source of Biological Material**

Male Sprague–Dawley rats were obtained from Charles River, Raleigh, NC.

## **2.11 Statement on Animal Welfare**

All animal procedures were in compliance with USDA laboratory animal use regulations. Additionally, all procedures were approved by the Institutional Animal Care and Use Committee of the University of Pittsburgh, the location of the laboratory where all experiments involving animals took place

## **2.12 Acknowledgements**

Research was supported partially through the National Institutes of Health (R01NS102725, R21NS109875) and the University of Pittsburgh Center for Biological Imaging (1S10RR028478-01), the Royal Society for an Industry Fellowship (J.V.M., INF/R1/180026) and the Centre for Doctoral Training in Diamond Science and Technology (EP/ L015315/1) with the Defense Science and Technology Laboratory (Dstl) (S.J.C.), the University of Arkansas's Women's Giving Circle, the National Science Foundation (CMI-1808286) and the Arkansas Biosciences Institute, the major research component of the Arkansas Tobacco Settlement Proceeds Act of 2000. MLM is also grateful for a Fulbright Dissertation Research Award. We acknowledge Errol Porter for consultation on microelectrode fabrication and the High-Density Electronics Center for use of microfabrication facilities. Scanning electron microscopy images were obtained in the Arkansas Nano & Biomaterials Characterization Facility at the University of Arkansas. We are grateful to Dr. Jonathan Moldenhauer and Professor David Paul at the University of Arkansas for designing and providing the circuit board for mounting the edge connector.

## 2.13 Figures

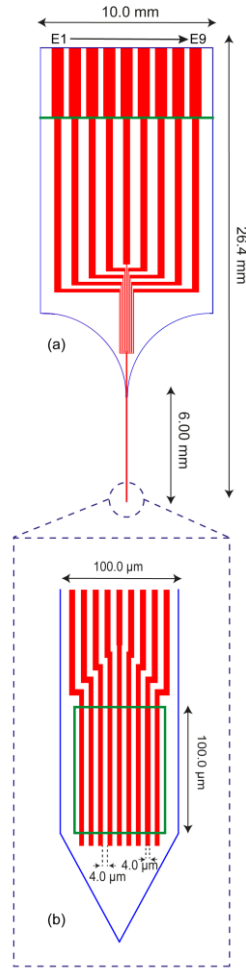


**Fig. 1** AutoCAD drawings of the probe and microelectrode array. (a) The view of the entire probe. The blue outline defines the shape of the probe in the substrate layer (SU-8 3050), the red areas are the contact pads, leads, and electrodes in the metal layer. (b) Magnified view of the tip of the probe containing the electrode array. The green outline indicates the openings in the insulation layer (SU-8 2000) over the contact pads and electroactive region of the microband electrodes. Microband electrodes are assigned names of E1 to E9 from left to right with the paddle oriented to the top of the page

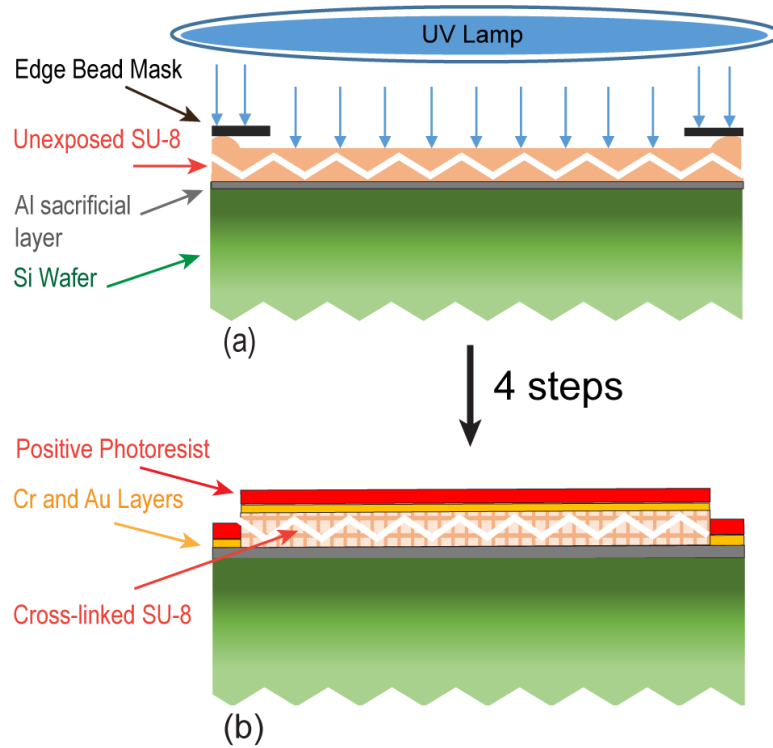


**Fig. 2** Process flow of whole wafer (not to scale). (a) Blanket UV-exposure of the SU-8 substrate layer, excluding the edge bead, after spin-coating and pre-baking.. (b) Subsequent removal of the edge bead with developer, post-baking of the remaining substrate SU-8, followed by coating of wafer with Cr and Au metal layers, and spin coating and baking of positive photoresist

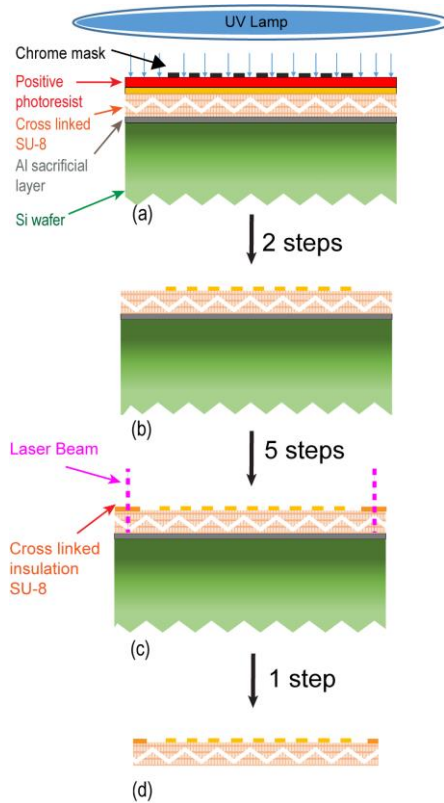


**Fig. 3** Expanded view of the process of a single probe (not to scale) that follow steps in Fig. 2. (a) Defining an image of the electrodes in the photoresist through UV exposure through a chrome mask. (b) Developing unexposed positive resist followed by etching of Cr and Au metal layers. (c) Spin coating, pre-baking, UV-exposure through an aligned insulation chrome mask, development, and post-baking of insulating SU-8 layer, followed by laser cutting to create trenches through both SU-8 layers in a probe shape. (d) Releasing probes from substrate by dissolution of the underlying aluminum layer in a KOH solution

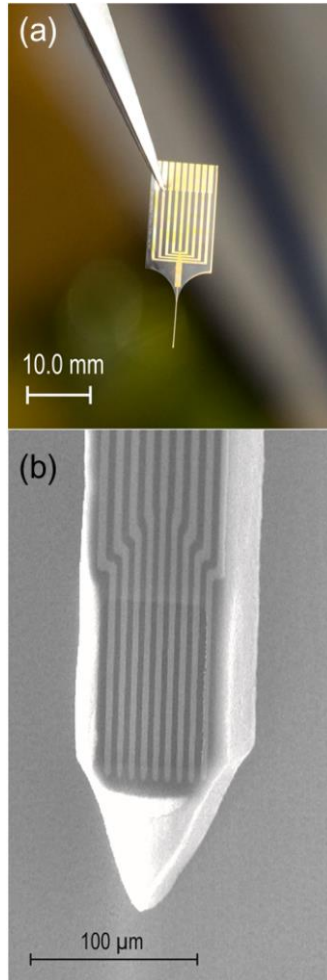


**Fig. 4** (a) Photograph of a completed probe. (b) SEM image of the microarray on the tip of the SU-8 probe. A faint rectangular outline can be observed over the array, which is the edge of the top layer of insulating SU-8 that borders an opening exposing the electrodes and defining their electroactive length



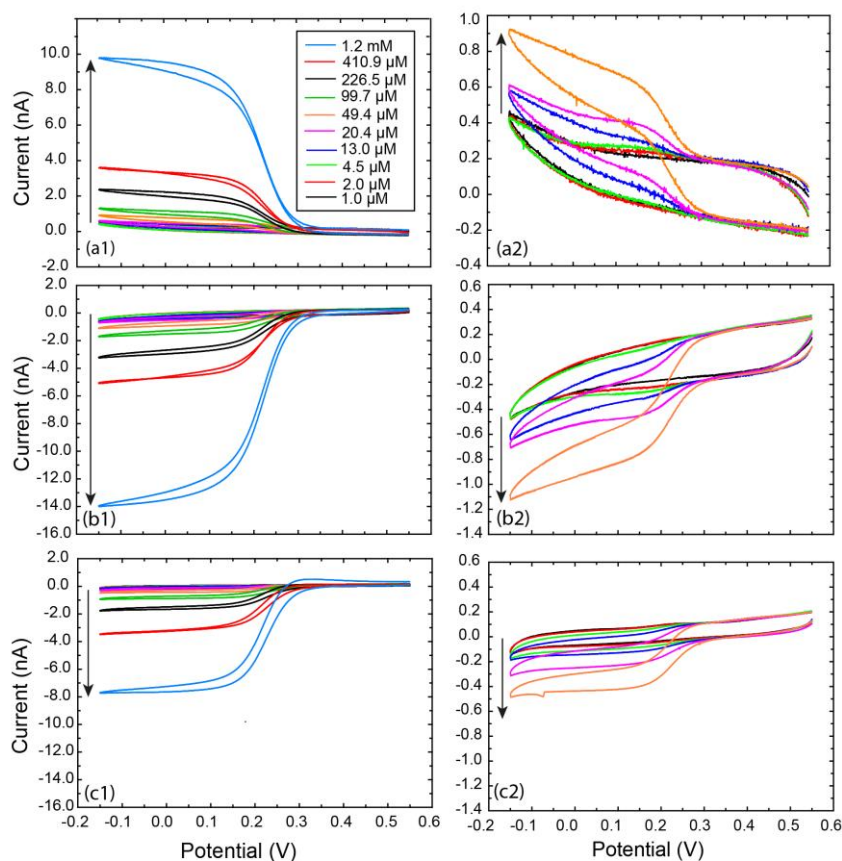


**Fig. 5** Electrochemical responses for different concentrations of  $\text{K}_3\text{Fe}(\text{CN})_6$  in 0.10 M KCl during redox cycling when (a1) and (a2) collectors are held at +0.550 V vs. Ag|AgCl (saturated KCl) (anodic, positive current) and while (b1) and (b2) generators undergo CV at a scan rate of 0.020 V/s (cathodic, negative current), and without redox cycling when (c1) and (c2) generators undergo CV at a scan rate of 0.020 V/s and collectors are left at open circuit. Arrows indicate responses in the direction of increasing concentration. (a1), (b1) and (c1) overlay responses for concentrations of 1.0  $\mu\text{M}$ , 2.0  $\mu\text{M}$ , 4.5  $\mu\text{M}$ , 13.0  $\mu\text{M}$ , 20.4  $\mu\text{M}$ , 49.4  $\mu\text{M}$ , 99.7  $\mu\text{M}$ , 226.5  $\mu\text{M}$  and 410.9  $\mu\text{M}$  and 1.2 mM. (a2), (b2) and (c2) are expanded views of (a1), (b1) and (c1), respectively, where the largest response corresponds to 99.7  $\mu\text{M}$

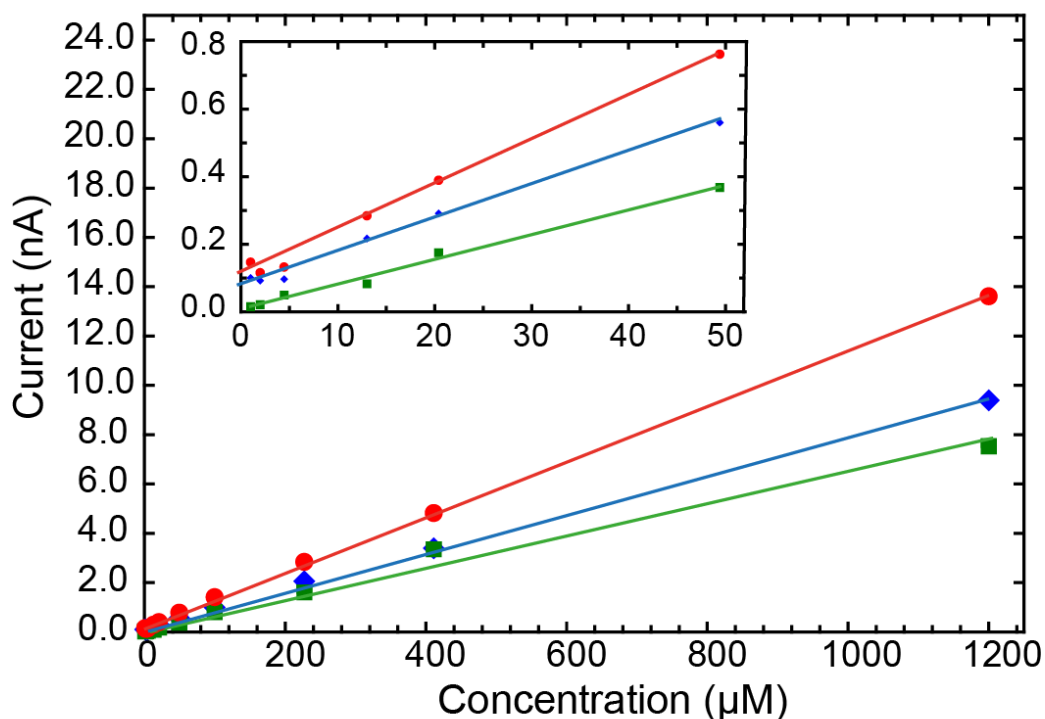


**Fig. 6** Calibration curves of background-subtracted, plateau current (measured at 0.0 V) on increasing concentrations of  $K_3Fe(CN)_6$  for generators without redox cycling (green squares), and for generators (red circles) and collectors (blue diamonds) with redox cycling. The absolute value of current has been plotted for a simpler overlay. The least squares fit and corresponding  $R^2$  values for curves for  $i_{GEN}$ ,  $i_{GEN}$ , and  $i_{GEN/RC}$  are:  $y = (6.38 (\pm 0.22) \times 10^{-3} \text{ nA } \mu\text{M}^{-1}) x + (0.11 (\pm 0.01) \text{ nA})$ ,  $R^2 = 0.990$ ;  $y = (1.12 (\pm 0.01) \times 10^{-2} \text{ nA } \mu\text{M}^{-1}) x + (0.17 \pm 0.03 \text{ nA})$ ,  $R^2 = 0.999$  and  $y = (7.77 (\pm 0.07) \times 10^{-3} \text{ nA } \mu\text{M}^{-1}) x + (0.14 \pm 0.03 \text{ nA})$ ,  $R^2 = 0.999$ ; respectively. Inset shows calibration curve for concentrations below  $50 \mu\text{M}$

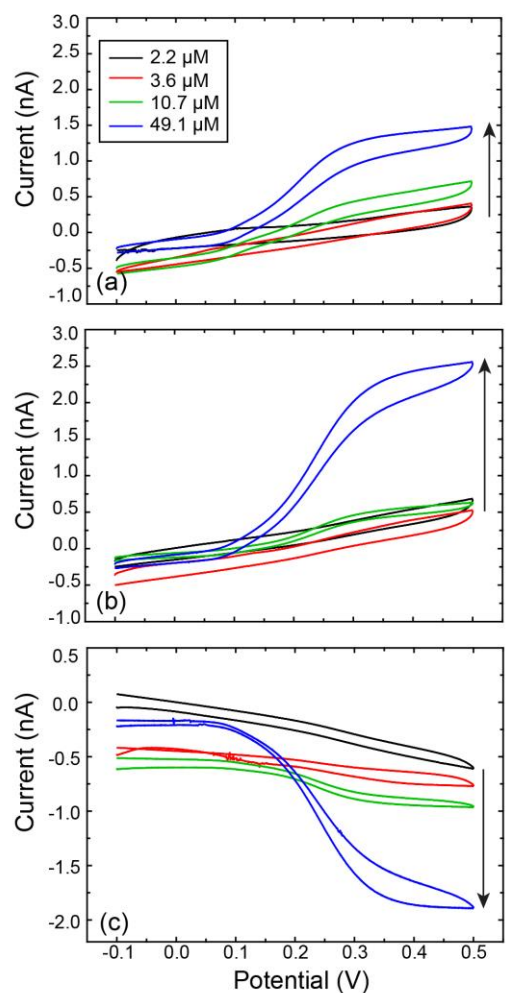


**Fig. 7** Electrochemical responses in different concentrations of dopamine in aCSF without redox cycling for (a) generators at 0.020 V/s, and with redox cycling for (b) generators at 0.020 V/s and (c) collectors held at -0.100 V vs. Ag|AgCl (saturated KCl). Arrows indicate responses in the direction of increasing concentration of dopamine: 2.2  $\mu\text{M}$ , 3.6  $\mu\text{M}$ , 10.7  $\mu\text{M}$  and 49.1  $\mu\text{M}$

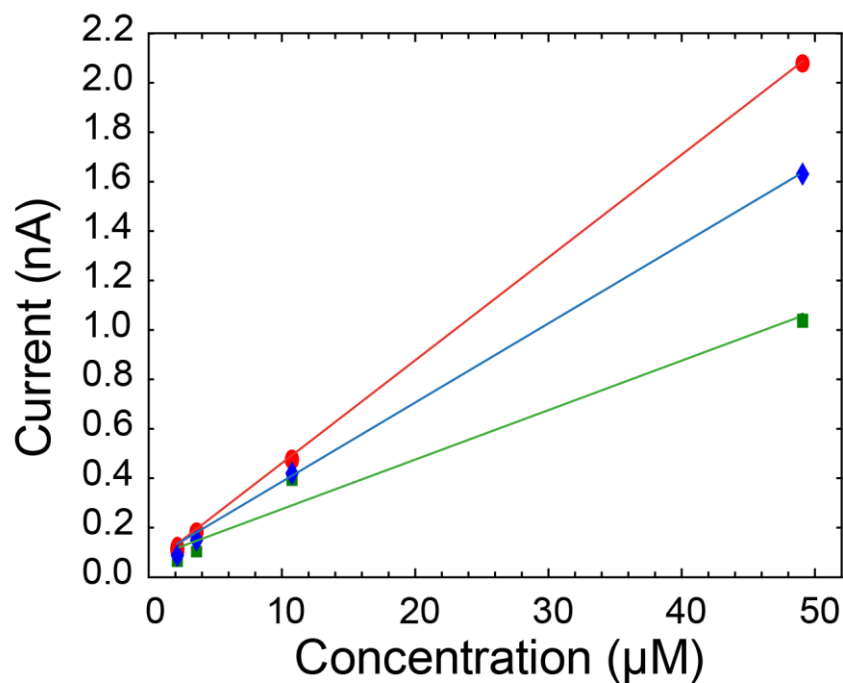


**Fig. 8** Calibration curve of background-subtracted, plateau current (measured at 0.4 V) on increasing concentrations of dopamine for generator without redox cycling (green diamonds), generator with redox cycling (red circles) and collector with redox cycling (blue squares).. The absolute value of current has been plotted for easier overlay. The least squares fit and corresponding  $R^2$  values for curves for  $i_{GEN}$ ,  $i_{GEN}$ , and  $i_{GEN/RC}$  are:  $y = (2.09 (\pm 0.17) \times 10^{-2} \text{ nA } \mu\text{M}^{-1}) x + (4.71 (\pm 0.34) \times 10^{-2} \text{ nA})$ ,  $R^2 = 0.975$ ;  $y = (4.20 (\pm 0.04) \times 10^{-2} \text{ nA } \mu\text{M}^{-1}) x + (2.60 (\pm 0.94) \times 10^{-2} \text{ nA})$ ,  $R^2 = 0.999$ ;  $y = (3.28 (\pm 0.03) \times 10^{-2} \text{ nA } \mu\text{M}^{-1}) x + (1.74 (\pm 0.60) \times 10^{-2} \text{ nA})$ ,  $R^2 = 0.999$  respectively

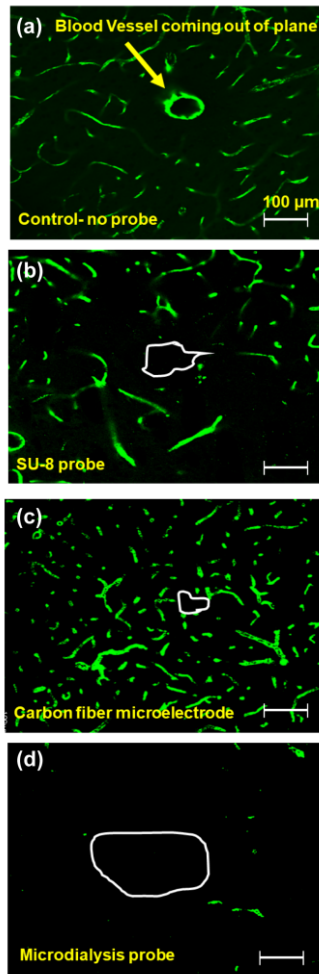


**Fig. 9** Fluorescence microscope images of tracks of an inserted probe. White outlines show the perimeter of the probe's track. The green streaks show blood vessels in the slice. The scale bar is the same for all images. (a) The control image was obtained from the opposite side of the brain in which the microelectrode array probe was inserted. (b) Track of the probe used for this study. (c) Track of a 5- $\mu\text{m}$  diameter carbon microfiber electrode. (d) Track of a typical 300- $\mu\text{m}$  diameter microdialysis probe. In the control image, the round green outline is the cross section of a blood vessel

## 2.14 References

1. Xu, X.; Zhang, S.; Chen, H.; Kong, J., Integration of electrochemistry in micro-total analysis systems for biochemical assays: Recent developments. *Talanta* **2009**, *80* (1), 8-18.
2. Niwa, O., Electroanalytical chemistry with carbon film electrodes and micro and nano-structured carbon film-based electrodes. *Bull. Chem. Soc. Jpn.* **2005**, *78* (4), 555-571.
3. Lowinsohn, D.; Peres, H. E. M.; Kosminsky, L.; Paixão, T. R. L. C.; Ferreira, T. L.; Ramirez-Fernandez, F. J.; Bertotti, M., Design and fabrication of a microelectrode array for iodate quantification in small sample volumes. *Sensors and Actuators B: Chemical* **2006**, *113* (1), 80-87.
4. Hu, M.; Fritsch, I., Redox cycling behavior of individual and binary mixtures of catecholamines at gold microband electrode arrays. *Analytical Chemistry* **2015**, *87* (4), 2029-2032.
5. Aggarwal, A. Studies Toward the Development of a Microelectrode Array for Detection of Dopamine through Redox Cycling. Dissertation, University of Arkansas, 2011.
6. Niwa, O., Electroanalysis with interdigitated array microelectrodes. *Electroanalysis* **1995**, *7* (7), 606-613.
7. Bard, A. J.; Crayston, J. A.; Kittlesen, G. P.; Varco Shea, T.; Wrighton, M. S., Digital simulation of the measured electrochemical response of reversible redox couples at microelectrode arrays: consequences arising from closely spaced ultramicroelectrodes. *Analytical Chemistry* **1986**, *58* (11), 2321-2331.
8. Oleinick, A.; Zhu, F.; Yan, J.; Mao, B.; Svir, I.; Amatore, C., Theoretical Investigation of Generator-Collector Microwell Arrays for Improving Electroanalytical Selectivity: Application to Selective Dopamine Detection in the Presence of Ascorbic Acid. *ChemPhysChem* **2013**, *14* (9), 1887-1898.
9. Seymour, J. P.; Wu, F.; Wise, K. D.; Yoon, E., State-of-the-art MEMS and microsystem tools for brain research. *Microsystems & Nanoengineering* **2017**, *3* (1), 16066.
10. Jaquins-Gerstl, A.; Michael, A. C., Comparison of the brain penetration injury associated with microdialysis and voltammetry. *Journal of neuroscience methods* **2009**, *183* (2), 127-135.

11. Hong, G.; Lieber, C. M., Novel electrode technologies for neural recordings. *Nat Rev Neurosci* **2019**, *20* (6), 330-345.
12. Dengler, A. K.; McCarty, G. S., Microfabricated Microelectrode Sensor for Measuring Background and Slowly Changing Dopamine Concentrations. *J Electroanal Chem (Lausanne)* **2013**, *693*, 28-33.
13. Zachek, M. K.; Park, J.; Takmakov, P.; Wightman, R. M.; McCarty, G. S., Microfabricated FSCV-compatible microelectrode array for real-time monitoring of heterogeneous dopamine release. *Analyst (Cambridge, U. K.)* **2010**, *135* (7), 1556-1563.
14. Roberts, J. G.; Sombers, L. A., Fast-Scan Cyclic Voltammetry: Chemical Sensing in the Brain and Beyond. *Analytical Chemistry* **2018**, *90* (1), 490-504.
15. Rodeberg, N. T.; Sandberg, S. G.; Johnson, J. A.; Phillips, P. E. M.; Wightman, R. M., Hitchhiker's Guide to Voltammetry: Acute and Chronic Electrodes for in Vivo Fast-Scan Cyclic Voltammetry. *ACS Chemical Neuroscience* **2017**, *8* (2), 221-234.
16. Hunsberger, H. C.; Setti, S. E.; Heslin, R. T.; Quintero, J. E.; Gerhardt, G. A.; Reed, M. N., Using enzyme-based biosensors to measure tonic and phasic glutamate in Alzheimer's mouse models. *JoVE (Journal of Visualized Experiments)* **2017**, (123), e55418.
17. Burmeister, J. J.; Pomerleau, F.; Huettl, P.; Gash, C. R.; Werner, C. E.; Bruno, J. P.; Gerhardt, G. A., Ceramic-based multisite microelectrode arrays for simultaneous measures of choline and acetylcholine in CNS. *Biosensors and Bioelectronics* **2008**, *23* (9), 1382-1389.
18. Burmeister, J. J.; Price, D. A.; Pomerleau, F.; Huettl, P.; Quintero, J. E.; Gerhardt, G. A., Challenges of simultaneous measurements of brain extracellular GABA and glutamate in vivo using enzyme-coated microelectrode arrays. **2020**, (1872-678X (Electronic)).
19. Zachek, M. K.; Takmakov, P.; Park, J.; Wightman, R. M.; McCarty, G. S., Simultaneous monitoring of dopamine concentration at spatially different brain locations in vivo. *Biosens. Bioelectron.* **2010**, *25* (5), 1179-1185.
20. Ngernsutivorakul, T.; White, T. S.; Kennedy, R. T., Microfabricated Probes for Studying Brain Chemistry. *Chemphyschem: a European journal of chemical physics and physical chemistry* **2018**, *19* (10), 1128.

21. Xi, Y. Interdigitated array electrode microprobe: Design, fabrication and characterization. University of Arkansas, 2005.
22. Atcherley, C. W.; Laude, N. D.; Parent, K. L.; Heien, M. L., Fast-scan controlled-adsorption voltammetry for the quantification of absolute concentrations and adsorption dynamics. *Langmuir* **2013**, *29* (48), 14885-14892.
23. Taylor, I. M.; Patel, N. A.; Freedman, N. C.; Castagnola, E.; Cui, X. T., Direct in vivo electrochemical detection of resting dopamine using Poly (3, 4-ethylenedioxythiophene)/Carbon Nanotube functionalized microelectrodes. *Analytical chemistry* **2019**, *91* (20), 12917-12927.
24. Pathirathna, P.; Balla, R. J.; Amemiya, S., Nanogap-Based Electrochemical Measurements at Double-Carbon-Fiber Ultramicroelectrodes. *Analytical Chemistry* **2018**, *90* (20), 11746-11750.
25. Hu, M.; Fritsch, I., Application of electrochemical redox cycling: toward differentiation of dopamine and norepinephrine. *Anal Chem* **2016**, *88* (11), 5574-5578.
26. HajjHassan, M.; Chodavarapu, V.; Musallam, S., NeuroMEMS: Neural Probe Microtechnologies. *Sensors (Basel)* **2008**, *8* (10), 6704-6726.
27. Sreenivas, G.; Ang, S. S.; Fritsch, I.; Brown, W. D.; Gerhardt, G. A.; Woodward, D. J., Fabrication and characterization of sputtered-carbon microelectrode arrays. *Analytical chemistry* **1996**, *68* (11), 1858-1864.
28. Metallo, C.; White, R. D.; Trimmer, B. A., Flexible parylene-based microelectrode arrays for high resolution EMG recordings in freely moving small animals. *J Neurosci Methods* **2011**, *195* (2), 176-84.
29. Zhuolin Xiang, S.-C. Y., Ning Xue, Tao Sun, Ultra-thin flexible polyimide neural probe embedded in dissolvable maltose-coated microneedle. *J. Micromech Microeng.* **2014**, *24*, 11-20.
30. Huang, S.-H.; Lin, S.-P.; Chen, J.-J. J., In vitro and in vivo characterization of SU-8 flexible neuroprobe: From mechanical properties to electrophysiological recording. *Sensors and Actuators A: Physical* **2014**, *216*, 257-265.
31. Takeuchi, S.; Ziegler, D.; Yoshida, Y.; Mabuchi, K.; Suzuki, T., Parylene flexible neural probes integrated with microfluidic channels. *Lab on a Chip* **2005**, *5* (5), 519-523.



32. Keekeun Lee, J. H., Ryan Clement, Biocompatible benzocyclobutene (BCB)-based neural implants with micro-fluidic channel. *Biosensors and bioelectronics* **2004**, *20*, 404-407.
33. A. H. A. Malavazi, J. A. B. G., R. J. M. Covolan, R. R. Panepucci, Design and microfabrication methodology of Su-8 based neural probes *XXIV Congresso Brasileiro de Engenharia Biomédica* **2014**, 2850-2853.
34. Nemani, K. V.; Moodie, K. L.; Brennick, J. B.; Su, A.; Gimi, B., In vitro and in vivo evaluation of SU-8 biocompatibility. *Materials Science and Engineering: C* **2013**, *33* (7), 4453-4459.
35. Read, T. L.; Cobb, S. J.; Macpherson, J. V., An sp<sup>2</sup> Patterned Boron Doped Diamond Electrode for the Simultaneous Detection of Dissolved Oxygen and pH. *ACS Sensors* **2019**, *4* (3), 756-764.
36. Li, A.; Chan, S. H.; Nguyen, N.-T., A laser-micromachined polymeric membraneless fuel cell. *Journal of Micromechanics and Microengineering* **2007**, *17* (6), 1107-1113.
37. Ghantasala, M. K.; Hayes, J. P.; Harvey, E. C.; Sood, D. K., Patterning, electroplating and removal of SU-8 moulds by excimer laser micromachining. *Journal of Micromechanics and Microengineering* **2001**, *11* (2), 133-139.
38. Green, R. A.; Ordonez, J. S.; Schuettler, M.; Poole-Warren, L. A.; Lovell, N. H.; Suaning, G. J., Cytotoxicity of implantable microelectrode arrays produced by laser micromachining. *Biomaterials* **2010**, *31* (5), 886-893.
39. Abercrombie, E. D.; Keefe, K. A.; DiFrischia, D. S.; Zigmond, M. J., Differential Effect of Stress on In Vivo Dopamine Release in Striatum, Nucleus Accumbens, and Medial Frontal Cortex. *Journal of Neurochemistry* **1989**, *52* (5), 1655-1658.
40. Matarèse, B. F. E.; Feyen, P. L. C.; Falco, A.; Benfenati, F.; Lugli, P.; deMello, J. C., Use of SU8 as a stable and biocompatible adhesion layer for gold bioelectrodes. *Sci Rep* **2018**, *8* (1), 5560-5560.
41. Nesbitt, K. M.; Jaquins-Gerstl, A.; Skoda, E. M.; Wipf, P.; Michael, A. C., Pharmacological mitigation of tissue damage during brain microdialysis. *Analytical chemistry* **2013**, *85* (17), 8173-8179.

42. Aggarwal, A.; Hu, M.; Fritsch, I., Detection of dopamine in the presence of excess ascorbic acid at physiological concentrations through redox cycling at an unmodified microelectrode array. *Analytical and bioanalytical chemistry* **2013**, 405.
43. Venton, B. J.; Cao, Q., Fundamentals of fast-scan cyclic voltammetry for dopamine detection. *Analyst* **2020**, 145 (4), 1158-1168.
44. Hajj-Hassan, M.; Fayad, R.; Berro, S.; Chodavarapu, V. P.; Musallam, S., Implantation of Elongated Porous Silicon Neural Probe Array in Rat Cortex. **2018**.
45. Bard, A. J.; Faulkner, L. R., *Electrochemical methods : fundamentals and applications*. 2nd ed.; Wiley: New York, 2001; p xxi, 833 pages.
46. Konopka, S. J.; McDuffie, B., Diffusion coefficients of ferri- and ferrocyanide ions in aqueous media, using twin-electrode thin-layer electrochemistry. *Analytical Chemistry* **1970**, 42 (14), 1741-1746.
47. Le Drogoff, B.; El Khakani, M. A.; Silva, P. R. M.; Chaker, M.; Vijn, A. K., Effect of the Microelectrode Geometry on the Diffusion Behavior and the Electroanalytical Performance of Hg-Electroplated Iridium Microelectrode Arrays Intended for the Detection of Heavy Metal Traces. *Electroanalysis* **2001**, 13 (18), 1491-1496.
48. Aoki, K.; Morita, M.; Niwa, O.; Tabei, H., Quantitative analysis of reversible diffusion-controlled currents of redox soluble species at interdigitated array electrodes under steady-state conditions. *Journal of electroanalytical chemistry and interfacial electrochemistry* **1988**, 256 (2), 269-282.
49. Niwa, O.; Morita, M.; Tabei, H., Fabrication and characteristics of vertically separated interdigitated array electrodes. *Journal of Electroanalytical Chemistry and Interfacial Electrochemistry* **1989**, 267 (1), 291-297.
50. Han, D.; Zaino Iii, L. P.; Fu, K.; Bohn, P. W., Redox cycling in nanopore-confined recessed dual-ring electrode arrays. *The Journal of Physical Chemistry C* **2016**, 120 (37), 20634-20641.
51. Niwa, O.; Morita, M.; Tabei, H., Highly sensitive and selective voltammetric detection of dopamine with vertically separated interdigitated array electrodes. *Electroanalysis* **1991**, 3 (3), 163-168.

52. Rice, M. E.; Gerhardt, G. A.; Hierl, P. M.; Nagy, G.; Adams, R. N., Diffusion coefficients of neurotransmitters and their metabolites in brain extracellular fluid space. *Neuroscience* **1985**, *15* (3), 891-902.
53. Wouters, K.; Puers, R., Diffusing and swelling in SU-8: insight in material properties and processing. *Journal of Micromechanics and Microengineering* **2010**, *20* (9), 095013.
54. Robbins, E. M.; Jaquins-Gerstl, A.; Fine, D. F.; Leong, C. L.; Dixon, C. E.; Wagner, A. K.; Boutelle, M. G.; Michael, A. C., Extended (10-Day) Real-Time Monitoring by Dexamethasone-Enhanced Microdialysis in the Injured Rat Cortex. *ACS Chemical Neuroscience* **2019**, *10* (8), 3521-3531.
55. Roberts, J. G.; Lugo-Morales, L. Z.; Loziuk, P. L.; Sombers, L. A., Real-time chemical measurements of dopamine release in the brain. *Methods Mol Biol* **2013**, *964*, 275-294.

**2.S Supplementary Information: Miniaturized Probe on Polymer SU-8 with Array of Individually Addressable Microelectrodes for Electrochemical Analysis in Neural and other Biological Tissues**

Mahsa Lotfi Marchoubeh, Samuel J. Cobb, Miguel Abrego Tello, Mengjia Hu, Andrea Jaquins-Gerstl, Elaine M. Robins, Julie V. McPherson, Adrian C. Michael, Ingrid Fritsch

This chapter is reformatted from the supporting information for a letter submitted to *Analytical Bioanalytical Chemistry*

Supplementary information includes CV responses for individual electrodes in the ferricyanide solution.

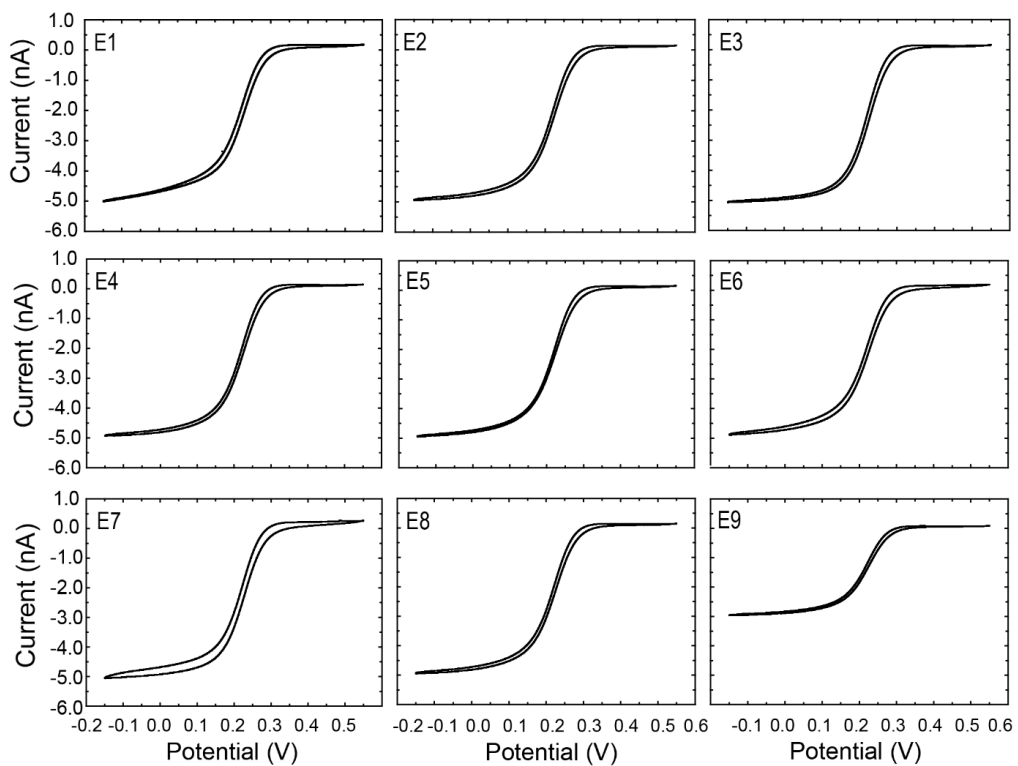


**Fig. S1** responses at 0.020 V/s of individual electrodes on a probe in a solution of 1.02 mM  $\text{K}_3\text{Fe}(\text{CN})_6$  and 0.10 M KC

**3. In situ Quantitative Analysis of Dopamine and Theoretical Considerations for Design Optimization for Redox Cycling at a Coplanar Array of Individually Addressable Electrodes with Dimensions Suitable for *in vivo* Detection on SU-8 Polymeric Substrate**

### 3.1 Abstract

Electrochemical characterization and design considerations for a microfabricated electrochemical device on an SU-8 chip substrate and insulated with a thin layer of SU-8 is reported. The device consists of nine individually addressable microelectrodes with an electrode width and gap of 4  $\mu\text{m}$  and electrode length of 100  $\mu\text{m}$ . First, electrochemical behavior of individual electrodes and redox cycling on the device is assessed with cyclic voltammetry of potassium ferricyanide and ruthenium (III) hexamine chloride as model compounds and obtained values are compared with theory. Then, a calibration curve for dopamine is obtained using redox cycling, and the detection limit is obtained as 800 nM on the generator electrodes. This is within physiological range of dopamine in the brain. In addition, the quality of electrode-electrolyte interface is evaluated by scan rate studies. The high capacitance at lower scan rates is indicative of imperfect interfaces between layers. Electrochemical impedance spectroscopy method is utilized to propose an equivalent circuit for a single electrode on SU-8 substrate. The proposed model indicated a layer of polymerized dopamine on the surface of the electrode. Finally, theoretical models are used to predict currents and detection limits for proposed optimized electrode designs.



### 3.2 Introduction

An electrochemical technique such as redox cycling provides amplified currents for electrochemically active species. This amplification is due to increased concentration gradients of molecules at oppositely polarized and closely-spaced microelectrodes.<sup>1, 2</sup> Amplification of the signal exponentially improves with smaller gaps between electrodes.<sup>3</sup> Also, redox cycling allows analysis of current at oppositely-charged electrodes, where species are generated at one set of electrodes and recycled at oppositely charged set and provides insights into solution composition, kinetics, and mechanisms of reactions.<sup>4-6</sup>

Redox cycling has been studied using electrode arrays with various geometries, mainly interdigitated arrays<sup>1, 7-11</sup> and ring/recessed microdisk arrays.<sup>12-14</sup> Advanced micro/nanofabrication techniques are used to fabricate these devices.<sup>12, 13, 15-20</sup> Most of these devices consist of electrodes that are not individually addressable.<sup>1, 2, 21-23</sup> Activation of individual electrodes at various gaps to better understand kinetics and following chemistry and to be able to differentiate and simultaneously measure catecholamines is a feat only achievable by individually addressable electrode arrays. These studies have been performed in our group previously..<sup>1, 2</sup>

Of the catecholamines, dopamine has been most extensively studied due to its diverse role in neurological functions.<sup>24-26</sup> Sampling of the extracellular fluid with microdialysis probe, has led to a wealth of information about the roles and effects of dopamine in the brain.<sup>27-30</sup> However, this method does not provide real time responses and can lead to tissue damage due to the size of the probes (>200  $\mu\text{m}$  in diameter).<sup>31</sup> Fast scan cyclic voltammetry (FSCV) using carbon fiber electrodes (4-20  $\mu\text{m}$  in diameter) provides real time electrochemical analysis with high temporal resolution (100 ms) of dopamine with minimal tissue damage, because of the

probe dimensions.<sup>32</sup> However, rapidly changing voltage used for this technique causes a large background current due to double-layer charging that overtakes faradaic current.<sup>33</sup> Thus, background subtraction is critical for quantitative analysis. This background subtraction leads to the inability of this method to measure basal or slowly changing levels of chemicals as they are embedded in the background current. In addition, because background current in vivo has limited stability, FSCV is typically not used for measurements that exceed 1 min without reestablishing background signal measurements.<sup>34</sup> Because redox cycling does not utilize fast scan rates, measurement of basal levels of DA is feasible in absence of high and unstable background currents.

Redox cycling has been used to detect and quantify dopamine in vitro on devices that are not suitable for in vivo studies.<sup>1, 35-39</sup> Some of these studies report detection limits for their devices and conditions; to the best of our knowledge, the lowest detection limit of 0.5 fM for dopamine achieved by redox cycling is by utilizing a device with 300 microband electrodes, with a gap and electrode width of 5  $\mu\text{m}$  and electrode length of 2 mm.<sup>40</sup> Other devices with various geometries have reported detection limits in the range of 0.5 nM to 2  $\mu\text{M}$ .<sup>38, 41, 42</sup> To the best of our knowledge, there are only two devices capable of redox cycling with suitable dimensions for in vivo analysis.<sup>10, 43</sup> Xi et al reported a dagger shaped probe with a 2 mm long and 70  $\mu\text{m}$  wide shank with 2-5 pairs of electrodes. The electrode's width, gap, and length are 3  $\mu\text{m}$ , 2  $\mu\text{m}$ , and 250  $\mu\text{m}$ , respectively. This device has a detection limit of 1  $\mu\text{M}$  for DA at 5 pairs of electrodes; however, the microfabrication process on silicon nitride substrate and etching of the device to create the shape of the probe is extremely rigorous, time consuming, and irreproducible. In addition, silicon nitride is a rigid substrate that is prone to breakage during insertion into the

tissue. Another device reported by Dengler et al. features three 10- $\mu\text{m}$  wide and 100- $\mu\text{m}$  long carbon-based electrodes with 8  $\mu\text{m}$  gaps. This probe is also patterned on silicon nitride substrate.

In a previous publication, we presented a miniaturized neural probe with suitable dimension for for in vivo and small volume analysis of dopamine with a detection limit of 1.2  $\mu\text{M}$ . This device is microfabricated on a laser cut, dagger shaped, SU-8 polymer substrate. SU-8 is a great candidate for implantable neural devices as it shows no biotoxicity<sup>44</sup> and enough rigidity to penetrate soft tissue without breakage but also enough flexibility to minimize tissue damage due to mechanical mismatch between the tissue and probe.<sup>45-47</sup> The shank of this probe is 6 mm long with width and thickness of 100  $\mu\text{m}$ , leading to very small tissue damage.<sup>48</sup> The device consists of nine microband electrodes with electrode width and gap of 4  $\mu\text{m}$  and a length of 100  $\mu\text{m}$ . A thin SU-8 layer insulates the device with only the contact pads and a window at the tip (70  $\mu\text{m}$  x 100  $\mu\text{m}$ ) exposed.

All the microfabricated devices mentioned above are insulated by a layer of polymer or silicon nitride. The purpose of this insulation is to define the geometry of the electrodes and provide an accurate value for electrochemically active areas. A concern for these devices is the quality of the adhesion or the seal between the metal layer, the substrate and insulation layers. Defects in the seal can be in the form of cracks or poor integrity of interfaces between these layers. These defects can be studied by performing charging current studies with cyclic voltammetry.<sup>49</sup>

Redox cycling has been used at a variety of different electrode geometries and configurations.<sup>8, 50, 51</sup> The most prominent designs are interdigitated array (IDA) electrodes<sup>22, 52, 53</sup> and the recessed disk-ring microelectrodes.<sup>12, 13, 54</sup> An equation was developed by Aoki et. al. to predict diffusion limited redox cycling current for the IDA design (Eq.1).

$$i_{lim} = m n F C * D \left[ 0.637 \ln \left( 2.55 \left( 1 + \frac{w}{w_g} \right) - \left( \frac{0.19}{\left( 1 + \frac{w}{w_g} \right)^2} \right) \right) \right] \quad \text{Eq. 1}$$

Here,  $i_{lim}$  is the same at the generators and collectors,  $m$  is number of generators and collectors,  $w$  is the width of an individual electrode, where generator and collector widths are and  $w_g$  is the width of the gap between anodes and cathodes. The length of the electrodes is denoted as  $l$ ,  $D$  is diffusion coefficient (assuming  $D_o$  and  $D_R$  are equal),  $F$  is the Faraday Constant,  $n$  is the number of electrons transferred and  $C$  is concentration ( $\text{mol}/\text{cm}^3$ ). This equation assumes infinite number of band electrodes with insignificant edge and end effects and demonstrates the significance of the gap width (compared to electrode width) for redox cycling. Other groups have also performed experimental and computer-simulated studies on the effects of geometry of the IDA on redox cycling performance and associating the gap between the electrodes to steady state current at the electrodes.<sup>55-57</sup> All these simulations are one dimensional and do not take into account different diffusion profiles at the ends of the microelectrodes. In addition, the array designs in these studies are not suitable for in vivo investigations, where probe size and active region of the brain constrains electrode dimensions and geometries, thus limiting analyte signal. Here, we consider these restrictions in evaluating our present electrode design and propose alternative widths and gaps to determine realistic expectations for signals obtainable from coplanar band arrays on a probe tip.

In our report describing successful fabrication of an in vivo probe intended for redox cycling, we only demonstrated preliminary electrochemical function of the electrodes.<sup>48</sup> In the work presented here, we establish a quantitative evaluation of the electrodes for these probe dimensions and offer predictions for improvement of array design. Redox cycling behavior of model compounds and dopamine using the electrode band array were evaluated. The

electrochemical responses are compared with theory, and detection limit and sensitivity are reported for dopamine. In addition, the background current of the electrodes is studied and is associated with the quality of the insulation layer seal with SU-8. Electrochemical impedance spectroscopy was utilized to propose an equivalent circuit for the electrodes on an SU-8 substrate. Furthermore, Eq. 1 is used to evaluate possible future designs with electrodes fitting on the same footprint and the enhancements in current and detection limits are reported.

### **3.3 Materials and Methods**

#### **3.3.1 Chemicals and Materials**

Unless otherwise stated, chemicals were reagent grade and used without further purification. Dopamine hydrochloride, calcium chloride, sodium dihydrogen phosphate monohydrate, and 4-(2-hydroxyethyl)-1-piperazineethanesulfonic acid (HEPES) (all ACS grade) were obtained from Alfa Aesar (Ward Hill, MA, USA). Magnesium sulfate, potassium ferricyanide (99.8% pure) and sodium chloride were obtained from EMD Chemicals (Gibbstown, NJ, USA). Sodium hydrogen carbonate and ruthenium hexaamine (III) chloride was obtained from J.T. Baker (Phillipsburg, NJ, USA). Sodium sulfate was obtained from Aldrich Chemical (St. Louis, MO, USA). D(+)-glucose (anhydrous) and potassium chloride were obtained from BDH/VWR (Radnor, PA, USA). Components for artificial cerebrospinal fluid (aCSF, 142 mM NaCl, 1.2 mM CaCl<sub>2</sub>, 2.7 mM KCl, 1.0 mM MgCl<sub>2</sub>, 2.0 mM NaH<sub>2</sub>PO<sub>4</sub>, pH 7.4) and phosphate buffered saline (PBS, 137 mM NaCl, 2.7 mM KCl, 10 mM Na<sub>2</sub>HPO<sub>4</sub>, 1.8 mM KH<sub>2</sub>PO<sub>4</sub>) were purchased from Sigma-Aldrich. Water (ACS reagent grade, 18 MΩ cm or greater) was obtained from Ricca Chemical (Arlington, TX, USA).

### 3.3.2 Design and Microfabrication of the Device

The design of the device, its justifications and microfabrication process have been well-documented by our group in a previous publication.<sup>48</sup> In short, the device consists of nine parallel individually addressable microband electrodes on an SU-8 substrate (Fig.1). An SU-8 top insulation layer covers all areas of the device except for exposed contact pads and the electrodes at the tip. Fig.1 (b) is a schematic showing the electrode array design that fits within a 70 x 100  $\mu\text{m}$  electroactive window at the tip of the shank. In the CAD drawing to make the fabrication masks, each electrode is 4  $\mu\text{m}$  wide and is separated by a 4  $\mu\text{m}$  gap from the next electrode. The exposed length of the probe at the tip is 100  $\mu\text{m}$ . The gold electrodes on the microfabricated device are 4.3  $\mu\text{m}$  wide with a gap of 3.7  $\mu\text{m}$  and a length of 99.2  $\mu\text{m}$ . The electrodes and leads are designed to fit on a shank with suitable dimensions for in vivo analysis with minimal tissue damage. For the work described herein, the 90  $\mu\text{m}$  thick SU-8 substrate was not laser machined to form the implantable shank. Instead, the SU-8 substrate was cut into rectangular chips. This was carried out by first creating a trench with the tip of a scalpel in an outline of the chip. The rectangular-shaped devices could be released from the substrate after 5 hours of soaking in concentrated potassium hydroxide solution that etched the underlying aluminum layer adhering the SU-8 to the wafer's surface. The devices were then stored in water prior to and between experiments.

### 3.3.3 Characterization of Individual Electrodes

All electrochemical experiments were performed with a bipotentiostat (760B, CH Instruments, Austin, TX), equipped with a Faraday cage and a picoamp booster (CH Instruments, Austin, TX). The reference electrode was Ag|AgCl in saturated KCl, and the Pt wire was used as the working electrode. To connect the device to the edge connector, it was aligned inside a

Molex zero insertion force (ZIF) edge connector with 1.00 mm pitch and 9 circuits (part number 52610-0972). For ease of connectivity and spatial availability, the edge connector was soldered onto a circuit board (OSHPark company), and the board was connected to the pin header leading to the potentiostat's leads. The cage's purge inlet was connected to argon gas (Ultra high purity, Airgas, PA). All solutions were kept under argon purge for at least 15 mins before each experiment. A conical cardboard cover was placed around the electrochemical cell inside the faradaic cage to protect the solution from convection flows due to argon purge.

Electrochemical impedance spectroscopy (EIS) experiments were performed with the CHI 760b potentiostat at 0.00 V, in a 0.1 to 10,000 Hz frequency range. Electrochemical characterization of individual electrodes on the device was performed by cyclic voltammetry (CV) in a 5.01 mM solution of  $[\text{Fe}(\text{CN})_6]^{3-}$  in 0.1 M KCl and a 5.06 mM solution of  $[\text{Ru}(\text{NH}_3)_6]^{3-}$  in 0.1 M KCl. Cyclic voltammetry was chosen for characterization due to its diagnostic capabilities. For the  $[\text{Fe}(\text{CN})_6]^{3-}$  solution, the potential was swept at 0.02 V/s from 0.55 V to -0.15 V and back to 0.55 V vs Ag|AgCl (saturated KCl). For the  $[\text{Ru}(\text{NH}_3)_6]^{3-}$  solution, the potential was swept at 0.02 V/s from 0.20 V to -0.40 V and back to 0.20 V vs Ag|AgCl (saturated KCl). Electrochemical characterization of single electrodes was first performed. Next, five adjacent band electrodes in the array were selected for the redox cycling study, for which the second and fourth electrodes were shorted together to serve as generators, and the first, third, and fifth electrodes were shorted together to serve as collectors. Before each redox cycling study, the CV response was recorded at the shorted generators, with the collectors at open circuit. Then, for the solutions containing  $[\text{Fe}(\text{CN})_6]^{3-}$  in 0.1 M KCl, CV at 0.02 V/s was performed at the generators from 0.55 V to -0.15 V and back to 0.55 V vs Ag|AgCl (saturated KCl), while the collectors were held at a constant anodic potential of 0.55 V, and for the solutions containing

$[\text{Ru}(\text{NH}_3)_6]^{3-}$  in 0.1 M KCl, CV at 0.020 V/s was performed at the generators from 0.20 V to -0.40 V and back to 0.20 V vs Ag|AgCl (saturated KCl), while the collectors were held at a constant anodic potential of 0.20 V.

For solutions containing dopamine in artificial cerebral spinal fluid (aCSF) (consisting of 100 mM NaCl, 5.0 mM KCl, 1.2 mM  $\text{NaH}_2\text{PO}_4$ , 5.0 mM  $\text{NaHCO}_3$ , 10 mM glucose, 2.5 mM HEPES, 1.2 mM  $\text{MgSO}_4$ , 1.0 mM  $\text{CaCl}_2$  at 7.4 pH), CV at 0.02 V/s was performed at the generators from -0.10 to 0.50 V and back to -0.10 V vs Ag|AgCl (saturated KCl), while the collectors were held at a constant cathodic potential of -0.100 V. Concentration studies were performed by spiking a solution of aCSF in the electrochemical cell with different volumes from a freshly prepared stock solution of 0.93 mM and 25.52 mM dopamine in fresh aCSF to achieve consecutively higher concentrations of dopamine: 0.71  $\mu\text{M}$ , 1.02  $\mu\text{M}$ , 3.28  $\mu\text{M}$ , 7.77  $\mu\text{M}$ , 38.02  $\mu\text{M}$ , 70.24  $\mu\text{M}$ , 127.69  $\mu\text{M}$ , 196.29  $\mu\text{M}$  and 219.08  $\mu\text{M}$ .

To measure plateau current from CV responses, the difference was taken between the plateau current (the current at -0.30 V for  $[\text{Ru}(\text{NH}_3)_6]^{3-}$ , -0.10 V for  $[\text{Fe}(\text{CN})_6]^{3-}$  and 0.40 V for dopamine) and the value of the background current at 0.1 and 0.5 V for  $[\text{Ru}(\text{NH}_3)_6]^{3-}$  and  $[\text{Fe}(\text{CN})_6]^{3-}$ , respectively.

### **3.4 Results and Discussion**

#### **3.4.1 Electrochemical Performance of the Device using Model Compounds**

CVs in a 5.01 mM solution of  $[\text{Fe}(\text{CN})_6]^{3-}$  in 0.1 M KCl and a 5.06 mM solution of  $[\text{Ru}(\text{NH}_3)_6]^{3-}$  in 0.1 M KCl were used to characterize single electrodes. The electrodes were characterized with both  $[\text{Ru}(\text{NH}_3)_6]^{3-}$  and  $[\text{Fe}(\text{CN})_6]^{3-}$  to assure for reproducibility and performance. The Characterization for  $[\text{Fe}(\text{CN})_6]^{3-}$  was carried out with a 30 min gap after the characterization of  $[\text{Ru}(\text{NH}_3)_6]^{3-}$ . A semi steady-state plateau current was achieved for both



model compounds because of the slow scan rates. The average current (for electrodes three to seven) at the plateau was  $-27.8 \pm 0.37$  nA for  $[\text{Ru}(\text{NH}_3)_6]^{3-}$  (measured at  $-0.30$  V), and  $-26.06 \pm 0.81$  nA for  $[\text{Fe}(\text{CN})_6]^{3-}$  (measured at  $0.00$  V) (Fig. S1 (a) E1-E9 and (b) E1-E9). Electrodes one and two on the array did not show an electrical response due to visible disconnection of the leads as a result of microfabrication issues.

The  $i_{\text{qss}}$  from a potential step experiment with a microband electrode is expressed by Eq. 2,<sup>58</sup>

$$i_{\text{qss}} = \frac{2\pi n F L C^* D}{\ln\left(\frac{64 D t}{w^2}\right)} \quad (2)$$

where  $n$  is the number of moles electrons needed to reduce the model compounds ( $n=1$  for  $[\text{Ru}(\text{NH}_3)_6]^{3-}$  and  $[\text{Fe}(\text{CN})_6]^{3-}$ ),  $F$  is the Faraday constant ( $96485.3$  C/mol  $e^-$ ),  $D$  is the diffusion coefficient ( $7.65 \times 10^{-6}$  cm<sup>2</sup>/s for  $[\text{Ru}(\text{NH}_3)_6]^{3-}$  and  $7.20 \times 10^{-6}$  cm<sup>2</sup>/s for  $[\text{Fe}(\text{CN})_6]^{3-}$ ),  $C^*$  is the bulk and initial concentration of the oxidized form of the redox species ( $5.06 \times 10^{-6}$  mol/cm<sup>3</sup> for  $[\text{Ru}(\text{NH}_3)_6]^{3-}$  and  $5.01 \times 10^{-6}$  mol/cm<sup>3</sup> for  $[\text{Fe}(\text{CN})_6]^{3-}$ ),  $w$  is the width of the electrode ( $4.3$   $\mu\text{m}$ ) and  $t$  is the time after stepping to a diffusion-limited potential. This equation can be used to predict the plateau current of a CV during slow scan rates at a microband electrode. In this case,  $t$  can be calculated as the time from  $E_{1/2}$  to where the plateau current was measured ( $t = 8$  sec for  $[\text{Ru}(\text{NH}_3)_6]^{3-}$  and  $12.5$  sec for  $[\text{Fe}(\text{CN})_6]^{3-}$ ). Considering these parameters, the  $i_{\text{qss}}$  is calculated to be  $26.52$  nA for  $[\text{Ru}(\text{NH}_3)_6]^{3-}$  and  $23.61$  nA for  $[\text{Fe}(\text{CN})_6]^{3-}$ . These values are not within the 95% confidence interval. One justification for this could be that Eq.1 is written for infinitely long and flat electrodes and does not consider the role of different diffusion profiles at the two ends and the sidewalls of the electrodes.

Of the seven active electrodes on the device, five adjacent ones were chosen for redox cycling characterization studies. For this publication, these electrodes will be referred to as electrode one to five. The second and fourth electrodes were shorted together and served as generator electrodes. The first, third, and fifth electrodes were shorted together and served as collector electrodes. The redox cycling responses overlaid with the response of a single electrode (electrode six) and two shorted electrodes (generators) are shown in Fig. S2 (a) and (b). At first, the generator response while the collectors were held at open potential were recorded. The plateau currents obtained for  $[\text{Ru}(\text{NH}_3)_6]^{3-}$  and  $[\text{Fe}(\text{CN})_6]^{3-}$  are 42.4 nA and 39.7 nA, respectively. These currents are about 1.6 times of the single electrode currents. This can be justified by the shielding of diffusion layers for closely spaced electrodes.<sup>58</sup> At low scan rates, when the diffusion layers have time to expand, they overlap with neighboring electrodes; therefore, the total current of the two electrodes is smaller than the doubled current of one electrode. The approximate length of the diffusion layer in one dimension can be calculated by  $\sqrt{2Dt}$  where D is the diffusion coefficient and t is time. For  $[\text{Ru}(\text{NH}_3)_6]^{3-}$  at 7.5 sec, and  $[\text{Fe}(\text{CN})_6]^{3-}$  at 12.5 sec (times to reach the quasi-steady state current), diffusion length is calculated to be 107  $\mu\text{m}$  and 134  $\mu\text{m}$ , respectively. Both values extend well beyond the neighboring electrode, confirming that shielding effect plays a role.

The experiments were then repeated with collectors held at oxidizing potentials. In this case, as the species are reduced on the generator electrodes, they diffuse to the adjacent collector electrode where they get oxidized. The oxidized species can diffuse back to the generator, and the cycle can be repeated multiple times until the species diffuse into the bulk of the solution.

The two important factors that characterize the efficiency of redox cycling are amplification factor (the ratio of generator response with the collectors on to the one with the

collectors off) and collection efficiency (the ratio of the collector electrodes response to the generators while collectors are on). The amplification factors are 2.51 and 2.37 for  $[\text{Ru}(\text{NH}_3)_6]^{3-}$  and  $[\text{Fe}(\text{CN})_6]^{3-}$ , respectively. The collection efficiencies are 0.84 and 0.85 for  $[\text{Ru}(\text{NH}_3)_6]^{3-}$  and  $[\text{Fe}(\text{CN})_6]^{3-}$ , respectively. These values are in agreement and better than previously reported values by our group for the same design of electrodes or other works with similar electrode geometry and dimensions.<sup>10, 48, 59</sup> This is probably due to improved fabrication processes utilized for this publication that leads to electrodes with fewer carbon and dust residues on the surface.

The equation Aoki et. al. developed as theoretical formula to predict the diffusion limited current during redox cycling (Eq. 1) makes a few assumptions. One is that there is no loss of compound to the bulk solution due to diffusion and therefore the current at the generators is the same as the collectors. In addition, it assumes that the number of generators and collectors is equal ( $m$ ). For this work, we set  $m$  to be 2.5, to account for a total of five electrodes used in redox cycling experiments. Another assumption for this equation that the diffusion coefficients of reduced and oxidized forms of the molecules are the same<sup>60</sup>. The value we use for  $D$  ( $6.93 \times 10^{-6} \text{ cm}^2/\text{s}$  for potassium ferri/ferrocyanide pair and  $7.65 \times 10^{-6} \text{ cm}^2/\text{s}$  for ruthenium (II) and (III) hexaamine chloride pair) in Eq. 1 is the average of  $D_{\text{O}}$  and  $D_{\text{R}}$  for these compounds reported by Konopka et. al.<sup>61</sup>  $w$  and  $w_g$  values are obtained from observing the device under the microscope ( $w = 4.3 \text{ }\mu\text{m}$  and  $w_g = 3.8 \text{ }\mu\text{m}$ ). Eq. 1 makes several other assumptions: (1) the array comprises of so many electrodes that the edge effects of the outermost electrodes are negligible; (2) the length-to-width ratio for each electrode is so large that end effects can be ignored; (3) the system is at steady state; and (4)  $w > 0.18 w_g$ . The experimental generator currents during redox cycling for 5.01 mM solution of  $[\text{Fe}(\text{CN})_6]^{3-}$  in 0.1 M KCl and a 5.06 mM solution of  $[\text{Ru}(\text{NH}_3)_6]^{3-}$  are 100.70 nA and 99.71 nA, respectively. The  $i_{\text{lim}}$  calculated for each compound are 89.11 nA and

85.32 nA for  $[\text{Fe}(\text{CN})_6]^{3-}$  and  $[\text{Ru}(\text{NH}_3)_6]^{3-}$ , respectively. Both experimental values are ~ 16-25% higher than the theoretical predictions. This can be justified by the fact that at least the first two assumptions do not hold for our system and that the end effects play a role in the diffusion profiles of these compounds.

### 3.4.2 Capacitive Behavior of the Microelectrodes on SU-8

Evaluation of the scan rate dependence of charging current for an electrode can reveal information about the capacitance at the electrode and its seal with insulation layers.<sup>49, 62</sup> For a microelectrode, at faster scan rates, minor defects (such as poor adhesion to the upper or lower substrates or cracks on the surface of the electrode), play a small role in the capacitance value of the electrode.<sup>62, 63</sup> In general, this is due to the effects of uncompensated resistance,  $R_u$ . A large  $iR_u$  drop in the cracks occurs at fast scan rates when the current is high, and a small  $iR_u$  drop appears at slow scan rates when the current is low. The smaller the  $iR_u$  drop, the greater the contribution from the portions of the metal in the cracks to the total electrode area, and thus, the higher the charging current.<sup>54</sup> Fig. S3 shows response of charging current to increasing scan rates for a single electrode in 0.1 M KCl. Area-normalized capacitance for each scan rate is calculated using  $C_d = i_c / Av$ , where  $i_c$  is the charging current at 0.0 V potential, A is the nominal area of the single electrode and  $v$  is the scan rate. Fig. 2 shows a plot of log of the normalized capacitance vs the log of scan rate. The slope of this line is an indication of the quality of the seal;<sup>49, 54, 64</sup> therefore for a macro electrode where the cracks and crevices play minimal role this slope should be zero.<sup>49</sup> For the device reported in this work, the slope of the log-log plot is -0.37. Other groups with defective seals have reported similar values for their micro/nano electrodes.<sup>49, 54, 64</sup> It can be concluded that the seal of the gold band electrodes to the SU-8 upper and lower

insulation layers for this work is not perfect and therefore the electroactive surface area of the electrode is bigger than observed under optical microscope.

In addition to higher electrochemically active surface area, the imperfect seal around the electrode leads to increased capacitance. For the microelectrodes discussed in this work, an area-normalized capacitance of  $303.1 \pm 16.8 \mu\text{F}/\text{cm}^2$  is obtained from the slope for lower scan rates (0.02 to 0.5 V/s) where crevices and defects play a role in the capacitance. This value is in close agreement with Pt microelectrodes on SU-8 with similar dimension to electrodes on our device and at the same scan rates by Altuna et. al.<sup>65</sup> By plotting normalized current vs. scan rates above 10 V/s, area-normalized capacitance unaffected by crevices and imperfect seal is calculated to be  $57.6 \pm 1.8 \mu\text{F}/\text{cm}^2$  which is in agreement with the expected value for similar electrode dimensions and electrolyte strength.<sup>66-72</sup>

### **3.4.3 A Model Electrochemical Circuit for a Band Electrode on SU-8 Substrate in KCl**

In an alternative treatment to Altuna et al.'s approach, electrochemical impedance spectroscopy (EIS) was performed on a single band electrode in 0.1 M KCl solution at 0.00 V with an amplitude of 0.005 V to better understand the electrochemical behavior of microfabricated gold electrodes on an SU-8 substrate. The spectra obtained from EIS studies in the frequency range of 0.1-10,000 Hz were evaluated. It can be seen in the Bode plots (Fig. 6 (b)) that the impedance phase shift is less than -90 degrees (average = -77.4 degrees) indicating non-faradaic pseudocapacitance by a constant phase element (CPE) in the equivalent circuit. Using ZView<sup>®</sup> software, an equivalent proposed circuit with a good match to the experimental data was developed (Fig 6(a)). The values for these circuit elements are reported in table 1.

Table 1: Fitted circuit elements

| Element    | Value                            |
|------------|----------------------------------|
| $R_s$      | $1.63 \times 10^4 \Omega$        |
| $R_1$      | $1.71 \times 10^7 \Omega$        |
| CPE1       | $4.83 \times 10^{-10} \text{ F}$ |
| $\alpha_1$ | 0.90                             |
| $R_2$      | $3.16 \times 10^8 \Omega$        |
| CPE2       | $1.17 \times 10^{-9} \text{ F}$  |
| $\alpha_2$ | 0.88                             |

Where  $R_s$  represents the solution resistance and the resistance along the electrode path on the SU-8 substrate,  $R_1$ , CPE1 and  $R_2$ , CPE2 represent resistances and capacitances as CPEs. The best fit model suggests parallel R-CPE components in series to each other which indicates the presence of two separate layers of material.<sup>73</sup> One layer is the electrode surface, and the other is possibly a layer non homogenous layer with a different dielectric constant. This layer could be the residual carbon layer from the laser-micromaching step, the residual insulating SU-8 2000 from the microfabrication step or polymerized dopamine from previous experiments on the electrode. The potential range and the pH for the previous experiments with dopamine are suitable for polymerization on the electrode,<sup>74</sup> however, comparing our EIS experiments with Altuna et. a shows similarity of EIS behavior and close CPE and phase shift.<sup>65, 75, 76</sup> Considering their probe was not exposed to dopamine, there seems to be a lower chance that the top layer on our electrode could be polymerized dopamine. In addition, analysis of the background aCSF current from dopamine experiments does not indicate lowering capacitance values as a function of increasing dopamine concentration, further ruling out the polydopamine hypothesis (Fig. S4).

We have however, previously observed the presence of residues on our electrodes. At this point we are unable to assign which parallel combination is the electrode and which is the layer on top. More studies need to be done to better understand this circuit model. A comparison of the current from circuit during linear potential scan at high and low scan rates will provide valuable insights into this proposed equivalent circuit. The high value for  $R_s$  also needs to be investigated further as the expected value should be in the range of  $1000 \Omega$  (obtained from Eq. 1)

$$R = \frac{l}{kA} \quad \text{Eq.1}$$

Where  $k$  is conductivity of 0.1 M KCl solution (12.9 mS/cm),  $A$  is surface area of the electrode ( $380 \times 10^{-8} \text{ cm}^2$ ) and  $l$  is the distance between the microelectrode and the reference electrode (0.3 cm).

#### 3.4.4 Redox Cycling of Dopamine using the Device

The same electrodes used for redox cycling of model compounds were used to characterize the response of in vitro dopamine in aCSF at different concentrations ranging between 0.70 to 220.0  $\mu\text{M}$ , with and without redox cycling. The CV responses are shown in Fig. 3.

The potential was swept between -0.100 V to 0.500 V at 0.020 V/s to oxidize the dopamine to the o-quinone, with the collectors held at a constant potential of -0.100 V to reduce the o-quinone form back to dopamine. The redox cycling responses are shown in Figure 5. The shape of the curves is sigmoidal, however, due to slower electron transfer kinetics of dopamine, they do not reach the steady state current as sharply as the model compound.<sup>77</sup> In the forward sweep at the generator both with and without redox cycling, past the  $E_{1/2}$  of dopamine, the anodic current at the electrode rises as dopamine is oxidized to for its o-quinone form. When RC mode

is on, these oxidized species diffuse to the collector currents and lead to cathodic currents. On the return sweep and at potentials more negative to  $E_{1/2}$ , the generation of o-quinone does not occur and the current at both electrodes drops towards zero.

The linear calibration curve for each mode is shown in fig. 4. For ease of visualization, the absolute values of currents are plotted. The slope of these lines are representations of sensitivity. The amplification factor ( $A_f$ ) is an efficient way to represent the amplification of signal at the generator electrodes due to shuttling of dopamine molecule between the two electrodes. Using slopes of the calibration curve, an amplification factor of 1.66 and a collection efficiency ( $C_c$ ) of 0.74 is achieved. These values are smaller than the values reported in the literature with various designs. This is because amplification factor and collection efficiency are dependent on the geometry of the electrodes. In this work, we intend to achieve a device with suitable dimensions for in vivo measurements and therefore the area available for electrochemical detection is very limited. By utilizing more sophisticated microfabrication methods, more electrodes with smaller gaps can be achieved in the future.

Using Eq. 1, with  $D = 7.5 \times 10^{-6} \text{ cm}^2/\text{s}$ <sup>78</sup> and  $n= 2$  mole  $e^-/\text{mole}$  molecules, a theoretical slope of  $3.74 \times 10^{-2} \text{ nA}/\mu\text{M}$  is calculated. The experimental slope of the line for the generator during redox cycling is  $2.85 \times 10^{-2} \text{ nA}/\mu\text{M}$ . The smaller slope for the experiment can be justified by the fact that dopamine o-quinone is known to undergo following chemistry, therefore making it unavailable to the generator electrode for re-oxidation.<sup>79</sup>

Detection limits were calculated (3 x standard deviation of the background divided by slope of the line) to be 0.98  $\mu\text{M}$ , 0.80  $\mu\text{M}$  and 1.09  $\mu\text{M}$  for generator alone, and generators and collectors during redox cycling, respectively. The background was obtained by performing CV in the blank aCSF solution ( $N = 3$ ). Compared to our previous work, there is an improvement in the



detection limit that is justified by cleaner electrodes.<sup>48</sup> Other devices presented in the literature have a wide range of detection limits, however the devices with detection limits in the range of low micromolar and sub micromolar all consist of more than 100 electrodes and lengths of more than 2 mm.<sup>7, 9, 41</sup> A device reported in the literature that has similar electrode design to the work presented here is reported by Xi et. al.<sup>10</sup> This device is an insertable Si<sub>3</sub>N<sub>4</sub> probe with IDA electrodes and has reported detection limits of 1.0 μM of dopamine at the collector electrode at a 5-pair IDA, consistent with our results. The detection limits for dopamine obtained by FSCV are in the low nanomolar range due to higher surface area of the carbon fiber electrode used for this technique. However, FSCV is incapable of differentiation of dopamine and norepinephrine<sup>80</sup> and due to background subtraction, basal levels and slowly changing concentrations of chemicals cannot be detected. Both issues can be alleviated using redox cycling.

### **3.4.5 Design optimization of the electrode array**

The device used here has been designed with electrode geometry to fit on a probe shank with suitable dimensions for in vivo analysis and compatible with the capabilities of microfabrication at the University of Arkansas (4 μm-wide electrodes and 4 μm-wide gaps). The 100 μm-wide shank has enough space to fit nine electrodes with enough space on the edges. This probes' shank has been shown to cause minimal tissue damage to the tissue of rat's brain.<sup>48</sup> The length of the electrodes (100 μm, through the 70 × 100 μm uninsulated window on the shank tip) was chosen to be comparable with FSCV electrodes (exposed carbon microfiber protruding from the tip of the glass pipette) for benchmarking.

To optimize the electrochemical performance of the device, other electrode dimensions were studied. Since the width of the probe and the length of the electrodes were chosen to comply with biological and FSCV considerations, proposed designs fit on the same footprint.

The proposed designs also consider the reasonable approach to fabricate the electrodes. Currently laser writing technology allows for electrodes as small as 600 nm to be patterned in a short amount of time. E-beam has also been used to resolve features as small as 500 nm, however the beam in this method moves very slowly and therefore producing features that are longer than a few hundred microns would be unreasonably time consuming. Another consideration for the method is the individual addressability of the electrodes in the current design. Available connectors in the market support a maximum of 20 pins (more pins are available for the electronics industry but manually aligning the probe pads in those connectors is impractical). Hence, if the number of electrodes is higher than 20, the collectors and the generators need to be shorted together to make two contact pads. This will lead to the loss of individual addressability feature of the electrodes as well as the possibility of gap studies where electrodes would be activated at various distances from each other. To avoid this, widening the pad of the probe should be considered.

The basis of these prediction for design is the equation developed by Aoki et. al. (Eq. 1). In the current design, there are 9 electrodes; however, only 5 of them were used for the studies in the publication. Fig. 5 shows the theoretical current ( $i_{lim}$ ) vs. the width of the gap for a 5.01 mM solution of  $[\text{Fe}(\text{CN})_6]^{3-}$  in 0.1 M KCl. For all proposed designs, the electrodes occupy the same footprint (100  $\mu\text{m}$  long, fitting in a 70  $\mu\text{m}$  wide window). The electrode width ranges from 600 nm to 6  $\mu\text{m}$ , the gap width ranges from 600 nm to 4  $\mu\text{m}$ . The value for number of electrodes ( $m$ ) is calculated based on how many electrodes can fit in the 70  $\mu\text{m}$  window at the tip of the device.

It can be seen from Fig. 5 that by decreasing the gap, the current increases. The prediction is compatible with the redox cycling theory that species shuttle between the electrodes and therefore, fewer molecules will be lost to diffusion when the gaps are small.

The present detection limit of the device (at the generators during redox cycling, using five electrodes on the device) is 800 nM. This is in the higher range of physiological concentration range of dopamine (10-1200 nM). The proposed design with electrode width and electrode gap of 0.6  $\mu\text{m}$  improves the detection limit (assuming noise does not change) to 60 nM. To be able to obtain detection limits for the lowest physiological ranges, a proposed design of stacked electrodes could be considered. This design has been proposed and evaluated by Aoki et al.<sup>41</sup> By adding three stacks of electrodes on top of the current array, the detection limit could theoretically be lowered by to 20 nM. The microfabrication of such device is challenging, and further studies need to be conducted on feasibility on SU-8 substrate.

Eq.1 was used for the predictions provided above which makes assumptions on the end effects, length to width ratios and number of electrodes. Additional 3D simulations would provide us with valuable information about these aspects. Numerical approximation using finite element methods are analyzed to understand 2D vs 3D single electrode diffusion systems, scan rate study, and design optimization. Potassium ferricyanide is the model compound of choice. In the 2D model, band electrode is simulated as a hemicylindrical system. It is assumed that the electrode length is much larger than the width, where electrode ends would not contribute to the overall diffusive mass transport. Unlike 2D, 3D model would include electrode end contributions. Also, a band electrode does not provide a true steady-state current at long times, thus making chemical analysis of redox species more challenging. Fabrication of design is a very demanding task. Lastly, finding an optimized design without the need for fabrication would positively influence the understanding of these chemicals. Preliminary results suggest (1) approximately 21% of single electrode current magnitude (2D vs 3D) contributes to the overall diffusive process; (2) a scan rate of 1 mVs<sup>-1</sup> seems optimal; and (3) approximately 10% of

collection efficiency can be gained from 4  $\mu\text{m}$  (width and gap, No. 9 electrodes) to 1  $\mu\text{m}$  (width and gap, No. 34 electrodes) and amplification factor would be enhanced from 3 to 10. This work is still in progress and more details of these studies will be published elsewhere.

### 3.5 Conclusions

The studies here discuss the electrochemical characterization of a microfabricated device on a polymeric SU-8 substrate and individually addressable electrode array using redox cycling. The cyclic voltammetry data obtained here was compared to the literature for model compounds and dopamine. The detection limit is 800 nM which is in the upper range of physiological concentration of dopamine. The seal between the electrodes and the insulation layer was evaluated by scan rate studies proposed by Wehmeyer et. al.<sup>49</sup> The data indicated high capacitance at lower scan rates which suggests defects in the integrity of the seal. EIS experiments were performed, and an equivalent circuit was proposed for a single electrode on SU-8 substrate. This model indicated the presence of a layer covering the electrode. This layer can be the particles accumulated on the surface of the electrode or polymerized dopamine. Finally, using equations developed for redox cycling by Aoki et. al. other possible electrode and gap widths are investigated. By reducing the width of the gap, the limiting current increases semi-exponentially, therefore improving the detection limit to lower physiological concentrations of dopamine. Preliminary 3-dimensional computer simulations are used to study the effect of factors not considered by Aoki (the end effects of the electrodes) and proposed future designs.

There remains a need to further improve the detection limits to be able to detect the whole range of basal levels of dopamine in the brain. This can be achieved by improving the design of the electrodes to include narrower gaps and more electrodes. In addition, stacking the electrodes vertically could provide a path to more sensitivity. These require new

microfabrication techniques, developed with the available instruments. The quality of the microfabrication also plays an important role in the electrochemical response of the device. The imperfections in the seal lead to high capacitances at lower scan rates which makes the current of sub-micromolar concentrations harder to distinguish from the background. These defects are artefacts of microfabrication processes and optimization for those processes will lead to significant improvements. Finally, the present literature provides little information about the end effects of band electrodes. These effects can be studied by 3D simulations of arrays and can lead to improved designs and theoretical predictions of currents.

## 3.6 Figures

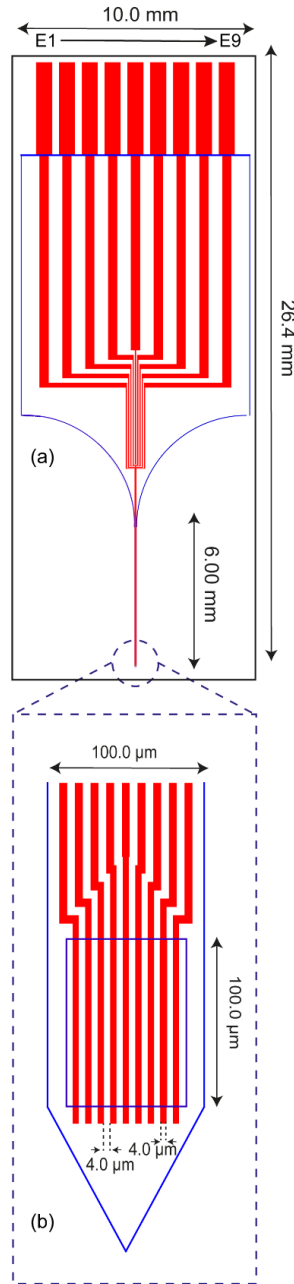


**Fig. 1** AutoCAD drawings of the device and microelectrode array on an SU-8 chip. (a) The view of the entire device. The blue outline defines the shape of the insulation layer, the red areas are the contact pads, leads, and electrodes in the metal layer and the black lines indicate the perimeters of the chip. (b) Magnified view of the tip of the device containing the electrode array. The window on the electrodes shows where they are exposed.

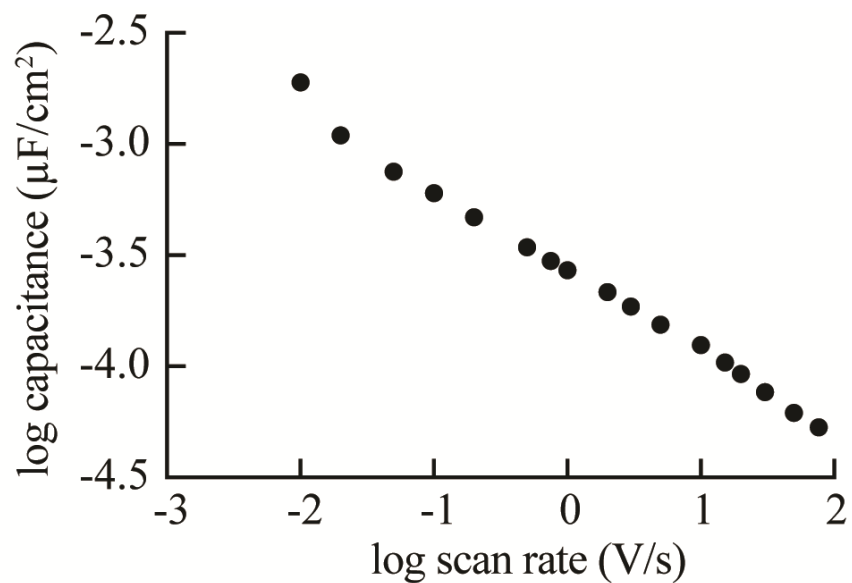


**Fig. 2** Dependence of log of normalized capacitance to log of scan rate for a single electrode in 0.1 M KCl. The measurements were obtained from data shown in Fig. S3, at 0.0 V vs Ag/AgCl. The line equation is  $y = -(0.37 \pm 0.01) x - (3.53 \pm 0.2)$  with  $R^2 = 0.995$



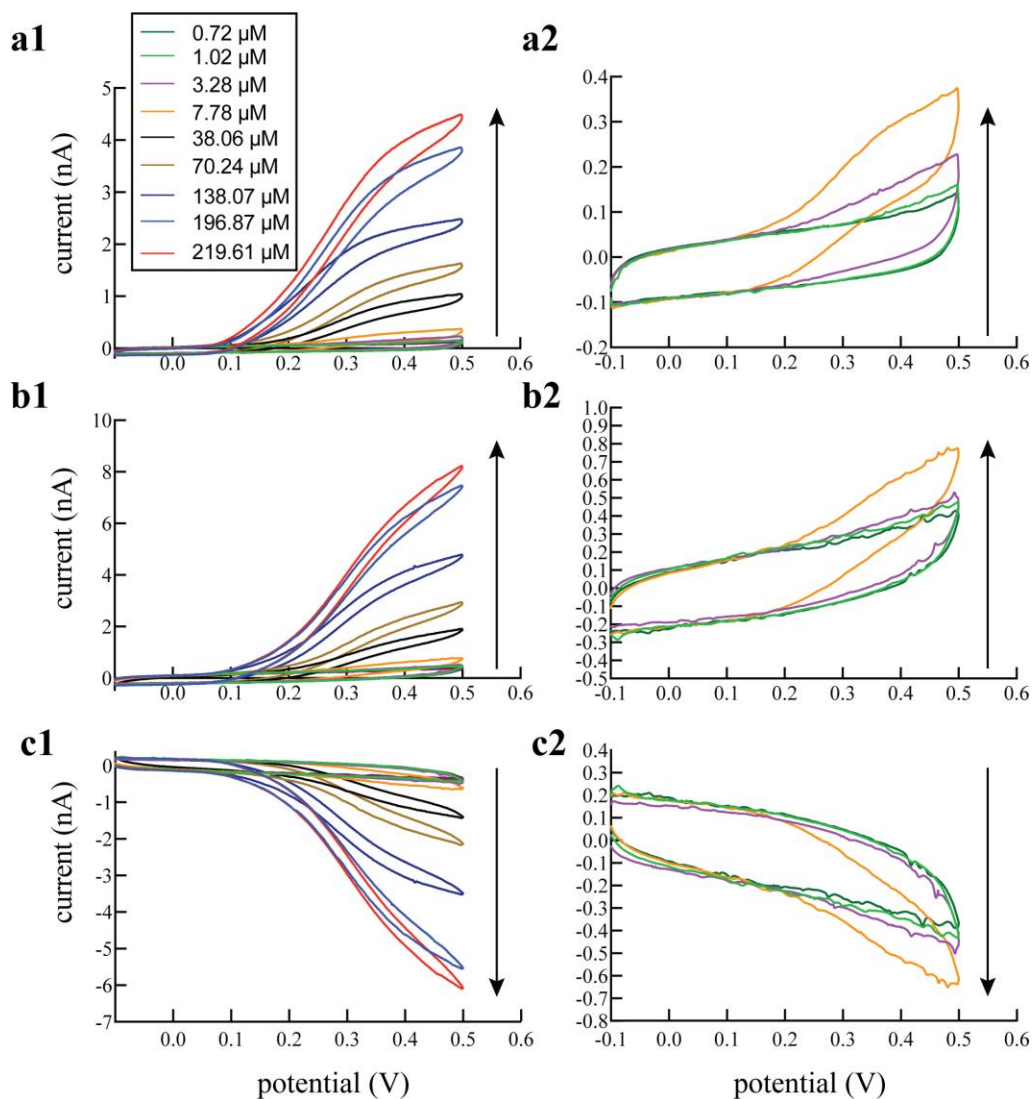


**Fig. 3** CV responses at 0.020 V/s for different concentrations of dopamine in aCSF for (a1) generators without redox cycling, (b1) generators with redox cycling and (c1) collectors with redox cycling, respectively. On the left, overlay CV responses for concentrations from 0.72  $\mu\text{M}$ , 1.02  $\mu\text{M}$ , 3.28  $\mu\text{M}$ , 7.78  $\mu\text{M}$ , 38.06  $\mu\text{M}$ , 70.24  $\mu\text{M}$ , 128.07  $\mu\text{M}$ , 196.87  $\mu\text{M}$  and 219.61  $\mu\text{M}$ . CVs on the right correspond to the lowest four concentrations from the CVs on the left

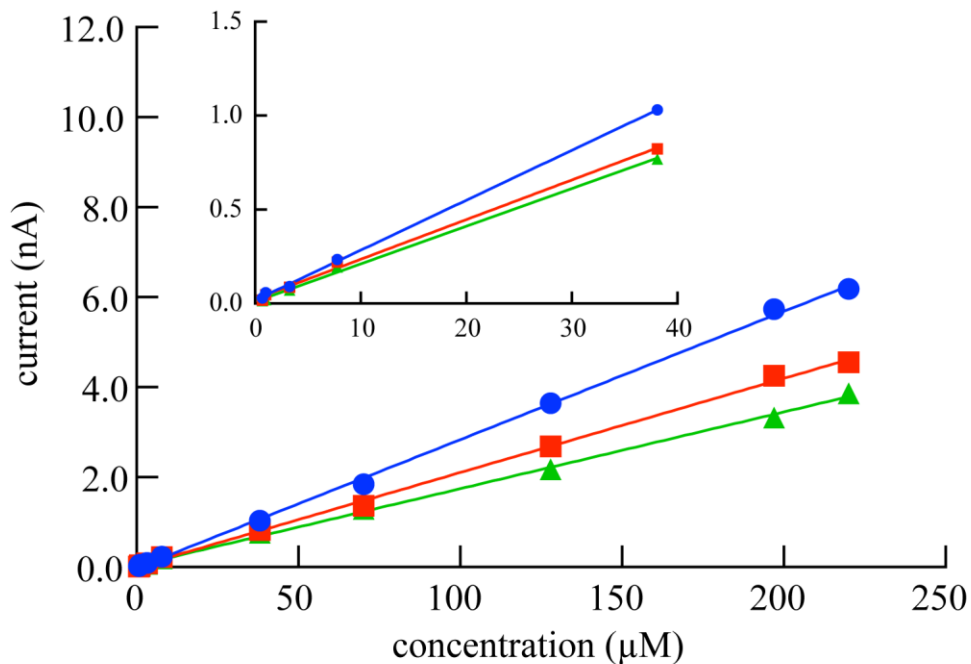


**Fig. 4** Calibration curve of background-subtracted, plateau current (measured at 0.4 V) on increasing concentrations of dopamine for generators without redox cycling (green), and for generators (blue) and collectors (red) with redox cycling. The absolute value of current has been plotted for a simpler overlay. The least squares fit and corresponding  $R^2$  values for curves for the generator without redox cycling, and the generator and collector with redox cycling are:  $y = (1.71 (\pm 0.12) \times 10^{-2} \text{ nA } \mu\text{M}^{-1}) x + (3.89 (\pm 0.04) \times 10^{-2} \text{ nA})$ ,  $R^2 = 0.999$ ;  $y = (2.85 (\pm 0.73) \times 10^{-2} \text{ nA } \mu\text{M}^{-1}) x - (1.88 (\pm 0.20) \times 10^{-2} \text{ nA})$ ,  $R^2 = 0.999$  and  $y = (2.09 (\pm 0.02) \times 10^{-2} \text{ nA } \mu\text{M}^{-1}) x + (0.14 (\pm 0.20) \times 10^{-2} \text{ nA})$ ,  $R^2 = 0.999$ ; respectively. Inset shows calibration curve for concentrations below 40.0  $\mu\text{M}$

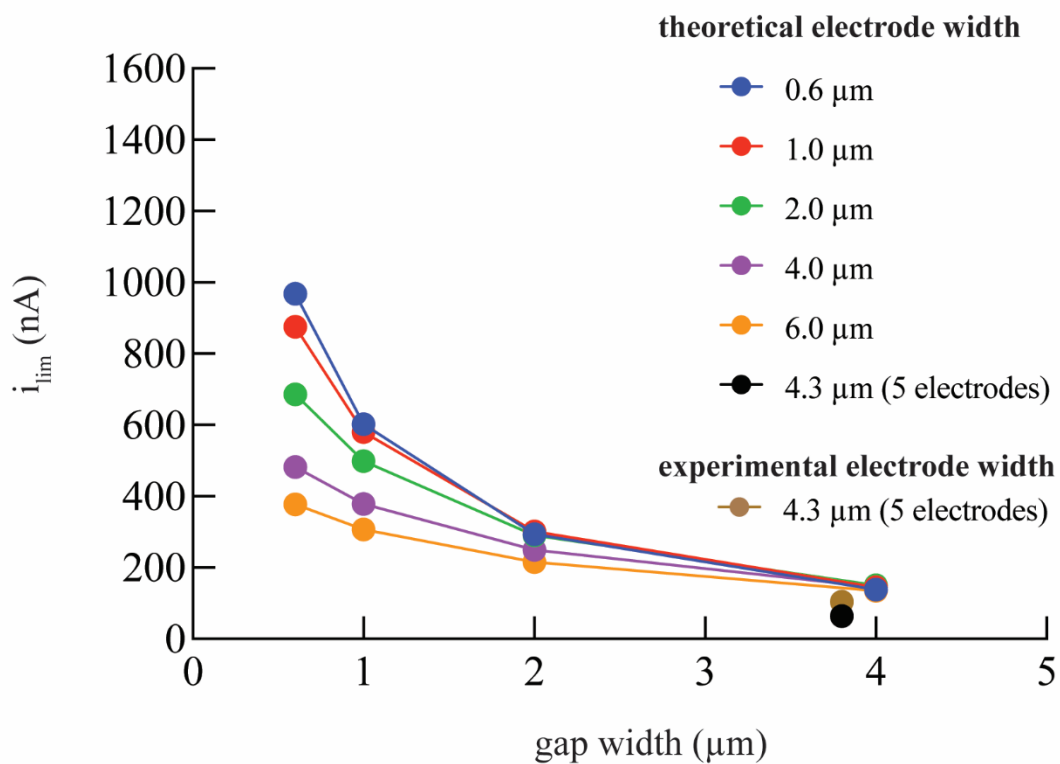


**Fig. 5** Prediction of current vs. gap for different electrode widths. Each curve corresponds to a certain width of electrode (0.6  $\mu\text{m}$ , 1  $\mu\text{m}$ , 2  $\mu\text{m}$ , 4  $\mu\text{m}$  and 6  $\mu\text{m}$ ). The two independent point correspond to the redox cycling performed for this paper with two generators and three collectors.

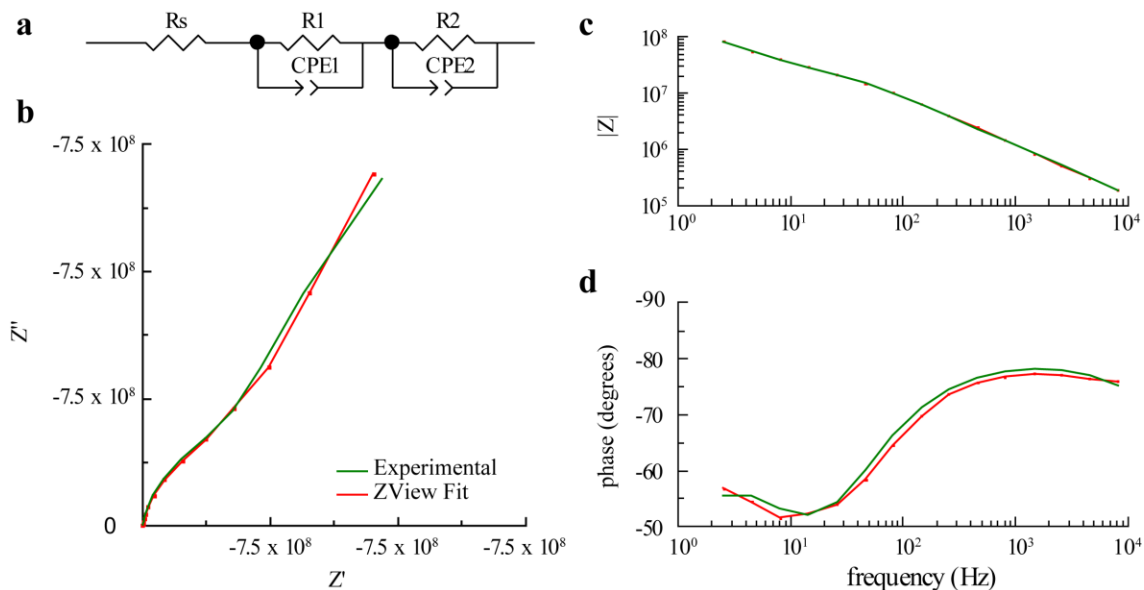


**Fig. 6** (a) equivalent circuit for a gold electrode on SU-8 substrate obtained from modeling the EIS data (b) Nyquist plot and (c) and (d) Bode plots of a single gold microband electrode on SU-8 substrate in 0.1 M KCl. The green line is the experimental data, and the red is the simulated values obtained from the equivalent circuit in the ZView software

### 3.7 References

1. Hu, M.; Fritsch, I., Redox cycling behavior of individual and binary mixtures of catecholamines at gold microband electrode arrays. *Analytical Chemistry* **2015**, *87* (4), 2029-2032.
2. Hu, M.; Fritsch, I., Application of electrochemical redox cycling: toward differentiation of dopamine and norepinephrine. *Analytical chemistry* **2016**, *88* (11), 5574-5578.
3. Wollenberger, U., Electrochemical biosensors-ways to improve sensor performance. *Biotechnology and Genetic Engineering Reviews* **1996**, *13* (1), 237-266.
4. Bard, A. J.; Crayston, J. A.; Kittlesen, G. P.; Varco Shea, T.; Wrighton, M. S., Digital simulation of the measured electrochemical response of reversible redox couples at microelectrode arrays: consequences arising from closely spaced ultramicroelectrodes. *Anal Chem.* **1986**, *58* (11), 2321-2331.
5. Hu, M.; Fritsch, I., Redox cycling behavior of individual and binary mixtures of catecholamines at gold microband electrode arrays. *J Anal Chem.* **2015**, *87* (4), 2029-2032.
6. Oleinick, A.; Zhu, F.; Yan, J.; Mao, B.; Svir, I.; Amatore, C., Theoretical Investigation of Generator-Collector Microwell Arrays for Improving Electroanalytical Selectivity: Application to Selective Dopamine Detection in the Presence of Ascorbic Acid. *Chem Phys Chem.* **2013**, *14* (9), 1887-1898.
7. Aoki, K.; Morita, M.; Niwa, O.; Tabei, H., Quantitative analysis of reversible diffusion-controlled currents of redox soluble species at interdigitated array electrodes under steady-state conditions. *Journal of electroanalytical chemistry and interfacial electrochemistry* **1988**, *256* (2), 269-282.
8. Dam, V. A. T.; Olthuis, W.; van den Berg, A., Redox cycling with facing interdigitated array electrodes as a method for selective detection of redox species. *Analyst* **2007**, *132* (4), 365-370.
9. Niwa, O., Electroanalysis with interdigitated array microelectrodes. *Electroanalysis* **1995**, *7* (7), 606-613.

10. Xi, Y. Interdigitated array electrode microprobe: Design, fabrication and characterization. University of Arkansas, 2005.
11. Zachek, M. K.; Park, J.; Takmakov, P.; Wightman, R. M.; McCarty, G. S., Microfabricated FSCV-compatible microelectrode array for real-time monitoring of heterogeneous dopamine release. *Analyt (Cambridge, U. K.)* **2010**, *135* (7), 1556-1563.
12. Ma, C.; Contento, N.; Gibson, L.; Bohn, P., Recessed Ring-Disk Nanoelectrode Arrays Integrated in Nanofluidic Structures for Selective Electrochemical Detection. *Analytical chemistry* **2013**, *85*.
13. Ma, C.; Contento, N. M.; Gibson, L. R.; Bohn, P. W., Redox Cycling in Nanoscale-Recessed Ring-Disk Electrode Arrays for Enhanced Electrochemical Sensitivity. *ACS Nano* **2013**, *7* (6), 5483-5490.
14. Menshykau, D.; O'Mahony, A. M.; del Campo, F. J.; Munõz, F. X.; Compton, R. G., Microarrays of Ring-Recessed Disk Electrodes in Transient Generator-Collector Mode: Theory and Experiment. *Analytical Chemistry* **2009**, *81* (22), 9372-9382.
15. Matylitskaya, V.; Kasemann, S.; Urban, G.; Dincer, C.; Partel, S., (Invited) Electrochemical Characterization of Nanogap Interdigitated Electrode Arrays for Lab-on-a-Chip Applications. *ECS Transactions* **2017**, *80* (10), 1295-1308.
16. Wahl, A. J. C.; Seymour, I. P.; Moore, M.; Lovera, P.; O'Riordan, A.; Rohan, J. F., Diffusion profile simulations and enhanced iron sensing in generator-collector mode at interdigitated nanowire electrode arrays. *Electrochimica Acta* **2018**, *277*, 235-243.
17. Partel, S.; Kasemann, S.; Matylitskaya, V.; Thanner, C.; Dincer, C.; Urban, G., A simple fabrication process for disposable interdigitated electrode arrays with nanogaps for lab-on-a-chip applications. *Microelectronic Engineering* **2017**, *173*, 27-32.
18. Sharma, D.; Lim, Y.; Lee, Y.; Shin, H., Glucose sensor based on redox-cycling between selectively modified and unmodified combs of carbon interdigitated array nanoelectrodes. *Analytica Chimica Acta* **2015**, *889*, 194-202.
19. Baek, S.; Kwon, S.-R.; Fu, K.; Bohn, P. W., Ion Gating in Nanopore Electrode Arrays with Hierarchically Organized pH-Responsive Block Copolymer Membranes. *ACS Applied Materials & Interfaces* **2020**, *12* (49), 55116-55124.

20. Fu, K.; Kwon, S.-R.; Han, D.; Bohn, P. W., Single Entity Electrochemistry in Nanopore Electrode Arrays: Ion Transport Meets Electron Transfer in Confined Geometries. *Accounts of Chemical Research* **2020**, *53* (4), 719-728.
21. Han, D.; Zaino Iii, L. P.; Fu, K.; Bohn, P. W., Redox cycling in nanopore-confined recessed dual-ring electrode arrays. *The Journal of Physical Chemistry C* **2016**, *120* (37), 20634-20641.
22. Aoki, K., analysis of reversible diffusion-controlled currents of redox soluble species at interdigitated arrays electrodes under steady state conditions. *J. Electroanal. Chem.* **1988**, *256*, 269-282.
23. He, D.; Yan, J.; Zhu, F.; Zhou, Y.; Mao, B.; Oleinick, A.; Svir, I.; Amatore, C., Enhancing the Bipolar Redox Cycling Efficiency of Plane-Recessed Microelectrode Arrays by Adding a Chemically Irreversible Interferent. *Anal. Chem. (Washington, DC, U. S.)* **2016**, *88* (17), 8535-8541.
24. Diehl, D. J.; Gershon, S., The role of dopamine in mood disorders. *Comprehensive psychiatry* **1992**, *33* (2), 115-120.
25. Dunlop, B. W.; Nemeroff, C. B., The role of dopamine in the pathophysiology of depression. *Archives of general psychiatry* **2007**, *64* (3), 327-337.
26. Iversen, S. D.; Iversen, L. L., Dopamine: 50 years in perspective. *Trends in neurosciences* **2007**, *30* (5), 188-193.
27. Borland, L. M.; Shi, G.; Yang, H.; Michael, A. C., Voltammetric study of extracellular dopamine near microdialysis probes acutely implanted in the striatum of the anesthetized rat. *Journal of neuroscience methods* **2005**, *146* (2), 149-158.
28. Gu, H.; Varner, E. L.; Groskreutz, S. R.; Michael, A. C.; Weber, S. G., In vivo monitoring of dopamine by microdialysis with 1 min temporal resolution using online capillary liquid chromatography with electrochemical detection. *Analytical chemistry* **2015**, *87* (12), 6088-6094.
29. Nesbitt, K. M.; Varner, E. L.; Jaquins-Gerstl, A.; Michael, A. C., Microdialysis in the Rat Striatum: Effects of 24 h Dexamethasone Retrodialysis on Evoked Dopamine Release and Penetration Injury. *ACS Chemical Neuroscience* **2015**, *6* (1), 163-173.

30. Shou, M.; Ferrario, C. R.; Schultz, K. N.; Robinson, T. E.; Kennedy, R. T., Monitoring dopamine in vivo by microdialysis sampling and on-line CE-laser-induced fluorescence. *Analytical chemistry* **2006**, *78* (19), 6717-6725.
31. Jaquins-Gerstl, A.; Michael, A. C., Comparison of the brain penetration injury associated with microdialysis and voltammetry. *Journal of neuroscience methods* **2009**, *183* (2), 127-135.
32. Venton, B. J.; Cao, Q., Fundamentals of fast-scan cyclic voltammetry for dopamine detection. *Analyst* **2020**, *145* (4), 1158-1168.
33. Robinson, D. L.; Hermans, A.; Seipel, A. T.; Wightman, R. M., Monitoring Rapid Chemical Communication in the Brain. *Chemical Reviews* **2008**, *108* (7), 2554-2584.
34. Rodeberg, N. T.; Sandberg, S. G.; Johnson, J. A.; Phillips, P. E. M.; Wightman, R. M., Hitchhiker's Guide to Voltammetry: Acute and Chronic Electrodes for in Vivo Fast-Scan Cyclic Voltammetry. *ACS Chemical Neuroscience* **2017**, *8* (2), 221-234.
35. Aggarwal, A. Studies Toward the Development of a Microelectrode Array for Detection of Dopamine through Redox Cycling. Dissertation, University of Arkansas, 2011.
36. Alayo, N.; Fernández-Sánchez, C.; Baldi, A.; Esquivel, J. P.; Borrísé, X.; Pérez-Murano, F., Gold interdigitated nanoelectrodes as a sensitive analytical tool for selective detection of electroactive species via redox cycling. *Microchimica Acta* **2016**, *183* (5), 1633-1639.
37. Kätelhön, E.; Hofmann, B.; Lemay, S. G.; Zevenbergen, M. A. G.; Offenhäusser, A.; Wolfrum, B., Nanocavity Redox Cycling Sensors for the Detection of Dopamine Fluctuations in Microfluidic Gradients. *Analytical Chemistry* **2010**, *82* (20), 8502-8509.
38. Vandaveer, W. R.; Woodward, D. J.; Fritsch, I., Redox cycling measurements of a model compound and dopamine in ultrasmall volumes with a self-contained microcavity device. *Electrochimica Acta* **2003**, *48* (20), 3341-3348.
39. Wolfrum, B.; Zevenbergen, M.; Lemay, S., Nanofluidic Redox Cycling Amplification for the Selective Detection of Catechol. *Analytical Chemistry* **2008**, *80* (4), 972-977.
40. Tabei, H.; Takahashi, M.; Hoshino, S.; Niwa, O.; Horiuchi, T., Subfemtomole detection of catecholamine with interdigitated array carbon microelectrodes in HPLC. *Analytical chemistry* **1994**, *66* (20), 3500-3502.



41. Niwa, O.; Morita, M.; Tabei, H., Highly sensitive and selective voltammetric detection of dopamine with vertically separated interdigitated array electrodes. *Electroanalysis* **1991**, 3 (3), 163-168.
42. Peng, W.; Wang, E., Preparation and characterization of a multi-cylinder microelectrode coupled with a conventional glassy carbon electrode and its application to the detection of dopamine. *Analytica Chimica Acta* **1993**, 281 (3), 663-671.
43. Dengler, A. K.; McCarty, G. S., Microfabricated Microelectrode Sensor for Measuring Background and Slowly Changing Dopamine Concentrations. *J Electroanal Chem (Lausanne)* **2013**, 693, 28-33.
44. Nemani, K. V.; Moodie, K. L.; Brennick, J. B.; Su, A.; Gimi, B., In vitro and in vivo evaluation of SU-8 biocompatibility. *Materials Science and Engineering: C* **2013**, 33 (7), 4453-4459.
45. Huang, S.-H.; Lin, S.-P.; Chen, J.-J. J., In vitro and in vivo characterization of SU-8 flexible neuroprobe: From mechanical properties to electrophysiological recording. *Sensors and Actuators A: Physical* **2014**, 216, 257-265.
46. Krishnamurthy, N.; Moodie, K.; Brennick, J.; Su, A.; Gimi, B., *In vitro and in vivo evaluation of SU-8 biocompatibility*. 2013; Vol. 33, p 4453-9.
47. Marchoubeh, M. L.; Cobb, S. J.; Tello, M. A.; Hu, M.; Jaquins-Gerstl, A.; Robbins, E. M.; Macpherson, J. V.; Michael, A. C.; Fritsch, I., Miniaturized probe on polymer SU-8 with array of individually addressable microelectrodes for electrochemical analysis in neural and other biological tissues. *Analytical and Bioanalytical Chemistry* **2021**, 1-15.
48. Lotfi Marchoubeh, M.; Cobb, S. J.; Tello, M. A.; Hu, M.; Jaquins-Gerstl, A.; Robbins, E. M.; Macpherson, J. V.; Michael, A. C.; Fritsch, I., Miniaturized probe on polymer SU-8 with array of individually addressable microelectrodes for electrochemical analysis in neural and other biological tissues. *Analytical and Bioanalytical Chemistry* **2021**, 1-15.
49. Wehmeyer, K. R.; Wightman, R. M., Scan rate dependence of the apparent capacitance at microvoltammetric electrodes. *Journal of Electroanalytical Chemistry and Interfacial Electrochemistry* **1985**, 196 (2), 417-421.
50. Niwa, O.; Morita, M.; Tabei, H., Fabrication and characteristics of vertically separated interdigitated array electrodes. *Journal of Electroanalytical Chemistry and Interfacial Electrochemistry* **1989**, 267 (1), 291-297.

51. Pathirathna, P.; Balla, R. J.; Amemiya, S., Nanogap-Based Electrochemical Measurements at Double-Carbon-Fiber Ultramicroelectrodes. *Analytical Chemistry* **2018**, *90* (20), 11746-11750.
52. Niwa, O.; Morita, M.; Tabei, H., Electrochemical behavior of reversible redox species at interdigitated array electrodes with different geometries: consideration of redox cycling and collection efficiency. *Analytical Chemistry* **1990**, *62* (5), 447-452.
53. Aggarwal, A.; Hu, M.; Fritsch, I., Detection of dopamine in the presence of excess ascorbic acid at physiological concentrations through redox cycling at an unmodified microelectrode array. *Analytical and Bioanalytical Chemistry* **2013**, *405* (11), 3859-3869.
54. Henry, C. S.; Fritsch, I., Microcavities Containing Individually Addressable Recessed Microdisk and Tubular Nanoband Electrodes. *Journal of The Electrochemical Society* **1999**, *146* (9), 3367-3373.
55. Odijk, M.; Olthuis, W.; Dam, V. A. T.; van den Berg, A., Simulation of Redox-Cycling Phenomena at Interdigitated Array (IDA) Electrodes: Amplification and Selectivity. *Electroanalysis* **2008**, *20* (5), 463-468.
56. Amatore, C.; Fosset, B.; Maness, K. M.; Wightman, R. M., Theory of electrochemical luminescence at double band electrodes. An examination of " steady-state" diffusion at ultramicroelectrodes. *Analytical Chemistry* **1993**, *65* (17), 2311-2316.
57. Fosset, B.; Amatore, C.; Bartelt, J.; Wightman, R. M., Theory and experiment for the collector-generator triple-band electrode. *Anal. Chem.* **1991**, *63* (14), 1403-8.
58. Bard, A. J.; Faulkner, L. R., *Electrochemical methods : fundamentals and applications*. 2nd ed.; Wiley: New York, 2001; p xxi, 833 pages.
59. Aggarwal, A. Studies toward the development of a microelectrode array for detection of dopamine through redox cycling. 2011.
60. Aoki, K.; Morita, M.; Niwa, O.; Tabei, H., Quantitative analysis of reversible diffusion-controlled currents of redox soluble species at interdigitated array electrodes under steady-state conditions. *J Electroanal Chem.* **1988**, *256* (2), 269-282.

61. Konopka, S. J.; McDuffie, B., Diffusion coefficients of ferri- and ferrocyanide ions in aqueous media, using twin-electrode thin-layer electrochemistry. *Anal Chem.* **1970**, *42* (14), 1741-1746.
62. Fox, K.; Armstrong-James, M.; Millar, J., The electrical characteristics of carbon fibre microelectrodes. *Journal of Neuroscience Methods* **1980**, *3* (1), 37-48.
63. Yamada, K.; Kitamura, F.; Ohsaka, T.; Tokuda, K., Microelectrodes with leak of solution. *Denki Kagaku Oyobi Kogyo Butsuri Kagaku* **1998**, *66* (3), 321-325.
64. Nagale, M. P.; Fritsch, I., Individually addressable, submicrometer band electrode arrays. 2. Electrochemical characterization. *Analytical Chemistry* **1998**, *70* (14), 2908-2913.
65. Altuna, A.; Bellistri, E.; Cid, E.; Aivar, P.; Gal, B.; Berganzo, J.; Gabriel, G.; Guimerà, A.; Villa, R.; Fernández, L. J., SU-8 based microprobes for simultaneous neural depth recording and drug delivery in the brain. *Lab on a Chip* **2013**, *13* (7), 1422-1430.
66. Lowinsohn, D.; Peres, H. E. M.; Kosminsky, L.; Paixão, T. R. L. C.; Ferreira, T. L.; Ramirez-Fernandez, F. J.; Bertotti, M., Design and fabrication of a microelectrode array for iodate quantification in small sample volumes. *Sensors and Actuators B: Chemical* **2006**, *113* (1), 80-87.
67. Pochay, P.; Wise, K. D.; Allard, L. F.; Rutledge, L. T., A Multichannel Depth Probe Fabricated Using Electron-Beam Lithography. *IEEE Transactions on Biomedical Engineering* **1979**, *BME-26* (4), 199-206.
68. Sreenivas, G.; Ang, S. S.; Fritsch, I.; Brown, W. D.; Gerhardt, G. A.; Woodward, D. J., Fabrication and characterization of sputtered-carbon microelectrode arrays. *Analytical chemistry* **1996**, *68* (11), 1858-1864.
69. Caston, S. L.; McCarley, R. L., Characteristics of nanoscopic Au band electrodes. *Journal of Electroanalytical Chemistry* **2002**, *529* (2), 124-134.
70. Morteza Najarian, A.; Chen, R.; Balla, R. J.; Amemiya, S.; McCreery, R. L., Ultraflat, Pristine, and Robust Carbon Electrode for Fast Electron-Transfer Kinetics. *Analytical chemistry* **2017**, *89* (24), 13532-13540.

71. Wipf, D. O.; Michael, A. C.; Wightman, R. M., Microdisk electrodes: Part II. Fast-scan cyclic voltammetry with very small electrodes. *Journal of Electroanalytical Chemistry and Interfacial Electrochemistry* **1989**, 269 (1), 15-25.
72. Jones, B. J.; Korzeniewski, C.; Franco, J. H.; Minter, S. D.; Fritsch, I., Spatially Directed Functionalization by Co-electropolymerization of Two 3,4-ethylenedioxythiophene Derivatives on Microelectrodes within an Array. *Journal of the Electrochemical Society* **2020**, 167 (16), 166511.
73. Orazem, M. E.; Tribollet, B., *Electrochemical Impedance Spectroscopy*. John Wiley & Sons, Incorporated: New York, UNITED STATES, 2017.
74. Łuczak, T., Preparation and characterization of the dopamine film electrochemically deposited on a gold template and its applications for dopamine sensing in aqueous solution. *Electrochimica Acta* **2008**, 53 (19), 5725-5731.
75. Altuna, A.; Berganzo, J.; Fernández, L. J., Polymer SU-8-based microprobes for neural recording and drug delivery. *Frontiers in Materials* **2015**, 2, 47.
76. Altuna, A.; Gabriel, G.; de la Prida, L. M.; Tijero, M.; Guimerá, A.; Berganzo, J.; Salido, R.; Villa, R.; Fernández, L. J., SU-8-based microneedles for in vitro neural applications. *Journal of Micromechanics and Microengineering* **2010**, 20 (6), 064014.
77. Randviir, E. P., A cross examination of electron transfer rate constants for carbon screen-printed electrodes using Electrochemical Impedance Spectroscopy and cyclic voltammetry. *Electrochimica Acta* **2018**, 286, 179-186.
78. Rice, M. E.; Gerhardt, G. A.; Hierl, P. M.; Nagy, G.; Adams, R. N., Diffusion coefficients of neurotransmitters and their metabolites in brain extracellular fluid space. *Neuroscience* **1985**, 15 (3), 891-902.
79. Ciolkowski, E. L.; Maness, K. M.; Cahill, P. S.; Wightman, R. M.; Evans, D. H.; Fosset, B.; Amatore, C., Disproportionation during electrooxidation of catecholamines at carbon-fiber microelectrodes *Analytical Chemistry* **1994**, 66 (21), 3611-3617.
80. Nakatsuka, N.; Andrews, A. M., Differentiating Siblings: The Case of Dopamine and Norepinephrine. *ACS Chemical Neuroscience* **2017**, 8 (2), 218-220.

**3.S Supplemental information: In situ Quantitative Analysis of Dopamine and Theoretical Considerations for Design Optimization for Redox Cycling at a Coplanar Array of Individually Addressable Electrodes with Dimensions Suitable for *in vivo* Detection on SU-8 Polymeric Substrate**

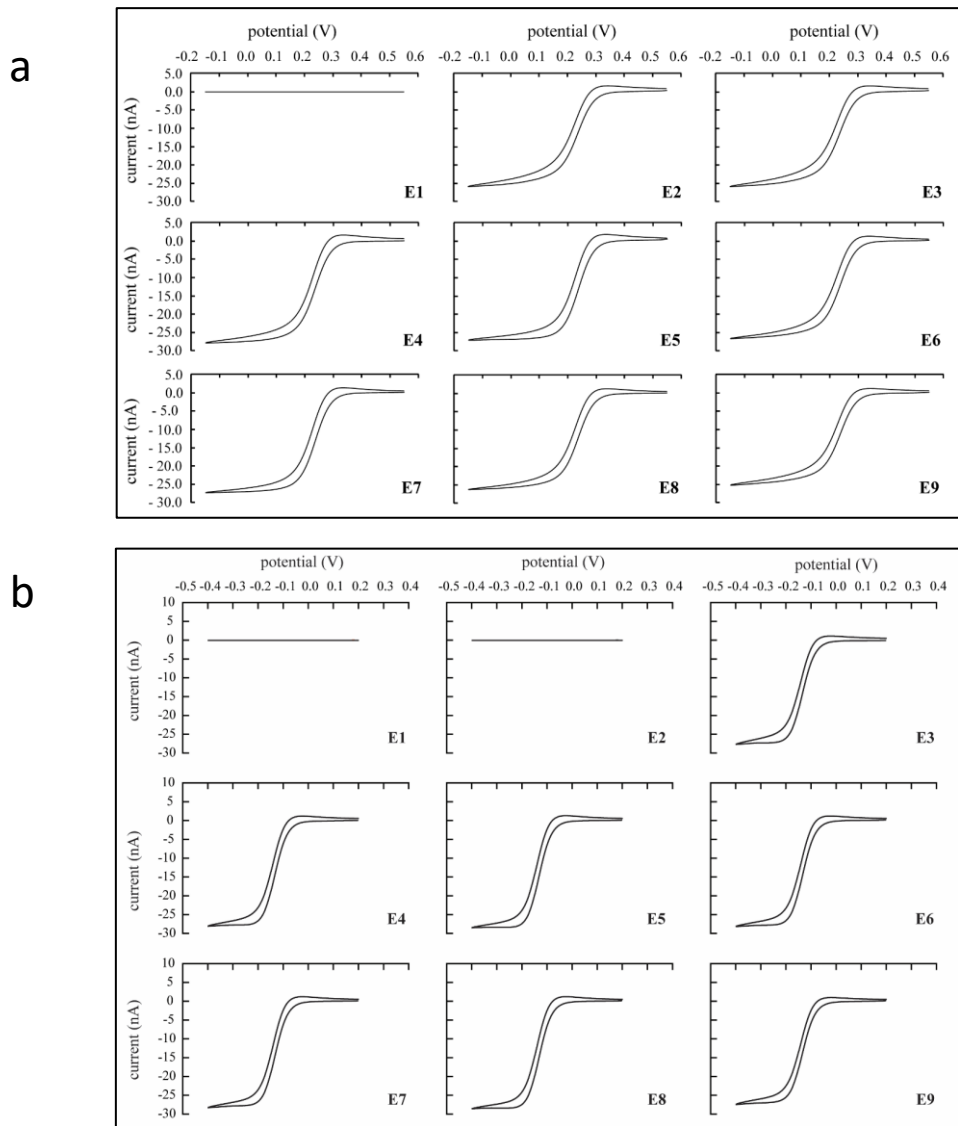


**Fig S1** CV responses at 0.020 V/s of individual electrodes (E1-E9) on a microfabricated device in (a) solution of 5.01 mM potassium ferricyanide in 0.10 M KCl (b) in a solution of 5.06 mM ruthenium hexamine chloride in 0.10 M KCl

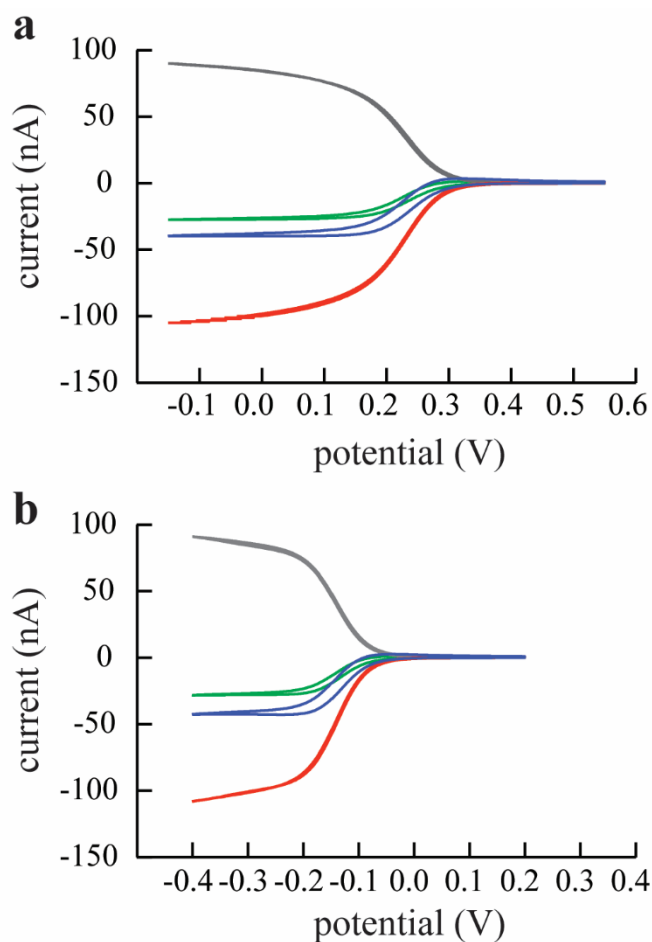


**Fig S2** Overlay of CV response for one electrode (green), generators (two electrodes shorted) with collectors off (blue), generators with collectors on (red), and collectors (three electrodes shorted) (gray) for (a) 5.01 mM solution of potassium ferricyanide. Collector current was held at 0.55 V vs. Ag|AgCl (saturated KCl) and (b) 5.06 mM solution of ruthenium hexamine chloride. Collector current was held at 0.2 V vs. Ag|AgCl (saturated KCl)

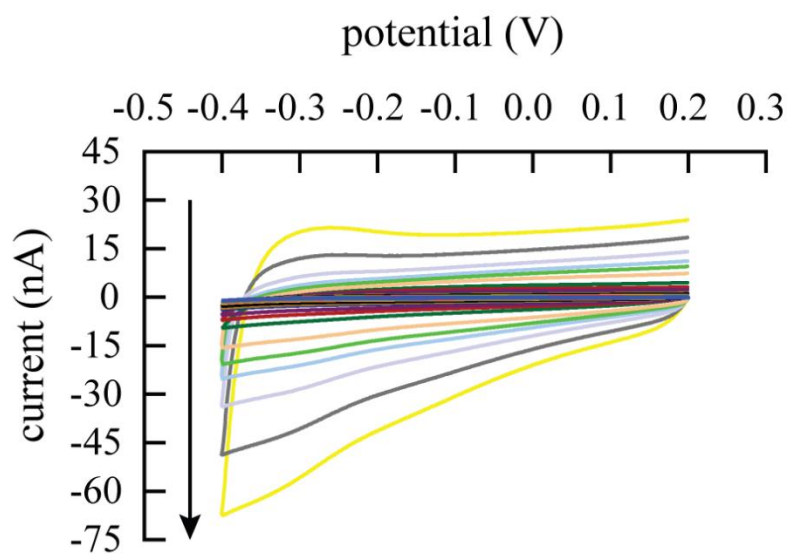


**Fig. S3** Scan rate study on a single electrode in 0.1 M KCl solution. Scan rate ranges from 0.01 V/s to 76.9 V/s



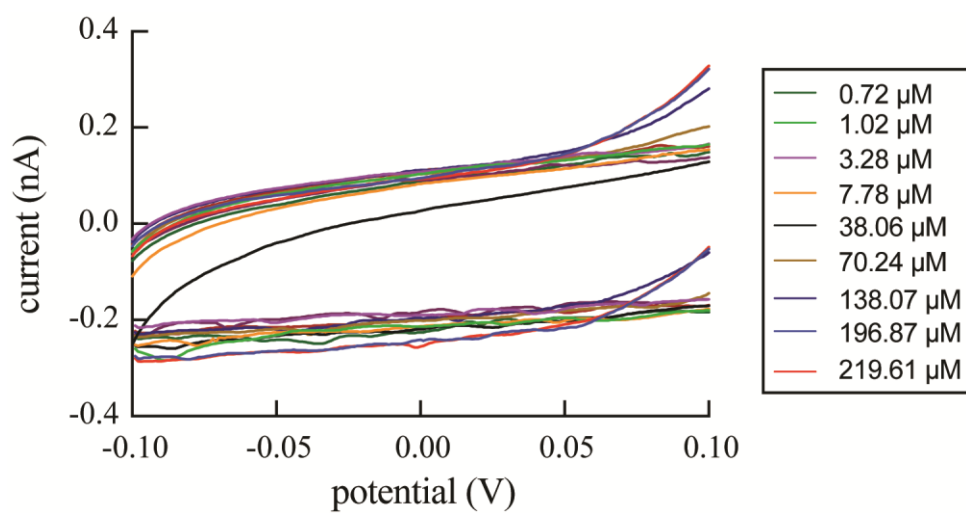


**Fig S4** Expanded view of the Charging region of cyclic voltammograms of dopamine for generators (collectors on) mode. The charging current does not show indications of change as a function of dopamine concentration change

## **4. Conclusion and Future Work**

## 4.1 Conclusion

The work described here focuses on the design, fabrication, and characterization of a novel neural probe suitable for *in vivo* detection of electrochemically active compounds. The device is designed with proper shank dimensions for minimally invasive insertion into brain tissue. The length of the shank allows for in-depth (up to 6 mm, after clearing the skull) measurements of concentrations of electrochemically active species in rat's brain. The probe is fabricated on a 100- $\mu\text{m}$  thick SU-8 substrate that provides a suitable balance between stiffness (leading to the straight path through the tissue and therefore accurately locating targeted regions using stereotaxic placement) and flexibility (causing less damage to the tissue and smaller chance of breakage during insertion). The probe consists of nine individually addressable microelectrodes, making the probe suitable for redox cycling studies with choice of distance between and grouping of activation of electrodes.<sup>1</sup>

A significant part of this work focuses on the design and microfabrication of the neural device. Here, we report the successful fabrication of the probe with an improved design. The improvements in the design include longer contact pads which allow for more convenient and precise alignment with the edge connector and wider window in the insulation layer at the tip providing leverage in case of alignment errors when patterning the insulation layer.

The microfabrication process for this probe is discussed in detail in this document. In short, a layer of SU-8 was deposited on an aluminum-coated silicon wafer. The wafer was then processed following microfabrication protocols explicitly established for this work and the metal electrodes were patterned. Next, a SU-8 insulation layer was spun coated and patterned on top of the device. Laser micromachining was used in the next step to create the individual shapes of the

probes. The laser created trenches around each probe, giving the potassium hydroxide solution access to the bottom aluminum layer so that individual devices were lifted from the wafer.

The device was then characterized electrochemically using the model compounds  $[\text{Ru}(\text{NH}_3)_6]^{3+}$  and  $[\text{Fe}(\text{CN})_6]^{3-}$ . For the redox cycling experiments in this dissertation, five adjacent electrodes were used. Two of these electrodes were shorted to act as generators and three as collectors. Each generator is flanked by two collectors. The generators are set to reduction potentials for the model compounds, and the collectors are held at oxidizing potentials. Under these conditions, amplification factors of 1.6-2.5 and collection efficiencies of 0.60-0.85 are reported.

The devices that showed electrochemical responses consistent with theoretical predictions for the electrolyte solution and model compounds were then used for redox cycling experiments with dopamine. In this case, the generator electrodes were set to oxidize dopamine and the collectors to reduce it. The detection limit obtained with this technique for dopamine was 800 nM for dopamine at the generators (redox cycling, generators on/collectors on mode), which is in the higher range of physiological concentrations of dopamine ( $10\text{-}1200\ \mu\text{M}$ )<sup>2,3</sup> and shows a significant improvement compared to the response obtained from generators on/collectors off mode (1500 nM).

In addition, some electrochemical studies were performed to understand the quality of the insulation provided by the top-coating SU-8 layer. Scan rate studies reveal the presence of capacitance-dependent behavior which indicates the presence of cracks and crevices in the material.<sup>4,5</sup> EIS studies were also performed to proposed a model equivalent circuit with a good fit.

To test the tissue damage of the probes, they were inserted into the brains of Sprague-Dawley rats in collaboration with the group of Professor Adrian Michael at the University of Pittsburgh. The results indicate that the probe made for this work does not cause extensive tissue damage. Damage to the tissue from the SU-8 probe is like that of the carbon fiber microelectrode and it is clear that the SU-8 probe offers the benefits of the smaller single carbon fiber electrodes but with the additional capabilities of multiple electrodes and redox cycling.

## **4.2 Future Work**

The accomplishments achieved to-date enable future work in testing the unique advantages of redox cycling in applications that benefit from probe-sized analysis.

### **4.2.1 Differentiation of catecholamines and their quantification *in vitro***

By having the capability to activate electrodes at certain potential and with various gaps, we can differentiate catecholamines using redox cycling. The following chemistry and the difference in internal cyclization rate for each catecholamine lead to different survival times for these molecules. Based on previous works in our lab (scaled for numbers and length of electrodes)<sup>6,7</sup> differentiation of dopamine and norepinephrine is feasible with the current probe. However, to be able to differentiate dopamine and epinephrine (with closer cyclization rate constants), a gap of 28  $\mu\text{m}$  is needed.<sup>7</sup> This means simultaneous measurement of dopamine and epinephrine on this probe is not practical with a two generator and three collector configurations. A proposed experiment is to set the outer most electrodes (e.g., electrodes 1 and 2 or both) as generator and the following electrodes as collectors. This way, the diminishing current of each catecholamine as a function of distance from the generator can be studied. These experiments can provide us with valuable information about the mechanism and kinetics of the following chemistry for the catecholamines.

The probe was initially designed with suitable dimensions and materials for *in vivo* measurements. Several additional considerations now need to be addressed to determine its function for *in vivo* studies. These include calibration, types of analytes and interferents and their concentrations, benchmarking against FSCV, immune response, reproducibility of signal, and more advanced differentiation among the catecholamines. To provide quantitative information, probes need to be calibrated pre-insertion, then inserted into the tissue, and finally re-calibrated post-insertion.<sup>8-11</sup>

A first experiment to be performed *in vivo*, would be to focus on dopamine and its detection because of numerous studies of dopamine using other electrochemical techniques in the literature with which to compare. Dopaminergic neurons are present in abundance in the striatum of the rat. A back of the envelope calculation that scales experimental data<sup>12</sup> to the dimensions and numbers of electrodes for the probe design suggests that redox cycling can detect basal levels of dopamine of around 200 nM. This cannot be achieved by FSCV because it requires subtraction of a high and varying background current.

The inability to distinguish dopamine from norepinephrine is another shortcoming of FSCV. Redox cycling achieves this by taking advantage of different reaction rates of the following reaction for catecholamine oxidation, where catecholamine o-quinone goes through an internal cyclization and become electrochemically inactive in the applied potential range. We have shown previously in our lab that differentiation can be achieved by varying the gap between the electrodes. This gap is translated into diffusion time which affects the survival possibility of the catecholamine o-quinone. These experiments involved bigger number and length of electrodes and on a device on a chip unsuitable for *in vivo* analysis. To differentiate these compounds *in vivo* using the probe, a probe with nine functioning electrodes is necessary. With

nine electrodes, a few configurations can be used that have generators and collectors either flanking each other (e.g. CGCGCGCGC or CCGGCCGGC) or one generator and a series of collectors (e.g. GCCCCCCC or GGCCCCCC). As mentioned before, since the number of electrodes is limited, differentiation of dopamine and norepinephrine with the flanking configuration might be a challenge.

Another important consideration is the immune response in the formation of glial accumulation around the probe and fouling of the electrodes by proteins in the blood. The role these factors play in changing or diminishing the electrochemical response of the probe need to be studied. More experiments need to be done with the probe implanted inside the brain. These experiments should be evaluated in two aspects. First, the electrochemical response of the probe before, during and after the implant should be studied to see how the response changes with fouling. Second, implanted tissue should be studied for signs of damage after varying times of implantation. Microdialysis near the implantation site can also provide valuable information about the effects of insertion and the immune response of the tissue.<sup>13</sup>

It is suggested that redox cycling studies first be performed in perfused slices of the brain and then expanded to *in vivo* experiments. Brain slices are obtained after perfusion of the tissue and therefore most fouling agents are absent from the environment making interpretation of the data more straight forward.

#### **4.2.2 Optimization of the probe**

The probe described in this dissertation was designed and made with the current capabilities at the University of Arkansas. The feasible resolution of the instruments available to us was ~4  $\mu\text{m}$ . However, more state-of-the-art tools are now available to researchers. It is clear that reducing the gap and increasing the number of electrodes on the device can lead to

significant changes in the probe's performance. By increasing the number of electrodes, two goals can be achieved: 1) improved amplification factors, collection efficiencies, and detection limits, and 2) feasibility of activation of more electrodes for kinetics and following chemistry studies which will lead to differentiation of catecholamines.

The best candidate for improved microfabrication is to use E-beam lithography. Currently, the University of Arkansas has one of these instruments in the Department of Physics. This instrument can pattern features as small as 500 nm.<sup>14</sup> However, various challenges are involved with the use of this instrument for microfabrication of the probe. The most important one is that the speed of the beam is very slow, and therefore developing features that are bigger than 1000  $\mu\text{m}^2$  are temporally impractical. This means that bigger features on the device (the leads and contact pads) should be patterned using conventional photolithography and the electrodes at the probe's tip be patterned using the E-beam. This requires alignment techniques and adjustments to photoresists as E-beam and UV lithography use different types of photoresists. All these approaches, however, are challenging.

In conclusion, the miniaturized neural device developed and characterized for this doctoral project is a valuable tool for studies of electrochemically active compounds in small volume and sensitive tissue environments. The microfabrication approach for this device is simple and involves laser micromachining of the substrate to create easy lift off from the carrier wafer. The unique design of this device makes it capable of performing redox cycling *in vivo* with minimal tissue damage.



### 4.3 References

1. Lotfi Marchoubeh, M.; Cobb, S. J.; Tello, M. A.; Hu, M.; Jaquins-Gerstl, A.; Robbins, E. M.; Macpherson, J. V.; Michael, A. C.; Fritsch, I., Miniaturized probe on polymer SU-8 with array of individually addressable microelectrodes for electrochemical analysis in neural and other biological tissues. *Analytical and Bioanalytical Chemistry* **2021**, 1-15.
2. Robinson, D. L.; Venton, B. J.; Heien, M.; Wightman, R. M., Detecting subsecond dopamine release with fast-scan cyclic voltammetry in vivo. *Clinical Chemistry* **2003**, *49* (10), 10.
3. Watson, C. J.; Venton, B. J.; Kennedy, R. T., In vivo measurements of neurotransmitters by microdialysis sampling. *Analytical Chemistry* **2006**, *78* (5).
4. Wehmeyer, K. R.; Wightman, R. M., Scan rate dependence of the apparent capacitance at microvoltammetric electrodes. *Journal of Electroanalytical Chemistry and Interfacial Electrochemistry* **1985**, *196* (2), 417-421.
5. Nagale, M. P.; Fritsch, I., Individually addressable, submicrometer band electrode arrays. 2. Electrochemical characterization. *Analytical Chemistry* **1998**, *70* (14), 2908-2913.
6. Hu, M.; Fritsch, I., Application of Electrochemical Redox Cycling: Toward Differentiation of Dopamine and Norepinephrine. *Analytical Chemistry* **2016**.
7. Hu, M.; Fritsch, I., Redox cycling behavior of individual and binary mixtures of catecholamines at gold microband electrode arrays. *Analytical Chemistry* **2015**, *87* (4), 2029-2032.
8. Bucher, E. S.; Wightman, R. M., Electrochemical analysis of neurotransmitters. *Annual review of analytical chemistry* **2015**, *8*, 239-261.
9. Cahill P.S., W. Q. D., Finnegan J.M., Mickelson G.E., Travis E.R., Wightman R.M., Microelectrodes for the measurement of catecholamines in biological systems. *Analytical Chemistry* **1996**, *68* (18), 3180-3186.
10. Zachek, M. K.; Takmakov, P.; Park, J.; Wightman, R. M.; McCarty, G. S., Simultaneous monitoring of dopamine concentration at spatially different brain locations in vivo. *Biosens. Bioelectron.* **2010**, *25* (5), 1179-1185.

11. Abercrombie, E. D.; Keefe, K. A.; DiFrischia, D. S.; Zigmond, M. J., Differential Effect of Stress on In Vivo Dopamine Release in Striatum, Nucleus Accumbens, and Medial Frontal Cortex. *Journal of Neurochemistry* **1989**, 52 (5), 1655-1658.
12. Hu, M.; Fritsch, I., Application of electrochemical redox cycling: toward differentiation of dopamine and norepinephrine. *Analytical chemistry* **2016**, 88 (11), 5574-5578.
13. Jaquins-Gerstl, A.; Michael, A. C., A review of the effects of FSCV and microdialysis measurements on dopamine release in the surrounding tissue. *Analyst (Cambridge, U. K.)* **2015**, 140 (11), 3696-3708.
14. Altissimo, M., E-beam lithography for micro-/nanofabrication. *Biomicrofluidics* **2010**, 4 (2), 026503.

## 5. Appendix



University of Pittsburgh

*Institutional Animal Care and Use Committee*

3500 Fifth Avenue  
Suite 206  
Pittsburgh, Pennsylvania 15213  
Tel: 412-383-2008  
Fax: 412-383-2020

# IACUC APPROVAL

Protocol #: 18103640  
PHS Assurance Number: D16-00118

**Principal Investigator:** Adrian Michael  
**Protocol Title:** Training in The Michael Lab (3)  
**Additional Titles:**  
**Funding Source(s):** NIH NS102725 - 01A1  
**Approval Date:** 10/15/2018  
**To Whom It May Concern:**

The University of Pittsburgh's Institutional Animal Care and Use Committee has reviewed and approved the research proposal referenced above.

The committee finds that the protocol meets the standards for humane animal care and use as set by the Animal Welfare Act and the NIH Guide for the Care and Use of Laboratory Animals.

Sincerely,

Frank J. Jenkins, PhD  
Institutional Animal Care and Use Committee

**The three year term of this protocol will expire on 10/15/2021. A full de novo rewrite and review must be completed and approved before this date to continue the project after this protocol expires.**

IS00013640